UNIVERSITÀ DEGLI STUDI DI MILANO

Scuola di Dottorato in Scienze Biologiche e Molecolari
XXV Ciclo

MODULATION OF PORE GATING BY "SENSOR" DOMAINS IN VOLTAGE-GATED K^+ CHANNELS.

Cristina Arrigoni

Tutor: Prof. Carlo Soave, Prof. Gerhard Thiel

Docente guida: Prof. Anna Moroni

Anno Accademico 2011-2012

Contents

PART I **1**

Abstract **1**

1 STATE OF THE ART **7**
1.1 Voltage-gated channels 7
1.1.1 Mechanism of voltage sensing 8
1.1.2 Conformational changes in the voltage sensor 12
1.1.3 Modularity of voltage-gated channels . . . 15

2 AIMS OF THE PROJECT **23**
2.1 Candidate domains for engineering a voltage-gated K^+ channel 23

3 RESULTS **27**
3.1 The fusion protein Kv_{Synth1} 27
3.1.1 Kv_{Synth1}: pore properties 29
3.1.2 Kv_{Synth1}: voltage sensor control 33
3.2 The relevance of the linker in Kv_{Synth} constructs. 40
3.3 Expression and purification of the recombinant Kv_{Synth1} 44

4 DISCUSSION (and future prospects) **51**

PART I (b) **55**

5 STATE OF THE ART **57**
5.1 HCN channels 57
5.1.1 Topology of HCN channels 58
5.2 cAMP modulation 60
5.2.1 Effect of cAMP on channel gating 60
5.2.2 The structure of the CNBD in HCN channels 61
5.2.3 Cooperativity of CNBDs 64

6 AIMS OF THE PROJECT **67**
6.1 A putative second binding pocket for nucleotides . 67

7 RESULTS **69**
7.1 Isoform specificity on the effect of c-di-GMP and compound n.11 79
7.2 Effect of compound n.11 on the native current I_f 81

8 DISCUSSION (and future prospects) **83**

References **88**

PART II - Published papers **102**

Part I

"Gli aspetti di cose per noi importantissime sono nascosti a causa della loro semplicitá. I veri fondamenti di un'indagine non colpiscono affatto l'uomo che la compie" *Ludwig Josef Johann Wittgenstein*

Abstract

Many proteins in nature show a modular topology, because it is possible to recognize functional modules responsible of distinguishable functions in the protein [1]. Voltage-gated can be considered modular proteins [55]. The superfamily of voltage-gated channels is composed of channels in which a pore-module is in charge of generating an ion conductance across the cell membrane, and other "sensor"-modules perceive different stimuli and transmit them to the pore, readjusting the conductance in response to changes within the cell. The sensor module in voltage-gated channels is the voltage sensing domain. It is composed of four transmembrane segments and it is able to feel the electrical properties of the membrane, such as changes in potential and, through a mechanical load applied by a short linker, to affect the gating of the pore (i.e. opening or closure of the channel) [2, 3]. A more sophisticated regulation is possible thanks to other modules fused to the same channel. Ligand-gated channels usually exhibit a C-terminal domain exposed in the cytoplasm, in contact with all the variable concentration of second messengers, able to modulate the activity of the channel. In this group, cyclic nucleotide-gated channels have a C-terminal domain, composed of a binding domain (CNBD) that respond to difference in concentration of cAMP or cGMP, and a C-linker region, connecting the CNBD to the pore. The CNBD acts as an allosteric domain, and modulate the channel opening upon cAMP binding [4].The idea that these domains evolved independently before fusing in a single protein, is strengthened by the fact that similar

domains are found in a large variety of proteins, that don't belong to channels family. For example, recently, a new enzyme was discovered, the voltage-sensing phosphatase (VSP) of Ciona intestinalis, whose voltage-sensor domain is fused to a phosphatase [5]. The CNBD of the hyperpolarized cyclic nucleotide-activated channels (HCN), has a conserved structure compared to that of the cAMP-dependent protein kinases [6]. My PhD thesis addresses two different topics, but in both cases I investigated how sensor-modules can give a sophisticated regulation of channel gating. In the first part, I approached the problem about how voltage-dependence originated in voltage-gated channels, in particular I obtained a voltage-gated K^+ channel fusing two unrelated protein modules: the voltage sensing domain of Ci-VSP [5] and the pore-channel PBCV-1 Kcv [7]. The fusion between a voltage sensor and a potassium channel with a quasi-ohmic behaviour generates a chimaeric protein called Kv_{Synth1}, an delayed outward rectifier potassium channel. Kv_{Synth1} retains the pore properties of Kcv (selectivity and filter gating) and the voltage dependence of the Ci-VSP (half activation potential, slope factor, shift of activation curve due to mutations). Moreover, the quality of the rectification is dependent on the length of the linker between the two modules. This highlights a mechanic role of the linker in transmitting the movement of the sensor to the pore, and shows that electromechanical coupling can occur without co-evolution of the two domains. In the second part, the allosteric modulation of the cyclic nucleotide binding domain of HCN channels has been studied on the basis of our findings in the crystal structure of the CNBD of the isoform 4 of HCN (hyperpolarized cyclic nucleotide-activated) channels. HCN are the molecular determinant of the I_f current, responsible of the autonomic regulation of the heart. In the structure of HCN4 CNBD a putative binding site for cyclic nucleotides in the C-linker region was found. Occupancy of this binding site by the prokaryote second messenger c-di-GMP can completely revert the effect of cAMP in the micromolar range. Docking a

large set of molecules in the binding pocket, another compound was identified, (N'-biphenyl-2-yl-N-[1-(3-cyanobenzyl)piperidin-4-yl]-N-(pyridin-3-ylmethyl)urea), able to give the same effect on cAMP modulation. The effect of these molecules is restricted to HCN4; this isoform selectivity underlies that, although the C-terminus of the three isoforms is structured in a similar way, the modulation can be different. Some different features of HCN1, HCN2 and HCN4 were already analysed previously [8]. These results highlight the presence of an second modulatory pathway in HCN channels, indicate a potential drug binding site for heart rate modulation and advance understanding of the mechanism of efficacy of cAMP binding in HCN channels.

1 STATE OF THE ART

1.1 Voltage-gated channels

Voltage-gated channels belong to a large family of ion channels with a crucial role in excitability, in maintaining the resting membrane potential and in the initiation and propagation of the nerve impulse [2]. The identification of the channels involved in the last phenomenon started from the early observation that in the axon the permeability to ion species is different when the membrane is at "resting" or under "excitation". In particular, the ionic current in the axon has two major components, the Na^+ and the K^+ conductances: when an action potential occurs, a strong inward Na^+ current depolarizes the membrane, and E_{Na} is the electromotive force. K^+ current is responsible to set the membrane potential again to a negative value, near to E_K (Fig.1.1). These two currents account for the action potential, they show distinguishable selectivity and separate kinetics, but both of them are voltage-dependent. The proteins that develop these currents, are Na^+ and K^+ voltage-gated channels [9].

Voltage-gated channels are a great example of how nature can produce a sophisticated protein device from simple bricks. Since these proteins use the membrane electric field to regulate cell functions, they acquired a tool to sense voltage. Within this large group, that includes Na^+, K^+, and also Ca^{2+} channels an accessory domain, the voltage sensor (VSD), senses the changes in the electrical field of the membrane and transmits the signal to

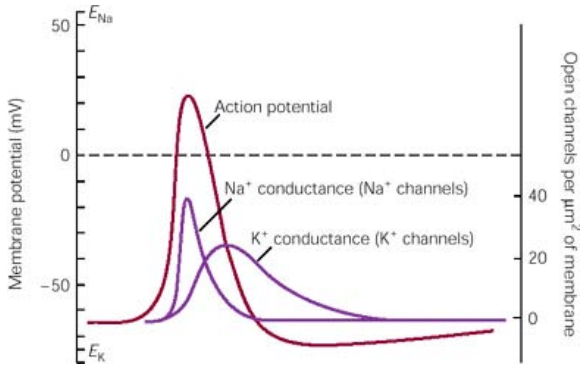

Figure 1.1: **Representative scheme of an action potential.** The sequential opening of voltage-gated Na^+ and K^+ channels generates the action potential. The Na^+ inward current depolarizes the membrane, while the K^+ conductance re-establishes the negative resting membrane potential.

the pore, affecting the open probability of the channel (Fig.1.2).

The voltage sensor, that controls this mechanism, is structurally conserved among these specialized proteins: it contains four transmembrane segments (S1-S4), in which the S4 is responsible of sensing electrical changes through a pattern of four arginines placed every third position along the α-helix [10–12].

1.1.1 Mechanism of voltage sensing

The effect of voltage sensor on the pore gating is well-understood in voltage-gated K^+ channels, and, more in particular, in Shaker, a eukaryotic Kv channel isolated from *Drosophila melanogaster* (Fig.1.4) [13–17]. Pore opening occurs after the motion of the VSD from a "resting" to an "active" state, and this conformational change is transmitted to the S5-S6 through the linker that connects the two modules (Fig.1.3) [2].

The translocation of the S4-helix is due to a large amount

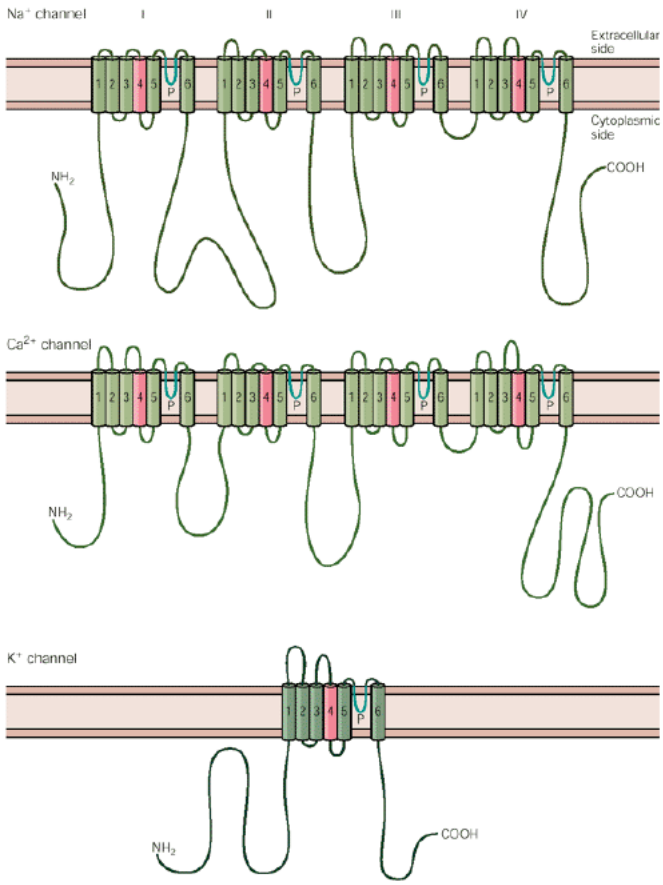

Figure 1.2: **Basic architecture of voltage-gated channels.** The cartoons show the composition of Na^+, K^+, and Ca^{2+} channels. The segments S1-S4 form the voltage sensing domain, while S5 and S6 organize the pore. Na^+ and Ca^{2+} channels are heterotetramers encoded by a single gene, while K^+ channels are composed of four identical subunits.

of positive charges that moves along five arginines residues of the segment. The first consideration is that positive charges are reorientated in response to a sudden change in the membrane potential, looking for a new position at a low energy level. For this reason, they generate fast transient currents, measurable in

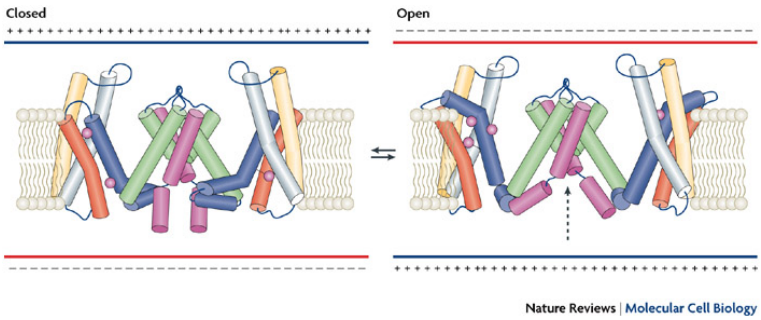

Figure 1.3: **Hypothetical transition close-to-open in Shaker.** The cartoon shows two subunits of a voltage-gated K^+ channel. When the membrane is depolarized the translation, rotation and tilting of the S4 segment (blue) is transmitted through the S4-S5 linker, which is in contact with the intracellular part of the S6 segment (magenta). In the closed position S6 is a straight alpha-helix, whereas in the open position it is bent, thereby opening the gate. The dashed arrow represents ion conduction through the open pore. The arginines are pictured in magenta.[2]

the absence of the ionic current by cut-open voltage clamp or two-electrode voltage clapm. An example is reported in Fig.1.4 [18].

The kinetics and the voltage-dependence of this "gating" current (represented by a Q-V curve) are a mirror of the behaviour of the ionic current, since they are correlated with the opening of the channel. Neutralization of many of these positive charges by mutagenesis affects the open probability of the channel, giving a different effect on the ionic current that depends on the contribution that aech of these aminoacids gives to the voltage sensor movement [14].
In Shaker, the voltage dependence of the channel is very steep, the open probability increases by a factor of 150 when ΔV is only 10mV. This corresponds to a large amount of charges moved in the sensor region: in fact, measuring gating currents in a patch where the number of expressed channels is known, it has been determined that every channels moves 13 e_o (electronic charge)

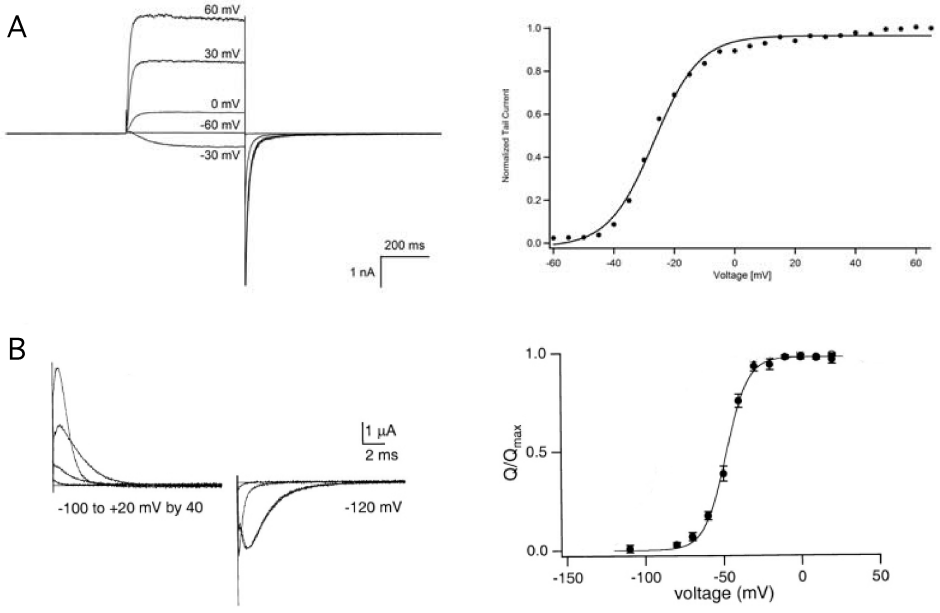

Figure 1.4: **Ionic and gating currents in Shaker.** Panel A: Ionic current trace of Shaker-IR (a mutant with removed inactivation) and voltage-dependence. The data are plotted with a Boltzmann function. The channel opens at depolarizing potentials, the calculated $V_{1/2}$ is about -27mV.Panel B: gating currents of Shaker recorded by cut-open voltage clamp. The trace show that this current is fast and transient, with left-shifted voltage-dependence respect the ionic current. [modified by [19]]

[19]. If the charges move through each voltage sensor of a Shaker channel, how does the pore integrate the motion of these independent elements to move from a closed to a open conformation? It has been demonstrated that a single wild type voltage sensor is able to gate the pore of one channel, when the other three sensor are mutated to neutralize all the basic charges [16]. The property of this mutated channel, in which the composition of the subunits is 1wt/3mut, is a left-shifted voltage dependence, indicating that lower energy level is required to open the channel. In fact, the three mutated subunits are locked in the active conformation, so that it is easy to move the channel in the open state. In particular, transition states are one fourth of the wild type, because each voltage sensor feels changes in the membrane potential independently from the others, and only the last step is cooperative, and leads to the final transition from the closed to the open configuration [16].

1.1.2 Conformational changes in the voltage sensor

Gating charges are a good marker of the conformational changes occurring in the voltage sensor during the transition between the resting and the active state. In voltage-gated channels is possible to recognize common structural features, especially concerning the voltage sensor. Many information were obtained from the crystal structure of voltage-gated K^+ channels solved by MacKinnon and co-workers [20–23] (Fig.1.5) and from the structure of a bacterial voltage-gated Na^+ channel [24], but the movement of the voltage sensor from the resting to the active state is still debated.

The two most famous models are the "helical screw" or "sliding helix" model and the "paddle" model. The first one assumes

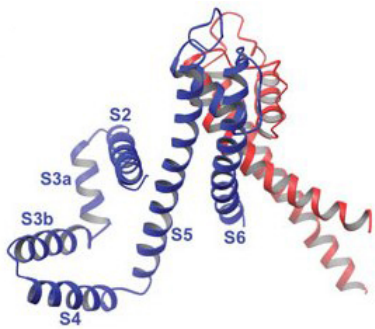

Figure 1.5: **X-ray structure of a chimera Kv1.2-2.1**. The crystal structure shows two subunit, in blue and in red. Voltage sensor is in the activated conformation, pore is open. The structure reveal that S3 is composed of two distinct helices, S3-S4. [2]

that the S4 moves outward of $\sim 13\mathring{A}$ and rotate 180° to transfer three charges per subunit, establishing new interactions with negative charges in S2 segment [13, 25, 26]. The "paddle" model is based on the observations arisen from the crystal structure in the active relaxed conformation. The N-terminal part of S4, together with part of the S3 (S3b), are involved in a large movement from the more intracellular side to the extracellular, so that they are free to move in the lipidic environment, with an extensive traslocation [23]. The difference between this two models is graphically summarized in Fig.1.6.

The absence of a structure in the resting state leaves a lot of opened questions, although some electrophysiology results showed that the "sliding helix" model can be supported. In Starace and Bezanilla [28] the authors converted the voltage sensor of Shaker in a proton pore, mutating the first and the second arginines of S4 in hystidines. The voltage sensor behaves like a proton pore, and this is possible only if the hystidines are in contact with aqueous crevices (see Fig.1.7) on both sides of the membrane. This behaviour can't be reconciled with the "paddle"

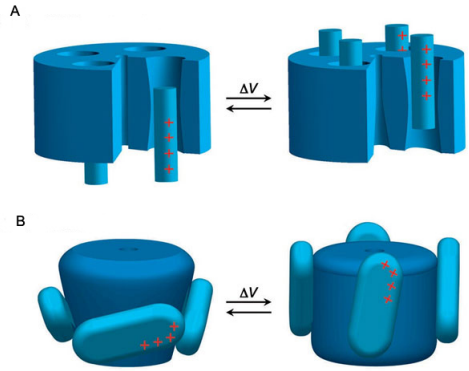

Figure 1.6: **Schematic representation of two models explaining voltage-sensor movement.** A: sliding helix model. The S4 moves outward along its axis. B: paddle model. Red crosses indicate gating charges. [27]

model, because the integrity of the protein/bilayer is not broken by aqueous crevices in the structure.

For these reasons, a structure of the voltage sensor in the resting position will be useful to understand the mechanism of the traslocation. The more recent information about the resting state are the results of long MD simulation [29]. These simulations show that S4 segment retains its helical conformation as it moves principally along its axis, and the whole transition comprises intermediate configurations, that may favor the nonconductive closed state of the pore. This is consistent with the X-ray structure of bacterial NaV channel [24] showing a closed pore domain with voltage sensors in the activated conformation. All these results fit with a model in which the first event of the inactivation is the closure of the pore, followed by independent inactivation of the VS [30]. Although MD can provide new evidence of the transition of the voltage sensor, a structure of the voltage sensor in the resting position will be useful to understand the mechanism.

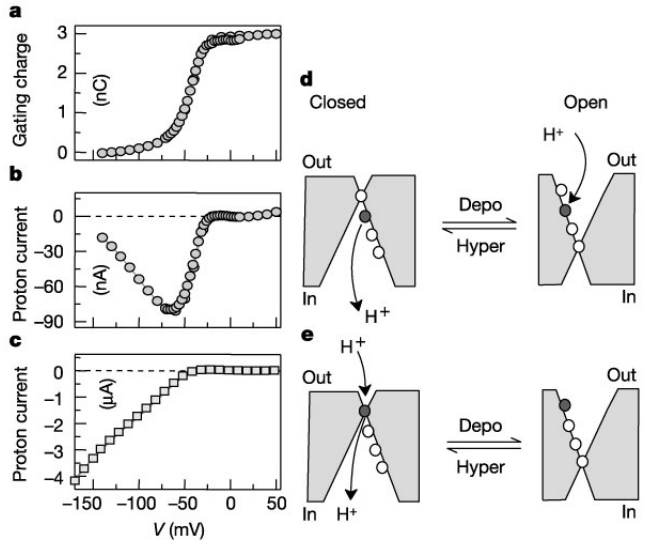

Figure 1.7: **Sliding helix model is supported by proton-pore experiments.** Proton transport and conduction: models of the conformational changes of the voltage sensor. R362 and R365 are two arginine residues of the S4 involved in gating charges movement. **(a)** Voltage dependence of the gating-charge movement of the Shaker R365H channel. **(b)** Voltage dependence of proton-transport current of the R365H channel. **(c)** Voltage dependence of proton channel current of the R362H channel. **(d)** Conformational changes during proton transport. In a proton gradient (inward), the histidine at 365 (filled circle) transports one proton each time the voltage sensor goes from the open to the closed conformation. **(e)** Representation of the R362H channel proton pore. Internal and external protons have simultaneous access to the histidine (filled circle) only in the closed position, which results in a continuous proton current when the sensor is closed. The protein core is grey. "Depo" and "hyper" indicate a more positive and a more negative membrane potential, respectively. [28]

1.1.3 Modularity of voltage-gated channels

Voltage-gated channels represent a structurally conserved superfamily, in which we can easily recognize distinct functional modules, the voltage sensor and the pore domain. The demonstration of the modularity of these proteins could suggest that Kv chan-

nels acquired the voltage dependence in one step, by fusion of two independent modules. This hypothesis is now supported by many evidence: (1) each modules, once detached from the original channel, could be still functional, even if showing different biophysical features [31, 32]; 2) the single domains that constitute Kv channels can be found in different proteins. The voltage sensing domain can be found also in the voltage-dependent phosphatase Ci-VSP isolated from *Ciona intestinalis* [5], or it can become a proton pore as in Hv1 [33]; 3) the modularity should imply that domains of different classes of channels can be swapped; 4) it should be possible to create a voltage-gated channel fusing two unrelated protein domains. The literature offers some successful examples about the evidence (1), (2) and (3); the results obtained in (4) will be presented in the "Result" section of this thesis. Concerning the functionality of isolated modules (1), it has been shown that the prokaryotic voltage-gated K^+ channel KmLv maintained a functional conductive pore once the voltage sensor is removed. The pore can be purified and reconstitution in proteoliposomes generated a ohmic current, an expected behaviour of a pore that lack of the gating mechanism of the voltage sensor [31]. Similar results were obtained from pore dissection in a voltage-gated Na^+ channel from *Silicibacter pomeroyi* [32]. Exemplary current traces recorded from the purified pore module are shown in Fig1.8

Concerning the presence of the typical ion channels-modules in enzymes (2), in 2005 Murata et al. published the characterization of Ci-VSP, a phosphoinositide phosphatase regulated by a voltage sensor, very conserved respect the one found in voltage-gated channels. It is composed of four transmembrane domains, and the S4 segment contains the conserved arginines motif responsible of the translocation of the positive charges generating the gating currents. In fact transient currents similar to gating currents have been recorded from Ci-VSP, and the derived Q-V curve showed a very right shifted and shal-

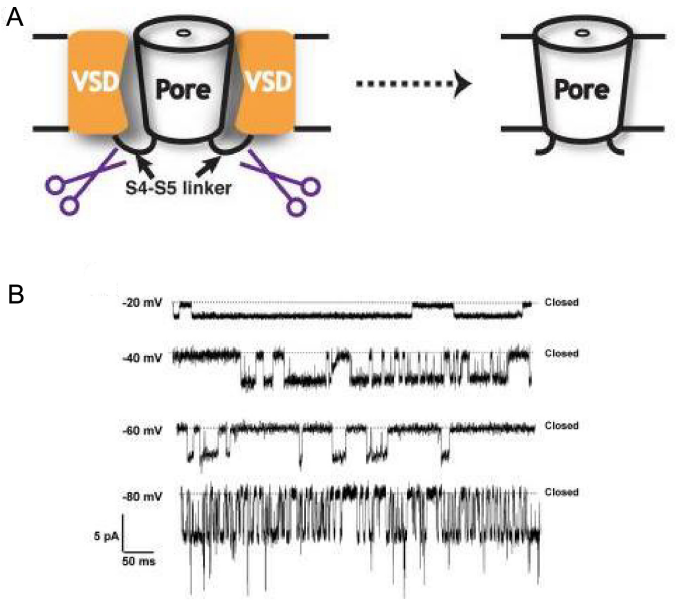

Figure 1.8: **Pore dissection of (Na(V)Sp1) sodium channel.** (A) The pore of a bacterial voltage-gated channel has been isolated from the voltage sensing domain. The pore module has been purified and reconstituted in proteoliposomes. (B) The pore generates a Na^+ current when inserted in the planar lipid bilayer. Representative single-channel traces. [32]

lower voltage-dependence respect to ion channels ($V_{1/2}$=+62mV, z=1.03) (Fig.1.9). This can suggest that a smaller amount of charges is moved upon depolarization [5]. The voltage sensor is connected to a phosphatase through a linker, and the two modules are coupled thanks to this covalent connection: the VSD motion rearranges the linker and turns on the phosphatase in the activated conformation, stabilized by PI(4,5)P2 (phosphatidylinositol 4,5- bisphosphate). The decreasing of the substrate decouples the VSD from the enzyme [34].

In the last years Ci-VSP has become a tool for understanding the mechanism of the voltage-dependence, because the voltage

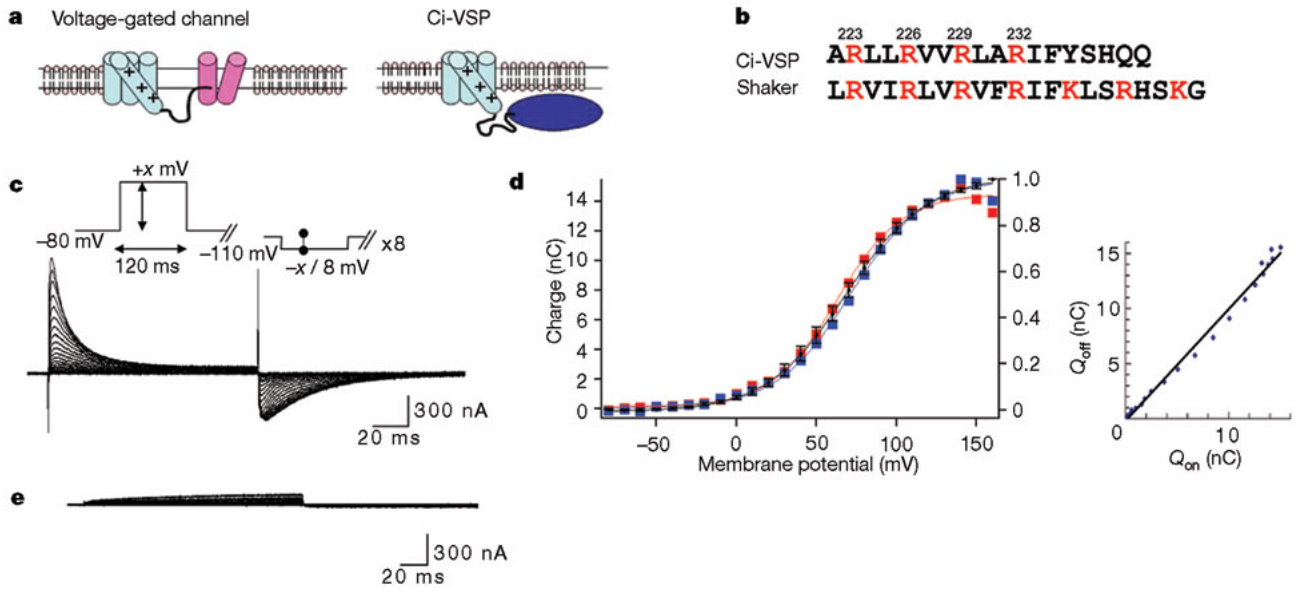

Figure 1.9: **Ci-VSP voltage sensor properties.** **(a)** Module structure of Ci-VSP and voltage-gated channel. **(b)** S4-like segment of Ci-VSP aligned with Shaker channel. **(c)** Currents recorded from a cut-open oocyte expressing Ci-VSP. A pulse was applied ranging from -80 to +160mV. **(d)** Voltage dependence of carried charge by OFF (blue squares) and ON (red squares) currents from a cut-open oocyte. $V_{1/2}$ were 62.7 and 71.8mV and z values were 1.26 and 1.10 for Q_on and Q_off respectively. **(e)** Records of Ci-VSP (R229Q/R232Q) show no gating charges. [5]

sensor can be characterized independently from the influence of a pore.
For example, it has been demonstrated that the VSD of Ci-VSP shows a "mode-shift" behaviour, very similar to that already studied in voltage-gated channels [35]. Mode-shift is a hysteresis found in these channels: after prolonged depolarization, more positive than +60 mV, the voltage sensors require stronger hyperpolarizations to return to their resting position. As a consequence, the voltage dependence of the gating charges in the Q-V curve shifts to more negative potentials compared with the Q-V obtained when holding the resting potential at -90 mV [36]. The physiological role of this mechanism is still not well-understood. Kv channels are activated when the membrane potential is at -50mV, after the onset of an action potential, and the mode-shift prevents the closure or the recover from inactivation before a resting of -70mV is reached again, avoiding too rapid firing [36]. It still matter of debate if the mode-shift is due to a relaxation, and a conformational change of the voltage sensor, or if it is due to an influence of the pore state (when it goes in the inactivated conformation). The finding that Ci-VSP exhibits a shift in the Q-V curve upon prolonged depolarization, seems to confirm that mode-shift is an intrinsic property of the voltage-sensor (Fig.1.10) [35].

The theory of the modularity implies that it should be possible to exchange modules between voltage-gated channels (3). The literature offers many attempts of replacing the pore or the voltage sensor of voltage-gated K^+ channels, but, although the results provided new interesting implications in understanding the mechanism of coupling between the domains, it was possible to obtain functional chimeras only if the substitution concerned small region of each module. The most famous example of replacement has been reported by Lu et al. [37]: they demonstrated that the pore domain is so conserved that Shaker machinery can gate KcsA pore, maintaining the hallmarks of an

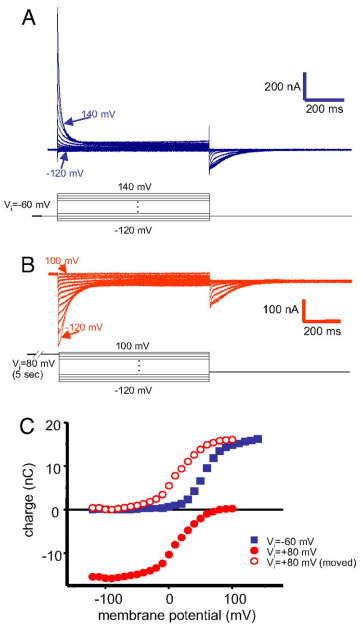

Figure 1.10: **Shift of Q-V in Ci-VSP.** (A) Family of sensing currents of Ci-VSP (blue traces) in response to a series of test pulses (shown in black below) ranging from -120 to 140mV from a holding potential of -60mV. (B) Family of sensing currents for the same oocyte (red traces) for a series of test pulses (shown in black below) ranging from -120 to 100 mV with a 5s conditioning prepulse to +80 mV precedes each pulse. (C) Relationship between total charge movement and test pulse amplitude (QâV curves) from an initial potential, Vi -60 mV (blue squares) and Vi +80 mV (red filled circles). (Modified from [35]).

outward rectifier channel. The limitation is that the channel is functional only if the C-terminus part of S5 and S6 remain unchanged. In fact, when the whole pore of Shaker is replaced by KcsA, the protein can reach the membrane but no detectable current is measured [38]. This evidence revealed the importance of the interactions between the S4-S5 linker region and the COOH terminus of the S6, that are essential in the gating mechanism of the channel [39], but it also underlined that eukaryotic voltage-gated channels coevolved for long time, in a way that the two

modules became indivisible.

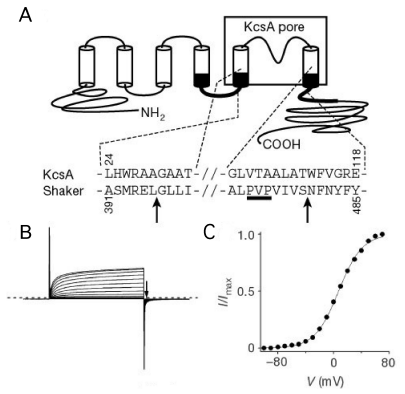

Figure 1.11: **Replacement of the Shaker pore module with that of KcsA.** (A) Topology of the KcsA-Shaker chimaeric channel and partial sequence of the parent channels around the splicing sites. (B) Current recorded from KcsA-Shaker channel, and (C) activation curve obtained fitting the data with Boltzmann equation. (Modified from [39]).

A similar strategy was used to demonstrate that it's possible to exchange part of the voltage sensor of a voltage-gated K^+ channel, Kv2.1 [40], with the homolog sequences from the prokaryotic channel KvAP, the voltage sensing phosphatase Ci-VSP [5] and the proton channel Hv1. Many chimaeric constructs were tested, and some of them are reported in Fig.1.12 but functional voltage-gated channels were obtained only when the replaced sequence corresponds to the so-called paddle-motif [20], including the S3b helix and the S4.

The authors concluded that the results pointed out that the paddle motif is a modular unit common to different voltage sensors, the only part that can be exchange between them, where the voltage sensing mechanism resides.

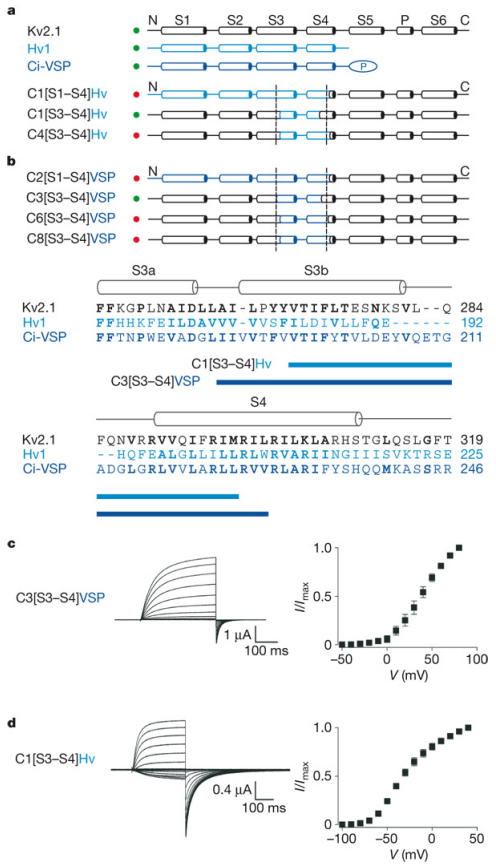

Figure 1.12: **Transfer of the voltage-sensor paddle motif from Hv1 or Ci-VSP into Kv2.1 channels. (a, b)** Overview of chimeras between Hv1 (a, light blue), Ci-VSP (b, dark blue) and Kv2.1 (black). Constructs that result in functional Kv channel activity when expressed in oocytes are indicated with green circles. The aminoacid alignment shows the sequence of Kv2.1, Hv1 and Ci-VSP in S3 to S4, highlighting (blue bars) the stretch of residues transferred to form the two chimeras indicated. **(c)** Current traces and tail-current voltageâactivation relationships for a chimera expressed in oocytes where the paddle of Ci-VSP was transferred into Kv2.1. **(d)** Current traces and tail-current voltageâactivation relationships for a chimera where the paddle of Hv1 was transferred into Kv2.1. (Modified from [40]).

2 AIMS OF THE PROJECT

2.1 Candidate domains for engineering a voltage-gated K^+ channel

The aim of my PhD project was to take a step further in the demonstration of the modularity of voltage-gated channels, approaching the problem from a different point of view, and answering the question: would it be possible to obtain a voltage-gated channel fusing together two modules, a voltage sensing domain and a pore domain, that are evolutionary unrelated? To create this chimera we needed to find two candidates with an essential feature: they were supposed to be a sort of "rudimental" proteins, providing the basic mechanisms of voltage-sensing (for the VSD) and permeation (for the pore), and at the same time operating independently. The ideal VSD was the one found in Ci-VSP described in 1.1.3, in which the voltage sensor is linked to a phosphatase. Although the two parts of the protein are strongly coupled as it was recently demonstrated [41], the voltage sensor is still functional when detached from the enzyme, and in particular, it maintains all its biophysical properties (voltage-dependence, mode-shift,...) as shown in Fig.2.1 [35, 42]. Nevertheless, although this module shows high similarity with voltage sensors found in ion channels, it was not known if it had been able to gate a pore.

A good candidate to play the role of the pore in a voltage-

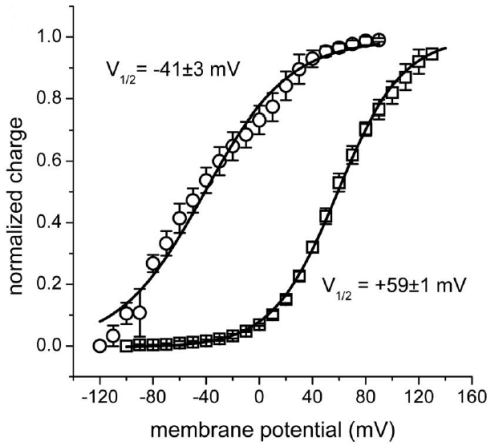

Figure 2.1: **Shift of Q-V in Ci-VSP voltage sensor, after deletion of the phosphatase.** The voltage sensor without the phosphatase (Ci-VSP with C terminus deletion from residue 244) also exhibits the Q-V shift on initializing the protein with prolonged depolarizations to +80 mV. Fit to single Boltzmann distributions showed $V_{1/2}$ of +59mV and -41mV for holding at-60 mV and conditioned to +80 mV, respectively. (Modified from [35]

gated channel could be the viral K^+ channel Kcv. Kcv is a small channel, encoded by the genome of the giant virus PBCV-1. Its 94 aminoacids form two transmembrane domains, jointed by the pore region that includes the canonical sequence of the selectivity filter of K^+ channels [7]. Four indentical monomers are organized in a tetrameric assembly (Fig.2.2[43]). Kcv lacks of regulatory domains, it is not supposed to be regulated by external stimuli. Because of its small size, it is a useful tool for understanding the basic principles of protein assembly, ion conduction and gating mechanisms.

Kcv is a robust and versatile channel, in fact it is heterologously expressed in *Xenopus* oocytes [7], in HEK cells [45] and the purified protein can be reconstituted in a functional channel in artificial lipid bilayer [43] (Fig.2.3). The most important

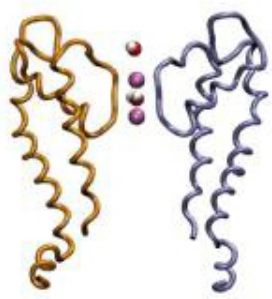

Figure 2.2: **Putative model of Kcv from molecular dynamics.** Two subunits are shown. The selectivity filter is alternatively occupied by two K^+ ions and two water molecules. [44]

biophysical property, for our purpose, is the quasi-linear current/voltage relationship, except for potentials more negative than -100 mV, where a rectification occurs due to a channel flickering at the level of the selectivity filter [44, 46]. This flickering is responsible of the "fast gasting" at extreme potentials, when the channel openings become exceedingly noisy because of unresolved closures. This is due to ion depletion in the selectivity filter when voltage pulls ions more rapidly out of the filter than they can be supplemented from the cytosol [44]. A second mechanism is called "slow gating", and it is related to very low open probability of Kcv, that spends most of the time in the closed state. The short second transmembrane domain seems to exclude the effect of a "bundle-crossing" similar to the one found in KcsA [47], so this feature recapitulates again to the selectivity filter [44].

From the electrophysiology characterization it is clear that the elementary mechanisms of ion conduction and gating can be performed by a single pore-module, as Kcv. The essential structure and function features make Kcv a good module to add new regulation. For this reason we tried to modify the properties of voltage-dependence of this pore-module in one step, by fusion

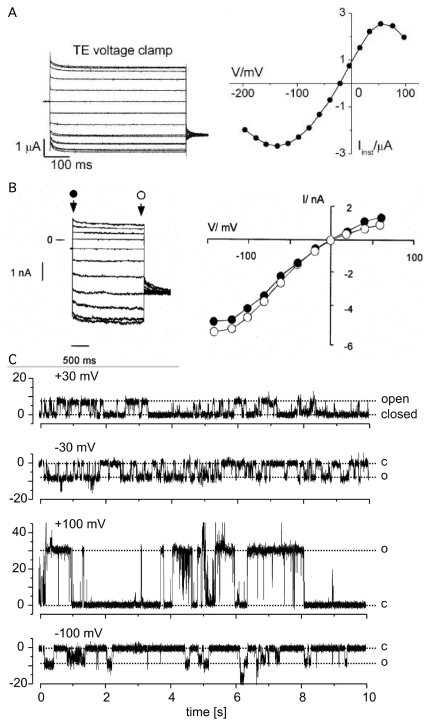

Figure 2.3: **Kcv biophysical properties** (A) Representative current trace and I-V curve of Kcv expressed in *Xenopus* oocytes. Kcv currents are developed instantaneously, the current-voltage relationship shows a quasi-ohmic behaviour, the channel is open over a wide range of positive and negative potentials. (B) Similar behaviour is observed in Kcv expressed in HEK 293 cells. In the graph are plotted the I-V curves of both the instantaneous and the steady-state current [44]. (C) Single-channel recording from lipid bilayer of the reconstituted protein Kcv in proteoliposomes [43].

of a domain usually in charge of this function in voltage-gated channels.

3 RESULTS

3.1 The fusion protein $\mathbf{Kv}_{Synth1}$

To test if the pore-module Kcv can be gated by Ci-VSP machinery, we created a fusion protein in which the voltage sensor of Ci-VSP (aminoacids 1-239) is directly connected to the N-terminus cytosolic slide-helix of Kcv (aminoacids 1-94).
The construct was obtained by overlap-PCR and cloned into BamHI and XhoI restriction sites of pSGEM vector (a modified version of pGEM-HE). T7-in vitro transcription system was used to produce mRNA. The fusion protein and the individual modules were expressed in *Xenopus* oocytes and the activity measured by two-electrode voltage clamp. VSD-injected oocytes do not show relevant currents, similar to water-injected oocytes, because it has been shown that this voltage sensor is not able to conduct any ionic current [5]. Kcv-injected oocytes generate the previously characterized current (Section 6.1): the main evident feature is the nearly-ohmic relationship of the current respect to the voltage. The fusion protein, Kv_{Synth1}, encodes for a functional channel, characterized by large currents compared to the one of VSD-injected oocytes, and very different from Kcv: the kinetic shares similar features with voltage-gated channels [48], because depolarized potentials generates time-dependent outward currents compared to the small remaining instantaneous component. The voltage-current relationship confirms the strong outward rectification of the chimera (Fig.3.1).

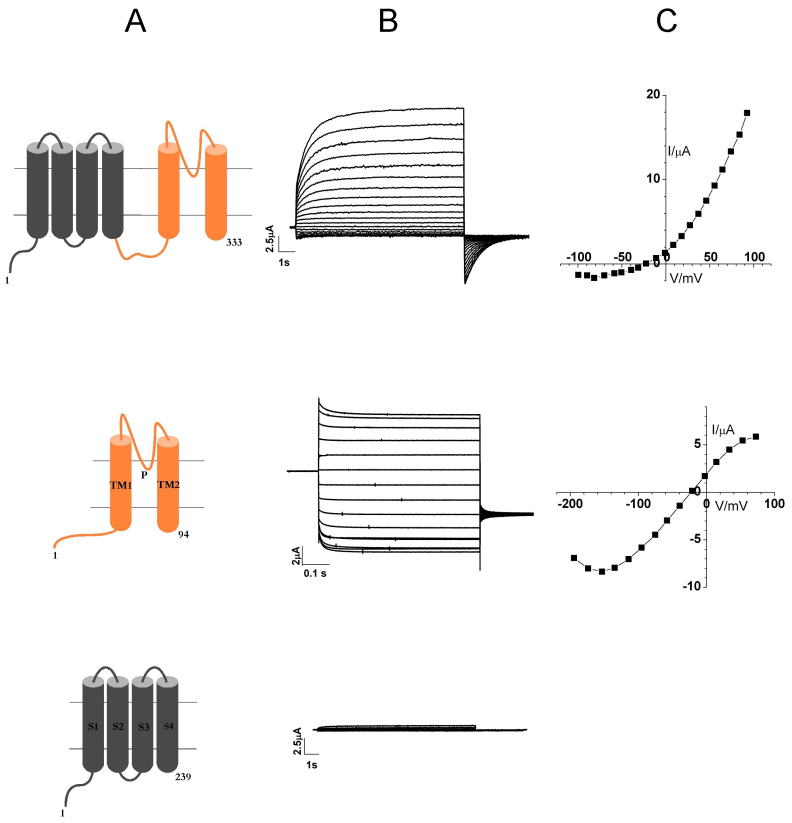

Figure 3.1: **Kv$_{Synth1}$ encodes for a voltage-gated channel.** Panel A: cartoons of the individual components and of the fusion protein KvSynth1. Grey cartoon: the voltage-sensing domain (aa 1-239) of Ci-VSP; S1-S4 indicate the 4 transmembrane domains. Orange cartoon: Kcv, viral K+ channel (aa1-94) ; TM1, TM2 and P indicate respectively the two transmembrane domains and the pore loop of Kcv. Panel B: Currents recorded by TE-voltage clamp in oocytes injected with the three constructs. Dotted line indicates zero current level. Voltage protocol: V$_{holding}$ -20 mV, test voltages +100 to -100 mV (-200 mV for Kcv), tail -80 mV. Test pulse length is 8.5 s for Kv$_{Synth1}$ and VSD-injected and 0.6 s for Kcv-injected oocytes. Panel C: corresponding steady-state I-V relationships of Kv$_{Synth1}$ and Kcv. All experiments were performed in $[K^+]$ 50mM.

3.1.1 $\mathbf{Kv}_{Synth1}$: pore properties

In order to asses if each module is intrinsically capable to play its specific role in the new chimera, we tested selectivity and permeability properties of Kv_{Synth1}. The data show that Kv_{Synth1} is still potassium selective, because it has the same Nernstian behaviour previously reported in Kcv (Fig.3.2); moreover, the replacement of external K^+ with an equivalent concentration of Na^+ shifts the reversal potential of the fully activated current of about -80 ± 6mV, so that the permeability ratio $\mathrm{P}_{Na}/\mathrm{P}_K$ is 0.05±0.01, very similar to the ratio measured in Kcv (0.03±0.01) [7] (Fig.3.3).

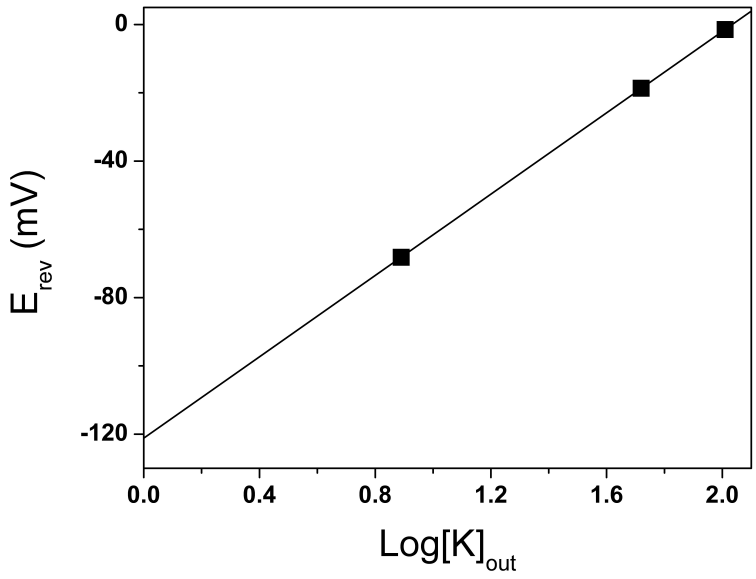

Figure 3.2: **Selectivity of $\mathbf{Kv}_{Synth1}$.** Nernst plot: Kv_{Synth1} current reversal potential (E_{rev}) plotted as a function of external K^+ concentration (Log[K]out) corresponding to 20, 50, 100mM. Black line is the linear regression to mean E_{rev} values (n=3). Slope factor is 58.5mV, very similar to the K^+ theoretical equilibrium potential [9].

It's important to notice that the typical behaviour observed in the current-voltage relationship of Kcv is maintained in Kv_{Synth1} during the full activation protocol (Fig.3.3). This protocol allows to record the single-channel like behaviour because (vedi libro).

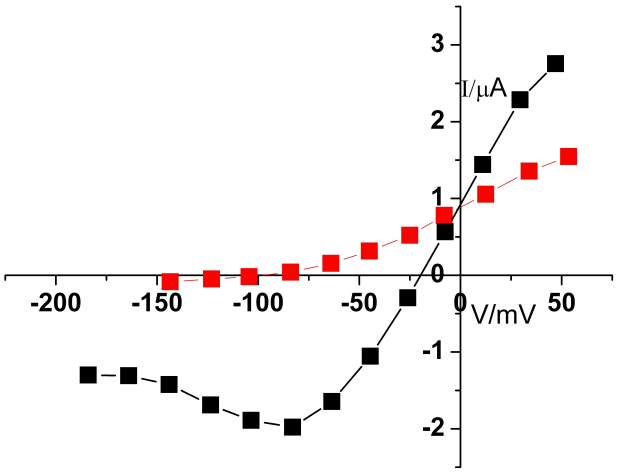

Figure 3.3: **Kv_{Synth1} selects K^+ over Na^+.** Current reversal potential recorded from the same oocyte was -20 mV in 50 mM $[K^+]$out (■) and -98 mV in 50 mM $[Na^+]$out (■). Voltage protocol: pre-pulse voltage step at +60 mV followed by testing voltages from +60 to -180 mV. Arrowhead marks the point of data collection.

The other Kcv properties that are preserved in Kv_{Synth1} are the blocking effect of Ba^{2+} on the inward component of the current, and the stability of the tetrameric assembly of the protein in SDS-PAGE. Infact, it has been previously reported that the potassium current of Kcv is blocked in a voltage-dependent manner by the divalent cation Ba^{2+} with a K_D of 1μM. In particular Ba^{2+} ions at the concentration of 1mM can completely remove the inward current measured at steady-state: the same effect has been recorded in oocytes expressing Kv_{Synth1}, when the external potassium solution is supplemented with 1mM BaCl_2.

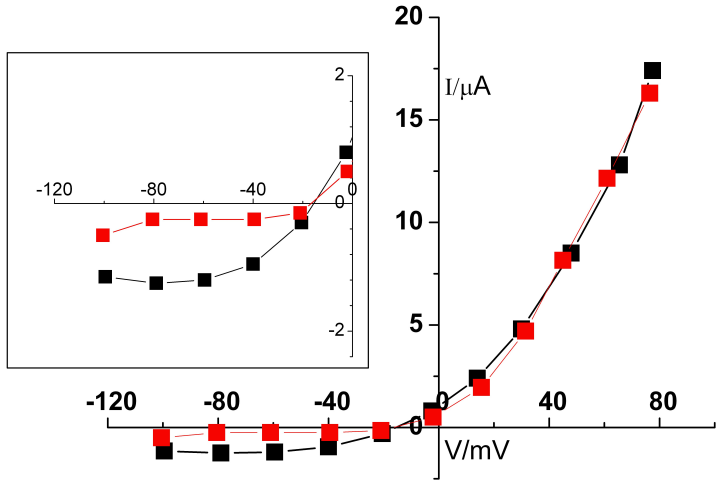

Figure 3.4: **Effect of Barium on Kv$_{Synth1}$ current.** Steady-state currents recorded in: (■) control solution (50 mM $[K^+]$out) and (■) +1mM $BaCl_2$. The addition of barium blocks the inward current and affects the outward current, as previously reported for native Kcv channel [7].

We also tested the pore mutation F305A that, as expected from our previous results with the Kcv mutant F66A ([7]), completely abolished the current in Kv$_{Synth1}$ (See Fig.3.7). This result confirms that the current recorded in Kv$_{Synth1}$-injected oocytes can not be considered an endogenous current. The purified protein Kcv is recognized in its tetrameric form in SDS-PAGE by the monoclonal antibody 8D6. Previous experiments of size exclusion chromatography demonstrated that a single molecule of antibody form a complex with a tetramer of purified Kcv (expressed and purified in Pichia pastoris [43]. This monoclonal antibody has been used to recognize the tetrameric form of the chimera Kv$_{Synth1}$, detecting it by western blot on crude lysate of oocytes expressing the channel.
The antibody is able to recognize both Kcv and Kv$_{Synth1}$, and this result highlights that the pore structure is reasonably still conserved and the chimera has a quaternary assembly that al-

lows the formation of a tetramer. Infact it's worth noting that Ci-VSP performs its function in the membrane as a monomer,as demonstrated by TIRF (total internal reflection fluorescent) microscopy experiments [49], but in our case, Kcv pore drives the arrangement of the protein structure.

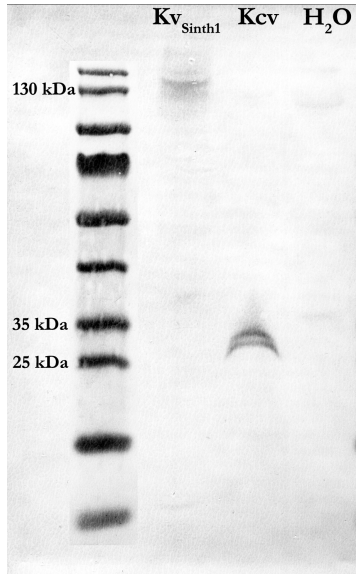

Figure 3.5: Western blot analysis performed total protein extract from oocytes with a monoclonal antibody (8D6) that recognizes the tetramer of Kcv, but not the monomer. The expected MW of Kcv and Kv_{Synth1} tetramers are 42,5 and 149 kDa, respectively. H_2O injected oocytes lysate is loaded for control.

3.1.2 Kv_{Synth1}: voltage sensor control

The contribution of the voltage sensor of Ci-VSP to the voltage dependence of Kv_{Synth1} is translated in a modified open probability of the channel respect to Kcv: the voltage sensor closes the pore at negative voltages and slowly opens it at depolarizing potentials. Tail currents recorded at -80mV with the same protocol in Fig.3.1 were plotted against applied voltages and fitted with a Boltzmann distribution

$$y = \frac{1}{1 + e^{\frac{zF(V - V_{\frac{1}{2}})}{RT}}}$$

where z, F, R, T have their usual thermodynamic meaning, and the instantaneous current was subtracted. The graph represented in Fig.3.6 shows that Kv_{Synth1} has a half-activation potential of +56mV and a z value of $\sim$1; the very positive activation potential and the shallow voltage dependence strongly resemble the slow and shifted behaviour of 'sensing' currents measured in Ci-VSP respect to voltage-gated K^+ channel (Fig.1.9). The voltage sensor closes the channel at negative potentials and opens it with a slow kinetics at voltages more positive than zero mV ($t_{1/2}$=450 $\pm$ 74 ms at +60 mV (n=4 oocytes)).

To demonstrate that the voltage sensor exerts a tight control on the pore, and that the potassium current developed by the channel is the direct effect of the state in which the voltage sensor is, we reproduce specific mutations in the voltage sensor whose phenotype has been previously characterized in Ci-VSP. The first mutation is the R229Q/R232Q in the fourth subunit of the VS: these aminoacidic positions consist of two positive arginines responsible of the traslocation of the charges along the α-helix, and their neutralization in Ci-VSP leads to a functional phosphatase,

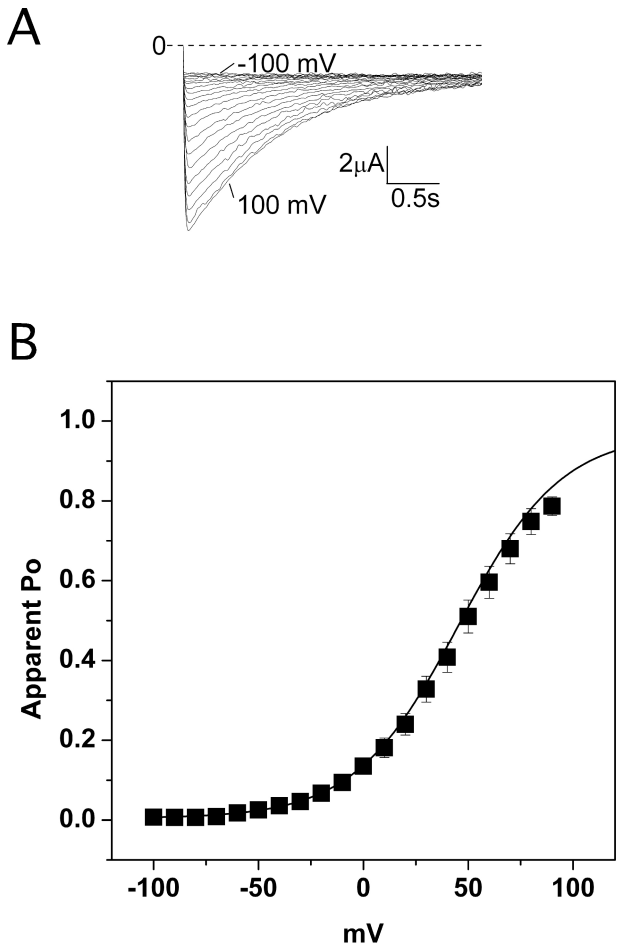

Figure 3.6: **Voltage dependency of $\mathbf{Kv}_{Synth1}$.** (B) Activation curve of Kv_{Synth1} constructed from tail currents (A) after subtracting the instantaneous current offset. Voltage protocol as in Fig.3.1. Data sets (n=6) were jointly fitted to a two-state Boltzmann equation. $V_{1/2}$=56 mV, z=0.92.

localized in the oocyte membrane, but insensitive to potential. Infact, when the mutations are placed in Kv_{Synth1}, we obtained a channel almost closed, with a quasi-Ohmic I/V relationship. The voltage sensor seems to be blocked in a conformation that is not more useful to open and regulate the pore. In a simi-

lar way Shaker conductance is affected when these arginines are replaced by neutral or negative charged aminoacids [50], suggesting that well-established mechanisms can be easily reproduced in this *bona fide* channel.

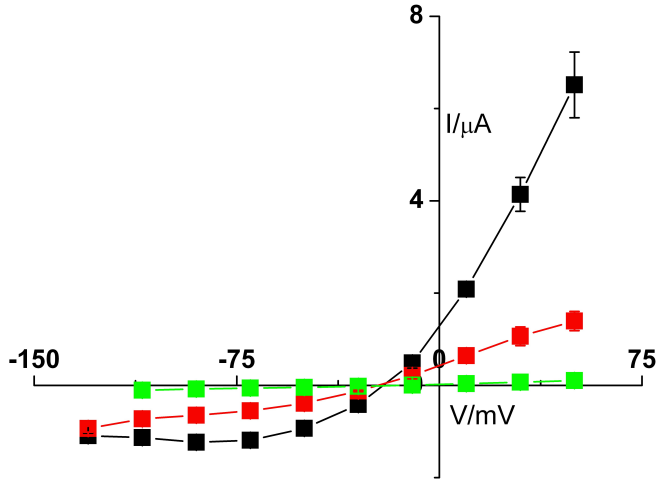

Figure 3.7: Steady state current/voltage relationships of the single mutant F305A (■), the double mutant R229Q/R232Q (■) and the wt Kv_{Synth1} (■). Points represent mean±(s.e.m) (n=6).Currents were recorded from a $V_{holding}$ of -20 mV. Test pulse is 600ms for Kv_{Synth1} wild-type and R229Q/R232Q. The low level of expression of the R229Q/R232Q mutant does not allow to apply long test pulses, due to endogenous current contamination that develops upon long depolarization.

Voltage sensor control is so effective that it is possible to affect the voltage dependence of Kv_{Synth1} mutating the arginine in position 217 (R217Q). This aminoacid does not contribute to gating charges [51], but probably interacts with a part of the voltage sensor that undergoes to a conformational change upon potential stimulus, and the effect of the mutation is a left shift of the Q-V curve to a value of $\sim$ 12mV [35]. Kv_{Synth1} R217Q generates a channel with a G-V curve that matches with "sensing" charges curve ($V_{1/2}$=17.9$\pm$0.3 mV). In figure 3.8 the G-V curves of both the wild-type and the mutant are plotted for comparison.

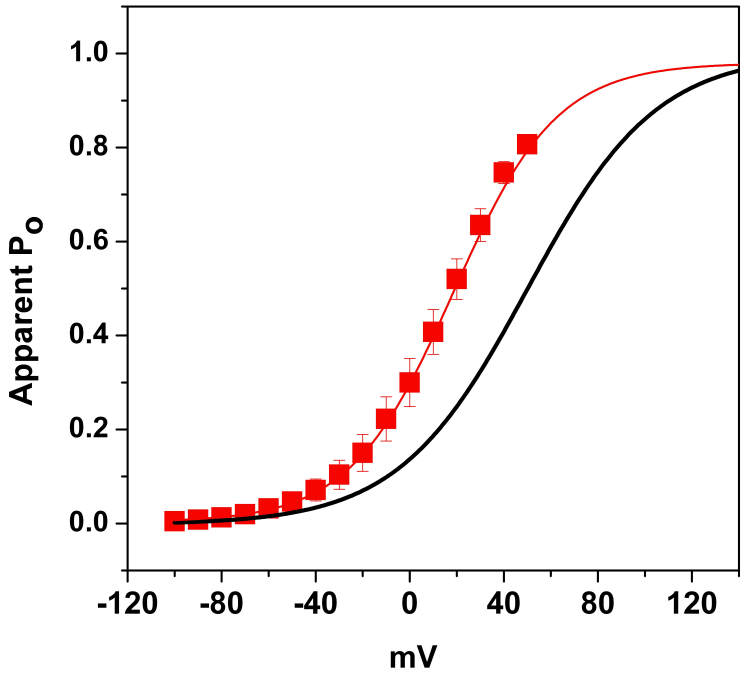

Figure 3.8: **Activation curve of the R217Q mutant.** The activation curve of the mutant (■) has been constructed as in Fig.3.6 (n=4). The activation curve of the wild-type is re-plotted for comparison (black line). $V_{1/2}$=18 mV, z=1.1.

As shown by the current traces and the I-V curve in Fig.3.9 (obtained by averaging n=3 oocytes with comparable levels of current for Kv_{Synth1} and Kv_{Synth1} R217Q) the mutated channel opens early respect to the wild-type, so that it has a more relevant inward current.

We used this mutant also to turn out the presence and, eventually, the influence of the relaxed state of the Ci-VSP voltage sensor on the Kcv pore. S4 enters in a relaxed state trough a conformational change, in which the α-helix turns into a 3_{10}helix, reaching a lower and more stable energy state, when the channel is stimulated for long time with depolarizing potentials. The effect of the relaxation is that the center point of the Q-V curve depends on the value and the duration of the holding potential. In voltage-gated channels this hysteresis has been for long time correlated to the development of slow inactivation, explained as a mechanical load that is imposed upon the voltage sensor by the pore domain [36]. But in the last years, it has been demonstrated that the voltage sensor of Ci-VSP also exhibit the typical "mode-shift" behaviour, with a left shift of the Q-V curve upon a prolonged depolarization at +80mV [35]. What could be the effect of this relaxation of the VS on Kcv pore? And, if an effect is observed, is it similar to the one found in voltage-gated channels? To investigate this, we recorded the current of Kv_{Synth1} R217Q applying a 5 seconds preconditioning pulse at -100mV or at +40mV, that represent respectively the potentials in which the voltage sensor is in the resting and in the active state. We took advantage of this mutant because the left shift of the G-V curve allowed us to pre-conditiong at a value of +40mV. More positive prolonged pulses can stimulate endogenous current in oocytes, affecting the results. What we observed with this protocol is shown in Fig.3.10: when the voltage sensor is initialized with a depolarizing pulse, the $V_{1/2}$ of the G-V curve settles to a more negative value, and this can be interpreted as an early opening of the channel, once the voltage sensor reached the lower

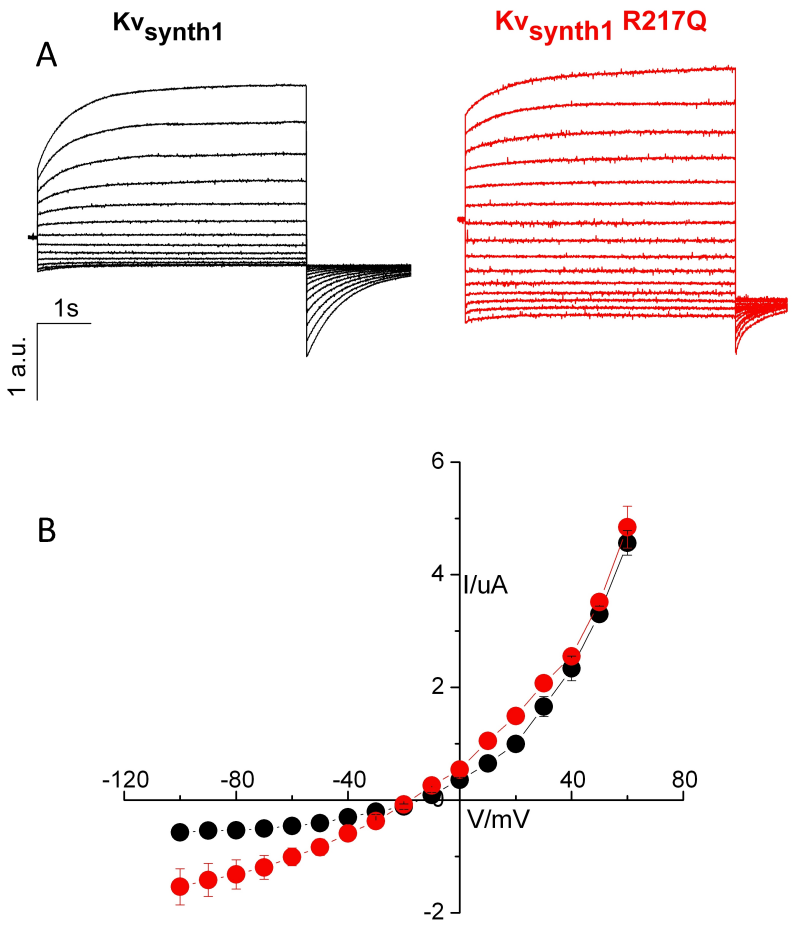

Figure 3.9: **Kv_{Synth1} R217Q.** Representative current traces and I-V curve of Kv_{Synth1} R217Q compared to the wild-type construct. The I-V curves show that the mutant (●) has a more prominent inward component of the current respect to the wild-type (●). The I-V curves are obtained from average of oocytes with similar level of current expression (n$\geq$ 3).

energy state. The two G-V curves plotted in Fig.3.10 go in the same direction of the Q-V curves of 'sensing' charges published in [35], but the value of the shift can be considered just qualitatively because the curves don't represent the full activation

of the channel: test pulses are shorter (1.2 seconds instead 10 seconds), to maintain the effect of the preconditioning voltages.

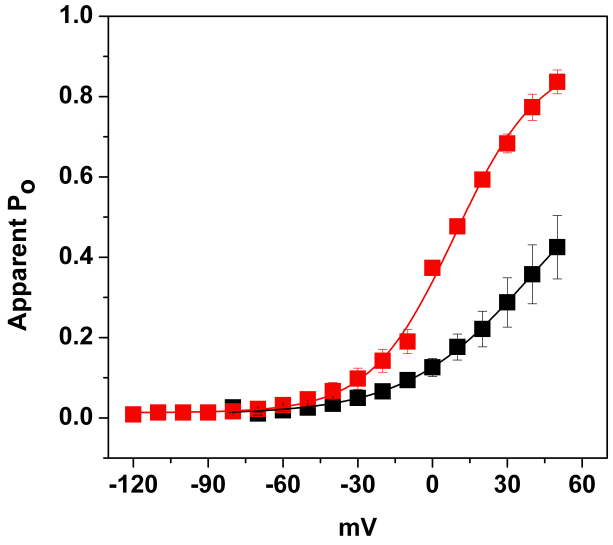

Figure 3.10: **The activation of the R217Q mutant depends on the pre-conditioning voltage.** The same R217Q expressing oocyte was subjected to the following protocol: pre-conditioning (5 s) at either -100 mV or + 40 mV; test pulses (1.2 s) from -120 mV to +30 mV. Tail currents (at -80 mV) are plotted for pre-conditioning at -100 mV (■) or at + 40 mV (■). The test pulses were kept short to maintain the effect of the preconditioning voltages; hence data do not reflect full activation of the channel.

All these results outline that the voltage sensor of Ci-VSP can control the pore opening, and, in particular, the properties of this independent module, i.e. the conformational changes that it undergoes, directly affect the development of the current through the pore. The effect of the mutations on Kv_{Synth1} described above, demonstrates that the channel behaves in a specular way respect how "sensing" charges feel the electrical field across the membrane. This suggests a simple but surprisingly

coupling between the two modules.

3.2 The relevance of the linker in Kv$_{Synth}$ constructs.

In Kv$_{Synth1}$ the slide-helix of Kcv is the only covalent linker between the pore and the voltage sensor, so it is presumable to hypothesize that this is the crucial point in which the coupling is established. Does Kv$_{Synth1}$ require a specific linker composition, or structure, or length? To assess if the linker plays a key role in the synthetic channel, we produced constructs in which the voltage sensor of Ci-VSP (aa1-239) is connected to Kcv combining in a different way the N-terminus of Kcv (aa 1-12) and the linker of Ci-VSP (aa 239-255) (see Fig.3.11).

Except for the construct Kv$_{Synth1.5}$, with a long linker of 28 aminoacids, all the other constructs express functional channels with large potassium currents. As it is shown by the more representative traces (Fig.3.12) every channel has different kinetic and fraction of the inward current respect to the total amount. Anyway, a dramatic change can be observed in Kv$_{Synth0.2}$, a chimera that strongly resembles Kcv, showing the rectification of the current at extreme negative potentials.

The same behaviour can be observed plotting the I-V curves of the chimeras with a linker of 20, 12, 6 and 4 aminoacids (Fig.3.13 A): the four channels show different level of inward current, that can be interpreted as a various ability of the linker to transduce the conformational change of the voltage sensor. To quantify the degree of rectification of Kv$_{Synth}$ constructs we measured the ratio between the current recorded at +60mV and at -100mV (I_{+60}/I_{-100}), exactly at the same distance from the reversal potential in an external solution of KCl 50mM (for Kcv

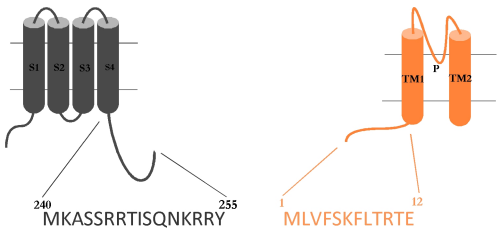

	aa n.	Linker sequence
$Kv_{Sinth0.2}$	4	TRTE
$Kv_{Sinth0.1}$	6	FLTRTE
Kv_{Sinth0}	8	SKFLTRTE
Kv_{Sinth1}	12	MLVFSKFLTRTE
$Kv_{Sinth1.1}$	16	MKASSRRTISQNKRRY
$Kv_{Sinth1.2}$	18	MKASSRRTISQNKRRYTE
$Kv_{Sinth1.3}$	20	MKASSRRTMLVFSKFLTRTE
$Kv_{Sinth1.4}$	20	MKASSRRTISQNKRRYTRTE
$Kv_{Sinth1.5}$	28	MKASSRRTISQNKRRYMLVFSKFLTRTE

Figure 3.11: **Kv_{Synth} constructs.** Cartoon representation of the voltage sensing domain of Ci-VSP and the pore Kcv. The sequences refer to the linkers of the two modules, that were combined to create all the Kv_{Synth} constructs. The table shows the linker composition: the color code is the same of the cartoons.

wild-type I_{+60}/I_{-100}=1). The average ratios calculated for ≥ 3 oocytes of each construct were plotted against the length of the linker and fitted with a logistic function, in which the lower asymptote is set to a value of 1, that corresponds to a channel with no rectification, as Kcv. The curve shows that the control of the voltage sensor is achieved when the linker is kept shorter than 20 aminoacids, and the saturating effect is reached between 12 and 6 aminoacids. In this range the properties of Kv_{Synth} don't change too much, and a linker of 6 aminoacids represents the extreme limit beyond which it is possible to observe an outward rectifier behaviour. $Kv_{Synth0.2}$, in fact, regains the typical properties of Kcv: the pore is perfectly functional, but the linker is

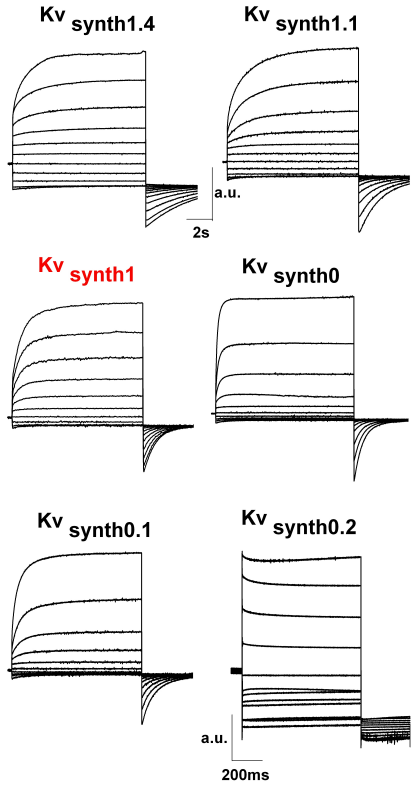

Figure 3.12: **Kv$_{Synth}$ constructs.** Representative current traces of Kv$_{Synth}$ constructs. The figure shows the current recorded in the constructs with different linker length. The inward current component decreases togheter with the linker lenght. Kv$_{Synth0.2}$, with a linker of 4 aminoacids, regains the properties of Kcv. The current traces are normalized to the value recorded at +60mV.

so short that probably the voltage sensor is screwed up and it can not exert any kind of regulation.
The idea that the length of the linker is the predominant feature in determining the quality of the outward rectification is supported by the fact that Kv$_{Synth1.4}$ and Kv$_{Synth1.3}$ have both a linker of equal length but different aminocidic composition: the degree of rectification is the same.

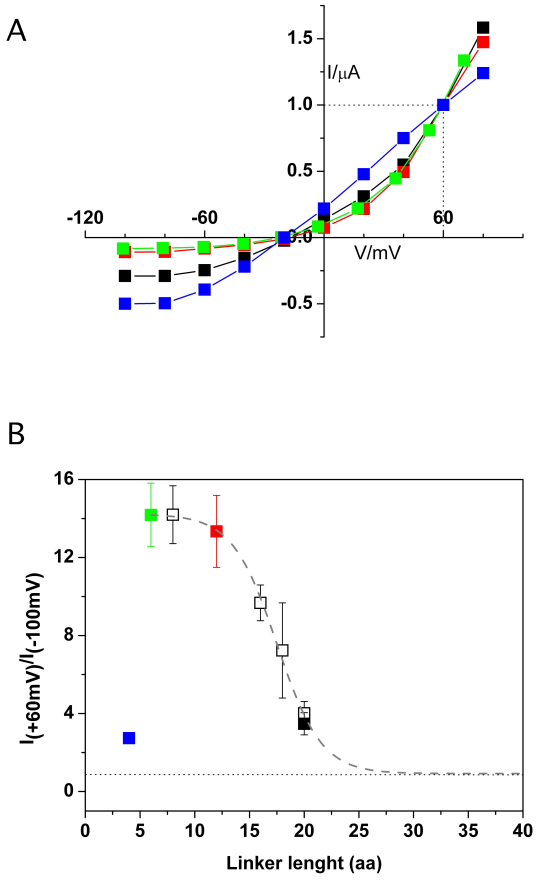

Figure 3.13: **Relationship between the linker length and the degree of rectification in Kv$_{Synth}$ constructs.** Panel A: I-V curves from Kv$_{Synth}$ 1.4 (■), 1 (■), 0.1 (■) and 0.2 (■) with a linker of respectively 20, 12, 6 and 4 aminoacids. The current is normalized at +60mV. Panel B: The degree of current rectification (I_{+60mV}/I_{-100mV}) is plotted as a function of linker length for all functional constructs. The degree of rectification of the constructs in Panel A are represented with the same color code. Data are mean±(s.e.m.). Experimental data (with the exclusion of the value corresponding to the construct with a 4 aa linker that loses the rectification) have been interpolated with a sigmoidal function (grey dashed line) in which the lower asymptote was set to 1, corresponding to the value measured in Kcv that lacks rectification (dotted line).

3.3 Expression and purification of the recombinant Kv_{Synth1}

In order to understand better the biophysical properties of the synthetic channel, structural studies and single channel measurements on the purified protein are required. The first step to approach a structural investigation is to express the protein in an heterologous system, such as *E. coli*. The coding region of the whole Kv_{Synth1} channel (residues 1-333) was cloned into three plasmids (pQE-32, pQE-70 and pGEX-6P-1) and each of them was transformed into three different *E. coli* expression strains (BL21(DE3), XL1-Blue and XL10-Gold).
A single colony for each strain was used for the initial expression test.
The expression test was carried out at 37°C using 1mM IPTG (isopropyl-β-D-thiogalactopyranoside) as induction molecule. The protocol used for the detection of the expressed protein is similar to [52]. The table 3.3 summarizes the results got from this first step.

Construct	Affinity tag	Vector	Promoter	*E. coli* strain	Expression level
Kv_{Synth1}	N-term His tag	pQE-70	T5	XL1-Blue	-
	C-term His tag	pQE-70	T5	XL10-Gold	-
	C-term His tag	pQE-70	T5	XL1-Blue	-
	C-term His tag	pQE-70	T5	SG009	-
	C-term His tag	pQE-70	T5	M15	-
	N-term His tag	pQE-32	T5	XL1-Blue	[+]
	N-term His tag	pQE-32	T5	XL10-Gold	[++]
	N-term His tag	pQE-32	T5	SG009	[+]
	N-term His tag	pQE-32	T5	M15	+
	N-term His tag	pGEX-6P-1	LAC	BL21*	-
	N-term His tag	pGEX-6P-1	LAC	XL1-Blue	-

Table 3.1: ***E. coli* Strains and Constructs for the Initial Expression Test**
Positive (+) and negative (-) signs indicate the relative expression level from Western blot: -, no visible band of expression; +, visible band. Multiple signs indicate relatively higher expression levels. The condition in brackets was chosen for further expression optimization.

As a result of the first expression test, the only construct that gave expression was the pQE-32::Kv_{Synth1} in all the three

tested *E. coli* strains (Table 3.3). In order to have a yield improvement, for the subsequent purification step, expression optimizations were set up at different temperatures and different concentration of IPTG . Initially the temperature was decreased to 30°C and the IPTG was used at the concentration of both 1mM and $500\mu M$. The expression was then monitored each hour for three hours and the expression level was detected by wester blot analysis (as described in [52]).
The best expression level at 30°C was achieved by the *E. coli* strain **XL10-Gold**. Further improvements were carried out only on this strain.
Since the protein detected by western blot seems to be partially degraded during the course of the three hours, two lower temperatures (28°C and 25°C) were used in the next optimization step.
Both 28°C and 25°C had no significant improvement in protein expression. For large-scale expression, the following protocol was adopted:

- *Temperature:* 30°C
- OD_{600}*:* 0.9
- *IPTG concentration:* 1mM
- *Induction time:* 3 hours

A preparative expression (1 L culture) of Kv_{Synth1} was conducted as described above. The cells were then harvested and resuspendend in the breaking buffer (150mM NaCl, 20mM Tris-Cl pH=8.0, 1mM PMSF, 0.1mg/ml DNAse, 5mM $MgCl_2$, 1mM EDTA, 0.125mg/ml lysozime and the inhibitor cocktail). The resuspension was incubated for 30min at $4°C$ and then sonicated $12 \times 20sec$. After an additional incubation on ice for 10min, the sample was centrifuged at 100000xg for 30min at $4°C$.
The supernatant was discarded and the pellet was resuspended in

10ml of resuspension buffer (100mM NaCl, 50mM KCl, 20mM Tris-Cl pH=8.0 and 5mM $MgCl_2$) as crude membranes. The membrane suspension was, then, divided into twelve eppendorf tubes and on each of them was added a different detergent (Table 3.2) at 10 times their critical micelle concentration (except for DM and OM that were added at 5.6x CMC and 2x CMC, respectively). After three hours of solubilization at room temperature, the samples were centrifuged at 100000xg for 1 hour at $4°C$. The supernatant and the pellet (completely dissolved in laemmli buffer in the same initial volume) were loaded onto SDS-PAGE and subjected to Western-blot analysis to test the solubilization efficiency.

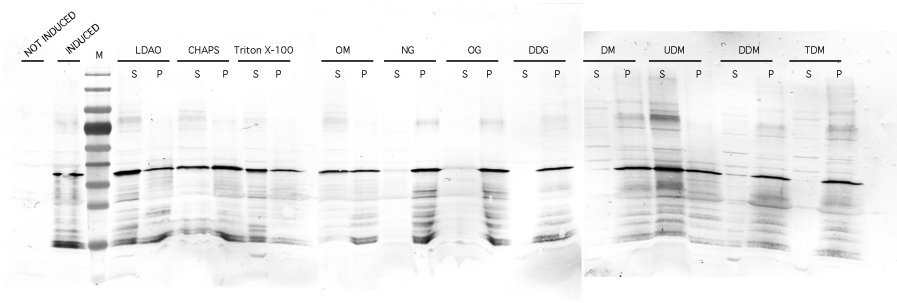

Figure 3.14: Western-blot analysis of the screened detergents (see Table 3.2). M: molecular weight marker (Fermentas); S: soluble fraction after spinning the solubilized samples at 100000xg for 1h; P: pellet fraction resuspended in Laemmli buffer. The band corresponding to the monomeric form of Kv_{Synth1} has a 40kDa molecular weight.

Based on the results of the western-blot analysis (Fig. 3.3), 5 detergents of the 11 screened were able to solubilize the protein, although a substantial portion of it remains in their pellet fraction. Of this five detergents, three were selected (LDAO, UDM and OM) for the next solubilization improvement, combining a higher detergent concentration (20xCMC) with a lower solubilization temperature ($4°C$). LDAO and UDM were chosen

Detergent	CMC (H_2O)	Used CMC
DDM n-Docecyl-β-D-Maltopyranoside	0.17mM	10x
DM n-Decyl-β-D-Maltopyranoside	1.8mM	5.6x
TDM n-Tridecyl-β-D-Maltopyranoside	0.033mM	10x
UDM n-Undecyl-β-D-Maltopyranoside	0.59mM	10x
OM n-Octyl-β-D-Maltopyranoside	19.5mM	2x
LDAO n-Docecyl-N,N-Dimethylamine-N-Oxide	1-2mM	10x
OG n-Octyl-β-D-Glucopyranoside	18-20mM	10x
DDG n-Dodecyl-β-D-Glucopyranoside	0.19mM	10x
NG n-Nonyl-β-D-Glucopyranoside	6.5mM	10x
DG n-Decyl-β-D-Glucopyranoside	2.2mM	10x
Triton X-100 Octylphenol Ethylene Oxide	0.23mM	10x
CHAPS*	8-10mM	10x

Table 3.2: **Detergents used in the solubilization screen.**
* CHAPS is an abbreviation for *3-[(3-cholamidopropyl)dimethylammonio]-1-propanesulfonate*

for their higher ratio "solubilized: not-solubilized", OM was, instead, selected because in the original solubilization screening it was used at a concentration of 2xCMC and the improvement was then carried out at 10xCMC. The new solubilization screening was prepared as discussed above and the samples were subjected to Western-blot analysis. The results are reported in Fig. 3.15. As the western-blot shows, the best results are achieved at $4°C$ with both UDM (20xCMC) and LDAO (10xCMC). Moreover LDAO appears to be able to solubilize more than 90% of the

protein, so it will be used in the subsequent purification steps.

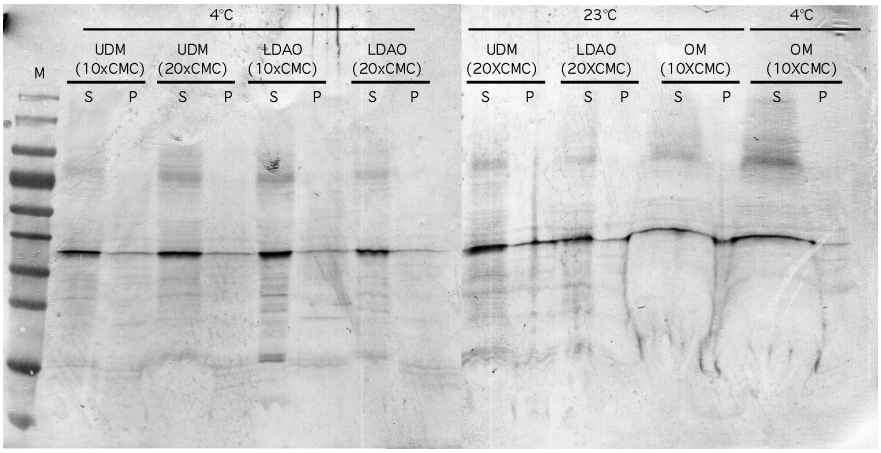

Figure 3.15: **Western-blot analysis of the screened detergents** (see Table 3.2). M: molecular weight marker (Fermentas); S: soluble fraction after spinning the solubilized samples at 100000xg for 1h; P: pellet fraction resuspended in Laemmli buffer.

For purification purpose, 4L of colture medium were inducted and prepared as described above. The cells were harvested and resuspended in the "breaking buffer" (20mM Tris-Cl, pH=8.0; 150mM NaCl; 5mM $MgCl_2$ and 1mM EDTA in the presence of 1mM PMSF, 0.1mg/ml DNase, 1x Inhibitor cocktail, $250\mu g/ml$ lysozyme). The mixture was then incubated on ice for 30min and sonicated (8x20sec). The membrane fractions were collected by a centrifugation at 100000xg fot 35min and the supernatant was discarded. The crude membranes were completely resuspended into the "solubilizing buffer" (20mM Tris-Cl, pH=8.0; 100mM NaCl; 50mM KCl; 5mM $MgCl_2$ in the presence of 1mM PMSF, 5mM imidazole and 750μM β-mercaptoethanol) and the detergent LDAO was added at the final concentration of 10mM. The mixture was incubated at $4°C$ for 3 hours and the unsolubilized fractions were spun down at 100000xg for 1 hour at $4°C$. The cleared supernatant was loaded onto 1.5ml of cobalt metal-affinity resin (Sigma). The resin was washed with 20 column

volumes of "washing buffer" (20mM Tris-Cl, pH=8.0; 100mM NaCl; 50mM KCl; 5mM $MgCl_2$; 5mM imidazole and 750μM β-mercaptoethanol in the presence of 10mM LDAO) and then eluted with 4 column volumes of "elution buffer" (20mM Tris-Cl, pH=8.0; 100mM NaCl; 50mM KCl; 5mM $MgCl_2$; 300mM imidazole and 5mM LDAO).
All the purification steps were analyzed by western-blot (Fig. 3.16). As the figure shows, the elution fractions (E1-3) appear to be degradated with a predominant band at 10kDa (asterisks), although a significant portion of the protein is in the monomeric and dimeric form. A bioinformatic prediction (via the XtalPred server [53]) revealed, in fact, that the N-terminal tail of Kv_{Synth1} (aa 1-100) is a random-coil domain, probably prone to itself degradation. The next optimization step will include the design of a new construct without the unfolded N-terminal domain of the protein, followed by two steps of purification (affinity gel and size-exclusion chromatography) to get a 90% pure protein for biophysical and structural studies.

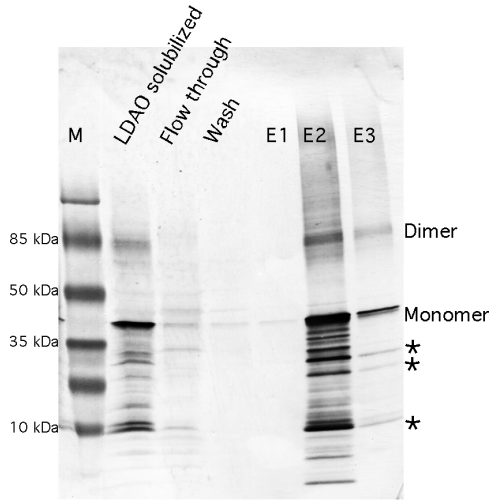

Figure 3.16: **Western-blot analysis of Kv_{Synth1} purification.** M: molecular weight marker (Fermentas); E1-3 elution fractions. The protein elutes in two fractions for a total volume of 5ml. The predominant forms of the protein are the monomer and the dimer, although a significant fraction is a low-molecular weight degradation (asterisks).

4 DISCUSSION (and future prospects)

Voltage-gated channels control different mechanisms in excitable cells, so they have been for a long time the object of a intense research [9]. The first studies started from the Hodgkin-Huxley model describing the action potential [54], to the identification of the proteins involved in this process as discrete identities. Then, with X-ray crystal structures and structure-function studies it was possible to provide the molecular description of the conformational changes in voltage-gated channels, that allow the coupling between sensing membrane potential and developing a conductance. Anyway, many aspects of their functioning is still unknown, because ion channels are sophisticated proteins, in which different control mechanisms are operating simultaneously. In Shaker there are three different type of inactivation of the conductance: N-, C- and P-type, and each of this can overlap with the voltage sensor control. Moreover some types of regulation can involve the recruitment of different subunits, affecting the behaviour of the channel. For these reasons, it could be difficult to isolate a single mechanism without the interference of other factors. An example is that the electrophysiology characterization of the prototype of voltage-gated K^+ channel, Shaker, had to be done removing the N-terminus of the protein, that causes inactivation of the current. Another case is the ambiguity in the assignment of the "mode-shift" to a voltage sensor properties or to an influence of the pore, as described in 1.1.3, due to the presence of C-type inactivation. Therefore, in order to understand the basic principles of voltage-dependence, it could

be useful to approach the problem recreating the mechanism *ab initio*, following what probably happened during the evolution, when the precursor of voltage-gated channel formed by fusion of two independent modules. The fusion of genes is one of the ways in which two proteins are brought together in a cell, to form a complex system of co-localized domains [1]. The results obtained by fusing the voltage sensor of Ci-VSP and the K^+ channel Kcv, strongly indicates that this is sufficient to transform a voltage-independent K^+ channel into a canonical Kv type outward rectifier. These finding has several corollaries. First, it is a common opinion that the voltage sensor of Ci-VSP shares high similarity with the one present in channels, but now we have demonstrated that it can not only control phosphatase activity but also gate a pore: the voltage sensor, although present in different proteins, has a unique way to work, so the basic function of voltage sensing is an intrinsic property of the domain, and the effect of its movement depends only on the module that it is fused to.
Second, a covalent link between the two modules, without any co-evolution of the interacting surfaces, is sufficient to provide a mechanical interaction, and, not an obvious consequence, the electrical coupling among them. In fact it has been shown that in Shaker channel, the most important interactions for the VSD-pore coupling occur between the S4-S5 linker and the -COOH terminus of the S6 segment [37]. However, in Kv_{Synth1} the coupling between the two modules is established without any pre-existent interaction. Third, the interaction between the two elements in Kv_{Synth1} is provided by a linker, that establishes the rectification of the chimera. The quality of the rectification, i.e. how the VSD triggers the attached channel pore domain to open only at depolarizing potentials, mostly depends on its length, in particular Kv_{Synth} constructs showed voltage-dependence with a linker in a range of 20-6 aminoacids, with optimal condition at 12-6 aminoacids linkers. We don't have any structural information on these linkers, to highlight if specific secondary structures

are preferred, although in two cases the same length gave the same rectification degree. The key role of the linker has been recently confirmed by μs MD simulation on the Kv1.2/Kv2.1 chimera [23], in which, during activation, outward S4 motion tightens the VSD-pore linker, perturbing linker-S6-helix packing. Fluctuations allow ions to enter the pore, and this state is stabilized by the linker-S6 [29].
Of course, without a crystal structure, it's difficult to know if interactions between the linker and the S6 are established in Kv_{Synth1} as in voltage-gated channels, but from this MD results the authors concluded that the length of the linker in voltage-gated channels is not of secondary importance: "The S4-S5 linker is tense in the activated state but relaxed in the resting state, perhaps explaining conservation of linker length: a shorter linker would inhibit channel closing, because S4 could not translate inward far enough, and a longer linker would inhibit opening, because even full S4 outward translation could not lead to an effective pull on the pore through the linker." [29]. This is consistent with what we found in Kv_{Synth}: short (4aa) and long (28aa) linkers cannot control properly the opening and the closure of the pore.
The last conclusion is that the versatility of the voltage sensor of the Ci-VSP, that can be adapted to different proteins, a channel or an enzyme, is in agreement with the theory that evolution has probably exploited the same gating pathway to regulate proteins involved in different cellular functions [55]. In allosteric proteins, if we define allostery as a "structural change, in the tertiary structure, the quaternary structure or both, induced by a small molecule or another protein" [1], the presence of a linker is required to co-localize two proteins that can establish an interaction. In our case the linker have a specific functional role: specific interactions could even improve the quality of the collaboration between the voltage sensor and the pore, and this is exactly what, in coevolved modules that form voltage-gated channels, the evolution did: in fact, "colocalization gives evolu-

tionary processes the opportunity to convert nonspecific binding interactions into interactions that have functional consequences" [1].
Moreover, Kv_{Synth1} can be considered a useful tool to investigate many aspects of the voltage-dependence mechanism. First of all, it would be interesting to measure "gating" currents in Kv_{Synth1} with cut-open voltage clamp technique, and to compare them with the current recorded from Ci-VSP, to see a possible influence of the presence of the pore. Moreover, gating currents, together with noise analysis could give information about the number of electronic charges required to open the pore. The shallow voltage-dependence of Ci-VSP [5] suggests that few charges are moved in this voltage sensor, but our results demonstrated that they are enough to trigger the pore opening. Since in voltage-gated channels the voltage sensors act independently with a final cooperative step, it would be interesting to understand how the voltage sensors of Kv_{Synth1} work together to open the pore.
Finally, Kv_{Synth1} can be a good candidate for crystallization, since it is nicely expressed and purified from *E.coli*. The crystal structure could give new insights about the coupling interactions between the two elements, and information about the linker structure in the different constructs that we tested in oocytes. Moreover, the right-shifted voltage-dependence of the chimera (inherited from Ci-VSP) respect to all the other Kv channels keeps the voltage sensor in the "resting" state in crystallization conditions (i.e. 0mV). The X-ray structure of this state will allow to compare the two extreme conditions that the channel is subjected to, when the membrane potential changes.

Part I(b)

La giraffa ha il cuore lontano dai pensieri. Si é innamorata ieri, e ancora non lo sa.

Stefano Benni

5 STATE OF THE ART

5.1 HCN channels

Within the superfamily of voltage-gated channels, there is a group of ion channels regulated by cyclic nucleotide ligands, that includes cyclic nucleotide-gated (CNG) channels and the hyperpolarization-activated cyclic nucleotide (HCN) channels. The two families exhibit high sequence similarity, they have similar structure, and similar mechanism of activation by cyclic nucleotides [56]. However HCN channels are voltage-dependent, whereas CNGs are virtually voltage-independent, so the effect of the cyclic nucleotide modulation on the current is different in the two groups. They play a fundamental role in a variety of physiological processes, sharing a regulation mechanism: opening in response to intracellular cyclic nucleotides, they translate this change in a variation of the membrane potential. The HCN family, like the CNG family, comprises several subunit types.There are four subunit isoforms, HCN1-HCN4, which can combine to form heterotetrameric channels in heart and brain [57–59]. HCN1 is expressed in photoreceprtors, dorsal root ganglia, cortex, cerebellum and sinoatrial node. HCN2 is expressed in sinoatrial node, dorsal root ganglia, and basal ganglia. HCN3 is widely expressed in brain, while HCN4 is expressed in the sinoatrial node and in subcortical areas [57–59]. HCN channels are cation channels,more permeable to K^+ than Na^+, and they are activated by membrane hyperpolarization. They are

the molecular basis of the time-dependent inward current known as I_f (funny), or I_h, and their function has been extensively described in the cardiac sinoatrial node [60, 61]. This area is the pacemaker of the heart, in which several types of channels cooperate to generate spontaneous rhythmic firing of action potentials. After an action potential, the membrane hyperpolarization activate these channels, that conduct an inward current and depolarize the cell, setting the membrane potential to the threshold of voltage-gated Ca^{2+} channels activation, leading to a new action potential [62]. Some neurotransmitters can increase the concentration of cAMP, accelerating the firing, and, as consequence, the heart beat. This effect is due to the regulation mechanism of cAMP (3'-5'-cyclic adenosine monophosphate) that bind to HCN channels, shifting the voltage dependence of the activation to more depolarizing potentials, the rate of channel opening and the maximal conductance [63].
In a similar way, HCN channels mediate pacemaker activity in the nervous system. Besides acting as pacemaker, HCN channels can also stabilize the membrane resting potential. In fact they are activated at rest, leading to an inward sodium current that depolarize the cell. This depolarization deactivates HCN channels, preventing too rapid firing [56]. Since they have an important role in the heart and brain activity, mutations in these channels are related to several diseases like bradycardia and epilepsy, as it was recently demonstrated [64, 65].

5.1.1 Topology of HCN channels

HCN channels present structural features common to the channels belonging to the superfamily of voltage-gated channels. They have six transmembrane segments, four of them (S1-S4) form the voltage sensor domain, while S5-S6 comprise the pore region, thought to be similar to that of KcsA, whose crystal structure has been solved. HCN channels have both intracellular N- and C-termini [56]. The N-terminus is different in every isoform, while

the C-terminus, connected to the end of S6 segment, is for the most part formed by cyclic nucleotide binding domain (CNBD) and the C-terminal called post-CNBD (Fig.5.1) [56].

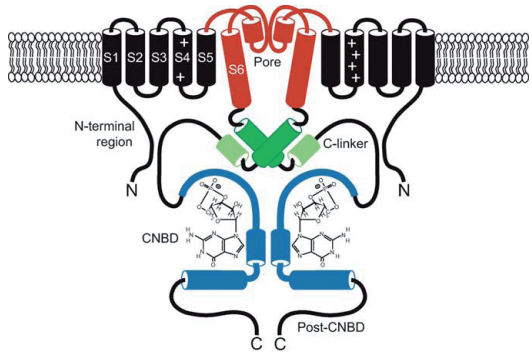

Figure 5.1: **HCN channels membrane topology** Cartoon representation of two monomeric subunits of an HCN channel. It' s possible to identify all the elements: the voltage sensor domain (black), the pore (red), the C-linker (green) connecting S6 with the CNBD (cyan) [56]

The selectivity filter has the conserved sequence found in e K^+ channels (GYG motif), but HCN channels are permeable to K^+ and Na^+ with a ratio of 4:1, and blocked by Cs^+ [66]. The voltage sensor contains the positive charged residues responsible of the S4 motion upon changes in membrane potential. HCN are moderately voltage-dependent, with an average of six equivalent charges moving to activate the channel, compared to $13e_o$ of Shaker, and they have slow activation kinetics [56]. The voltage dependence is different in tetramers formed by identical subunits. Both the S4 movement and the activation gate appear to be conserved between HCN and Kv channels. Because they open in response to voltage steps with opposite polarity, it is presumable that the coupling between the two elements is different [67]. The three isoforms of HCN channels, when expressed as homotetramers, show different kinetics and voltage dependence. HCN1 has the faster kinetic and less negative threshold of activation,

the current reaches the saturation level at less negative potential respect HCN2 and HCN4 [68].

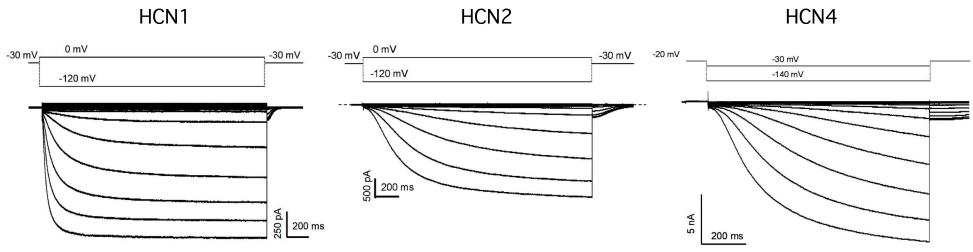

Figure 5.2: **Representative current traces of heterologously expressed HCN1, HCN2, HCN4 homotetramers.** Current traces are recorded at hyperpolarized voltage steps. The traces clearly show that HCN1 exhibits the fastest kinetic and the more positive voltage dependence. In fact, the current developed by HCN1 reaches saturation at less negative voltages respect HCN2 and HCN4. (From www.chantest.com)

5.2 cAMP modulation

5.2.1 Effect of cAMP on channel gating

HCN channels are activated by the membrane hyperpolarization, but channel opening can be modulated by cyclic nucleotides, in particular cAMP and cGMP [56, 63]. These molecules can bind in a pocket within the CNBD, affecting the open probability of the channel: binding of cAMP at nanomolar concentration shifts the voltage-dependence to more depolarized potentials, speeds the kinetics and increases the maximal conductance of the channel [56]. Nevertheless the intensity of the effect is different in HCN1 respect HCN2 and HCN4: in the latter the shift due to cAMP binding is around 17mV, while in HCN1 is only 3 mV [68]. Similar effects are obtained by cGMP, but 10-fold higher

concentration of ligand is required, due to lower affinity of this agonist [69].

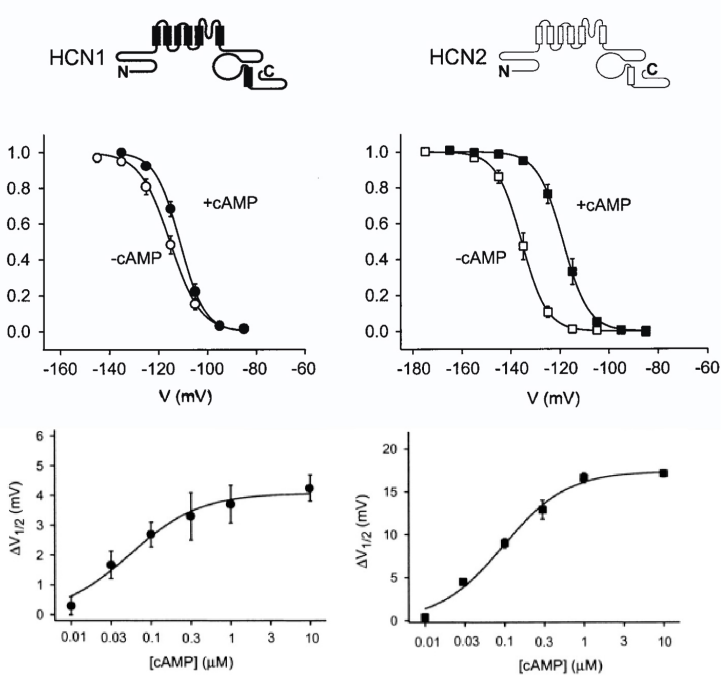

Figure 5.3: **HCN1 and HCN2 voltage-dependence and cAMP dose-response curve in patch-clamp measurements.** The heterologous expression of HCN1 and HCN2 show that the activation curve of HCN1 is right-shifted respect to HCN2. The presence of cAMP shifts HCN1 $V_{1/2}$ of about 3mV, and HCN2 $V_{1/2}$ of about 17mV. The dose-response curves reveal a K_d for cAMP of 60nM for HCN1, and 100nM for HCN2 (Modified from [70]).

5.2.2 The structure of the CNBD in HCN channels

The CNBD is the cytosolic regulatory domain in charge of the response of the channel to the binding of cyclic nucleotides. Despite a difference in the channel gating effect recorded in elec-

trophysiology of HCN1 respect to HCN2/4, the three crystal structures appear very similar (Fig.5.4), in agreement with the high sequence identity ($\sim$ 90%) [8, 71, 72]. The cytosolic region crystallized is composed of two subdomains: the **CNBD** and the **C-linker**. The CNBD consists in the binding pocket for nucleotides, and it is formed by four α-helices with a β-roll in between. The β-roll architecture is composed of eight antiparallel β-strands. The binding site for nucleotides looks like a pocket formed by helices C and P and β-sheet 7; in particular the comparison between the unbound and bound structures of an homolog CNBD from *M.loti* show a movement of 8$\mathring{A}$ of the C-helix acting as a gate that seems to trap the molecule of cAMP in the pocket [73].

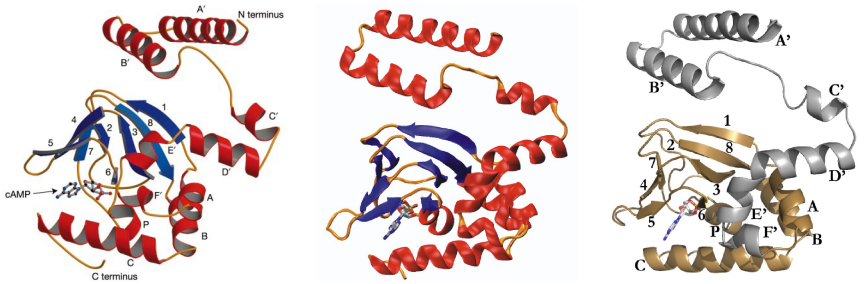

Figure 5.4: **Structures of C-terminal domain of three HCN isoforms.** Ribbon representation of a single subunit of C-linker/CNBD with the cAMP bound in the pocket, of mouse HCN2 [71], human HCN4 [72] and mouse HCN1 [8]. Each helix is marked with a letter.

The CNBD assembles as a tetramer in presence of cAMP. The tetramerization of the CNBD subunits is usually correlated to the removal of tonic inhibition from the pore of HCN channels, facilitating pore opening [8, 71, 72]. The inhibitory effect is supported by the fact that the deletion of CNBD in HCN channels accelerates the activation kinetics and shifts the voltage dependence to more positive voltages [4]. Although the three

isoforms don't diverge so much in the structure, HCN1 has a different response to cAMP (lower shift of $V_{1/2}$). In a previous study published by our laboratory we demonstrated that HCN1 has a higher propensity to tetramerize at basal levels of cAMP [8]. The crystal structure has been obtained also in presence of cGMP: this nucleotide allocates in the same binding pocket, but in syn configuration, instead of the anti configuration found in the cAMP-bound CNBD [71]. It has been shown that the affinity of cGMP for HCN2 is lower respect to cAMP ($K_{1/2}$ cAMP=0.09μM; $K_{1/2}$ cGMP=1.4μM in inside-out patches) [74]. This reduced efficacy of cGMP has been investigated in HCN2. In particular, the insertion of a point mutation in the C-helix, I636D, converts the cAMP effect into the one of cGMP, and viceversa.The authors suggest that cGMP is only a partial agonist in wild-type channels because it is unable to sufficiently stabilize movement of the C helix, or that because the C helix is in a different conformation with cGMP bound than with cAMP bound, and the mutation causes the C helix to adopt a cAMP-like configuration in presence of cGMP [75].
Most of the intersubunits contacts in the three crystals are in the C-linker. The C-linker connects the last transmembrane segment to the cyclic nucleotide binding pocket, is made of six α-helices interspersed by short loops. The C-linker has a characteristic fold, in which the first two helices (A',B') form an antiparallel helix-turn-helix motif interacting with the helices C' and D' of the neighbouring subunit (Fig.5.5. These interaction has been likened to an "elbow on shoulder", and it involves hydrogen bonds, hydrophobic interactions and salt bridges [71]. Electrophysiological data derived from HCN1/2 chimeras assigned differences in cAMP modulation to differences in the C-linker region [70]. All these results suggested that cAMP binding induces a significant rearrangements at the level of the "elbow on shoulder", and, consequently, to the whole C-terminal region.

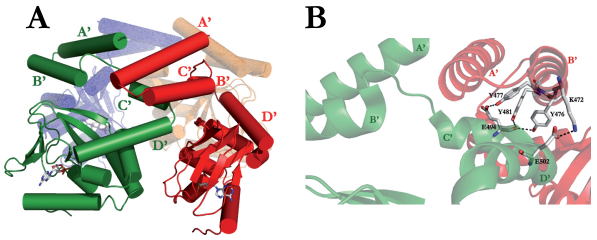

Figure 5.5: **Elbow-on-shoulder between two C-terminal domain neighbouring subunits.** (A) Cylinder representation of a tetramer from the side view with the cAMP bound. Helices B' and C' of the red subunit interact with helices C' and D' of the green subunit. (B) Residues involved in the interaction in HCN2 [71].

5.2.3 Cooperativity of CNBDs

Quite a few mechanisms have been suggested to explain cyclic nucleotide activation of HCN channels, but they are still evolving in relation to the more recent data [76, 77]. The **MWC** model was proposed to explain this mechanism (Fig.5.6 B): it's a classic allosteric model (the same used to explain haemoglobin behaviour), with transitions from the closed to open state stabilized by a constant amount of bound ligand. It is based on the assumption that there are four identical binding sites, and the channel opening occurs with a single concerted final transition of the whole protein [56]. To address this limitation two are models were proposed.
The first is the **dimers of dimers**: the CNBDs are organized as dimers; the dimer undergoes to a concerted transition from closed to open, but both dimers must be open to enhance opening of the pore [78]. This model implies that the CNBDs are organized in a two-fold symmetry in the apo-state (unbound), but they recover the four-fold symmetry when they are fully ligated, as the crystal structure shows (Fig5.6 A).
Anyway, the model that fit in the best way with the crystal structure, could be the **modular gating** model (Fig.5.6 C) [56]. The

activation of HCN channels can be described as the interaction between four modules:the pore, the voltage sensor, the C-linker and CNBD. Each module is in equilibrium between two possible conformations, and they are coupled so that the conformation of one module can be influenced by another module. This model is used to explain why in the crystal the C-linker is in the resting conformation, which is inhibitory for the pore, while the CNBD is bound by the ligand. The absence of the pore in the crystallized construct can promote the resting state of the C-linker, although the CNBD is "loaded".

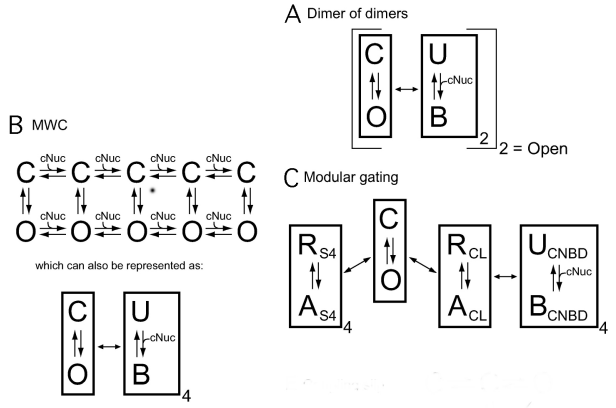

Figure 5.6: **Proposed models for cAMP modulation in HCN channels.** Schematic representation of dimers of dimers (A), MWC (B) and modular gating (C) models. (Modified from [56])

The last results, obtained with Isotermal Titration Calorimetry (ITC) on isolated C linker-CNBD [79] and patch-clamp fluorometry [76, 77], provided new insights in the description of the cooperativity between the four CNBDs.
By ITC experiments it was possible to measure two affinity states in HCN2, an high affinity state (0.1μM), due to the binding of the first cAMP molecule, and a lower affinity state ($\sim 1\mu$M) where all the binding sites are completely occupied. The same experiments on HCN1 highlighted that only the lower affinity state is measur-

able, so the authors suggested that the changes induced by the high affinity binding of cAMP have already occurred. This could explain the different effect of cAMP on HCN1 in terms of channel opening. The authors suggested that a negative cooperativity can be derived from their data: the binding of the first molecule decreases the affinity for the other binding sites. The difference in binding affinity was also observed on the whole channel by patch-clamp fluorometry, but with different conclusions. These experiments are done with a fluorescent analog of cAMP, allowing to track binding event and current flow at the same time. The more relevant results from these experiments were that in HCN2, two molecules of cAMP are enough to modulate channel opening, and that the cooperativity of HCN channels is a high complex process. The subunits substantially differ for binding affinity: the binding affinity for the second ligand is larger than the first ligand to be bound, and similarly the affinity for ligand 4 is larger that that for ligand 3. However, although in these cases we can observe a positive cooperativity, the affinity for ligand 3 is smaller than that for ligand 2. This suggests a negative cooperative effect. The channel is stabilized only in the states with zero, two or four ligands: it is possible to suppose that the activation process occurs thanks to a dimeric organization [76].

6 AIMS OF THE PROJECT

6.1 A putative second binding pocket for nucleotides

In our laboratory we crystallized the C-terminal region of HCN1, HCN2 and HCN4 in presence of cGMP. Carefully analyzing these structures, we found an unexplained electron density in all the three proteins, particularly marked in HCN4. This additional density is c-GMP specific, and it is located in the C-linker region, close to the tetramerization interface of the subunits. Several rounds of refinement showed that the density corresponds to a cGMP molecule (Fig 6.1). The presence of a cyclic nucleotide in a region, so important in the transmission of the signal due to cAMP binding to the pore, suggested us to explore the possibility that occupancy of this site by a cGMP molecule could affect the properties of the channel.

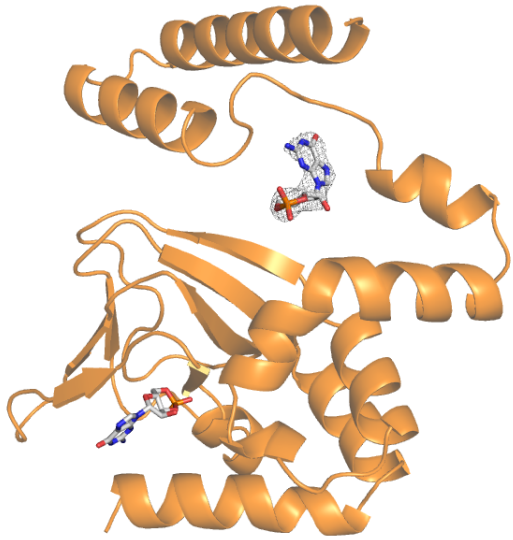

Figure 6.1: **Additional electron density in HCN4.** Crystal structure on the C-linker/CNBD of HCN4. The cAMP molecule is bind in the canonical pocket in the CNBD. A cGMP molecule is bound in the C-linker region, in the loop between helices B' and C'. (Fig. by M. Lolicato)

7 RESULTS

Although it is known that channels that regulate the pacemaker activity are modulated not only by cAMP, but also by cGMP, so far there is no evidence if cGMP has an effect on HCN4. The only measurements available showed the effect of cGMP on the native current I_f [63]. For this reason we tested the effect of cGMP on HCN4 homotetramers, to compare its effect with that reported for HCN2. Moreover, the presence of a cGMP molecule in the putative binding site in the C-linker, suggested us that cGMP could bind there when it is added at high concentration, giving a feedback regulation. The experiments were performed expressing HCN4 in mammalian HEK 293 cells. Inside-out patch clamp recordings from these channels showed a behaviour very similar to that reported for the native current I_f. cGMP was applied on excised-patches after recording the current in control solution; the effect of cGMP is concentration-dependent, the K_D derived from fitting experimental data with the Hill equation is 13.2μM, while n is 0.72. The maximal shift is 12mV, smaller than that cAMP induces on the current (Fig.7.1). All this data are consistent with the effect of cGMP on HCN2 (ref), where cGMP gives similar modulation of cAMP. To exclude that cGMP exerts side effects on the current by binding in the second pocket, high concentrations of nucleotide were tested. Five and 10mM cGMP were added to bath solution in excised patches, resulting in the same 12mV shift of the current. cGMP have no effect even when the canonical binding pocket was fully ligated by cAMP (5mM).

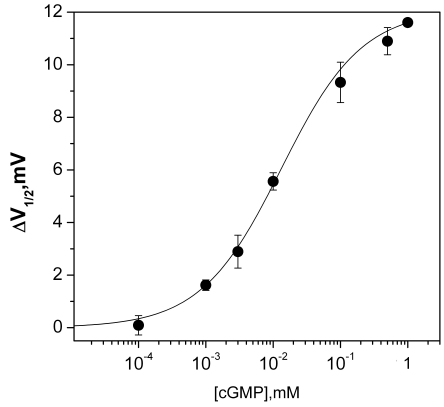

Figure 7.1: **Dose-response curve of cGMP on HCN4 current.** Experiments were performed in excised patches of HEK cells transfected with hHCN4. Experimental data (n$\geq$ 3) were averaged and fitted with Hill equation. K_d=13.2μM; n=0.72. Exp. performed by S. Zucca.

At this point we excluded occupancy by cGMP of the second binding site could exhert any measurable effect on the current. A more detailed analysis of the structure revealed that the portion of the protein in which the second cGMP was found, is rich of charged residues that create a deeper tunnel (compared to the cGMP electron density) able to allocate a bigger molecule. Starting from this consideration, we tried to fit a molecule of c-di-GMP in the pocket, obtaining a good overlap with the electron density and interaction with the charged residues of the "tunnel". Cyclic -di-GMP is a signalling molecule found in bacteria that is composed by two molecules of cGMP bound at the cyclic phosphate level (Fig.7.2). So we tested the effect of c-di-GMP *in vivo* in whole-cell configuration, adding the agonist in pipette solution [64].

The presence of 100μM c-di-GMP in the pipette solution did not affect the currents of HCN4, that appeared indistinguishable from the control. Anyway, a dramatic effect could be observed if

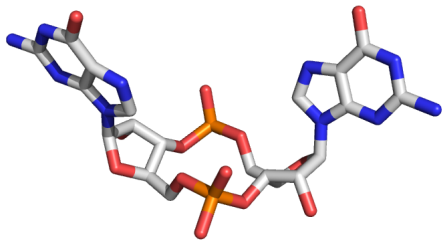

Figure 7.2: **c-di-GMP molecule.**

the same experiment was done in presence of cAMP. Compared to the activation curve obtained with cAMP alone, the presence of the c-di-GMP completely abolishes the effect of cAMP, shifting back the activation curve to control position (Fig.7.3).

This reverting effect of c-di-GMP on cAMP modulation is measurable also in excised patches. In single-step experiments, the current is recorded in control solution. cAMP addition at saturating concentration increased the current, and the c-di-GMP shifted back the current to the control recordings. This demonstrated that c-di-GMP directly affects HCN4 current (Fig.7.4).

Whole-cell experiments revealed a K_d of 1.58 ± 0.24 μM and a n value of 1.2 (Fig.7.5). We obviously tried to co-crystallize HCN4 CNBD in presence of this molecule, to demonstrate that c-di-GMP binds in the second pocket, and to analyze the interaction between the dinucleotide and that portion of the protein. Unfortunately any attempt to get crystals with good diffraction patterns failed, probably because the conformational changes occurring from c-di-GMP binding, destabilizes protein organization.

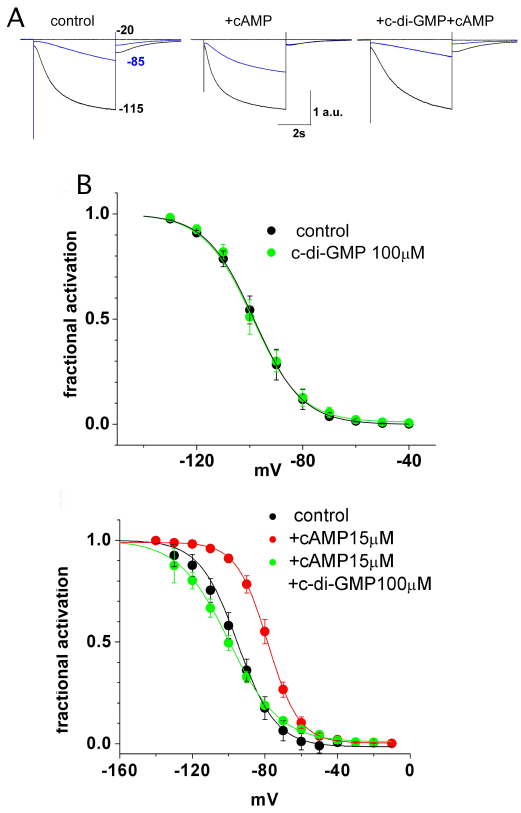

Figure 7.3: **Effect of c-di-GMP on HCN4 current.** The effect of c-di-GMP was tested in HEK cells transfected with hHCN4 in whole-cell configuration. (A) Representative current traces recorded in control solution, plus cAMP, and plus cAMP and c-di-GMP. (B) Top panel: Activation curves from experimental data obtained with and without c-di-GMP 100μM in pipette solution. $V_{1/2(+c-di-GMP)}$=$-$99.0$\pm$0.6, $V_{1/2(control)}$=$-$98.4$\pm$0.6 mV. Bottom panel: Activation curves from experimental data recorded in pipette control solution, with cAMP 15μM and with both cAMP 15μM and c-di-GMP 100μM. $V_{1/2(control)}$=$-$94.9$\pm$0.3, $V_{1/2(+cAMP)}$=$-$78.4$\pm$0.2, $V_{1/2(+c-di-GMP+cAMP)}$=$-$94.8 $\pm$ 0.6 mV. Data are obtained from average of n$\geq$ 3 experiments.

At the same time we could solve the structure at 3.7 A of the protein co-crystallized with another di-nucleotide, the c-di-

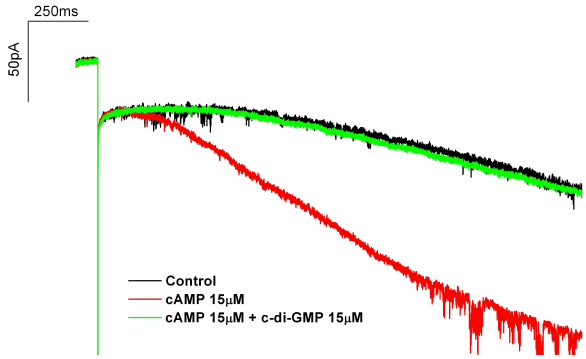

Figure 7.4: **The c-di-GMP affects directly cAMP modulation.** Single-step current trace recorded at -140mV of hHCN4 in inside-out configuration. Current recorded in control condition (black line) increases upon the addition of 1mM cAMP (red line). The c-di-GMP completely reverts the effect of cAMP, the current goes back to the level measured in control solution (green line). Fig. by S. Zucca.

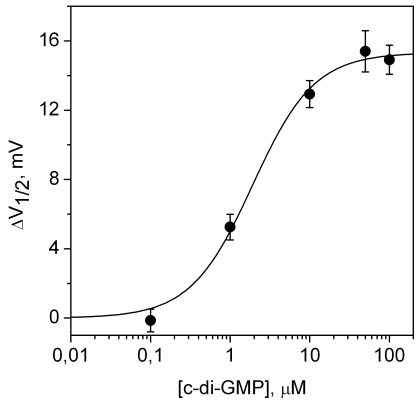

Figure 7.5: **Dose-response curve of c-di-GMP on HCN4 current.** Experiments were performed in whole-cell configuration in HEK cells transfected with hHCN4. Experimental data (n$\geq$ 3) were averaged and fitted with Hill equation. K_d=1.58 $\pm$ 0.24μM; n=1.2. Fig. by S. Zucca.

AMP, bound in the second pocket in the C-linker region. The crystal structure is at low resolution, so it is not possible to see

the side chains interacting with c-di-AMP, that binds only in two monomers on a total of sixteen found in the cell unit of the crystal. For comparison, cGMP was found in each monomer of the cell unit. Electrophysiology experiments showed that adding 100μM c-di-AMP in the pipette solution counteracts the effect of cAMP, displaying the same effect of c-di-GMP (Fig.7.6). This underlies that also this dinucleotide can dramatically perturb the CNBD structure, but it probably establishes different interactions, allowing the formation of a stable crystal. Another explanation can be that the presence of fewer molecules of c-di-AMP allows the tetramers to keep an ordered structure.

In silico docking the c-di-GMP in the binding pocket identified in the C-linker of HCN4, in three different poses, revealed that the glutamate in the position 566 could be an interaction point. It has been shown before that this aminoacid is conserved in HCN2, and is related to epilepsy when is mutated in aspartic acid [65]. This mutation causes a pronounced left-shift in the activation curve of HCN2, but the channel is still able to bind and respond to cAMP, with the same maximal shift of the $V_{1/2}$ recorded in the wild-type. The mutation E566K in HCN4 showed a similar behaviour to what has been reported in HCN2 [65]. In control pipette solution the $V_{1/2}$ is -129.3 ± 0.2 mV; experiments with cAMP 15μM causes a shift to a $V_{1/2}$ of -114.1 ± 0.1 mV. Furthermore, as expected by our docking results, the c-di-GMP doesn't influence the effect of cAMP, as shown in Fig. 7.6 the two curves are superimposed. The residue E566 is clearly involved in the interaction with the c-di-GMP, and this confirms that the dinucleotide binds in the non-canonical pocket within the C-linker.

As a control experiment, the c-di-GMP was docked in the canonical binding site of HCN4 structure after removal of cAMP. The docking software failed to get output a score because the molecule is too large for that pocket.

At this point, we collected several evidences that in the C-linker there is a binding pocket that can regulate the response

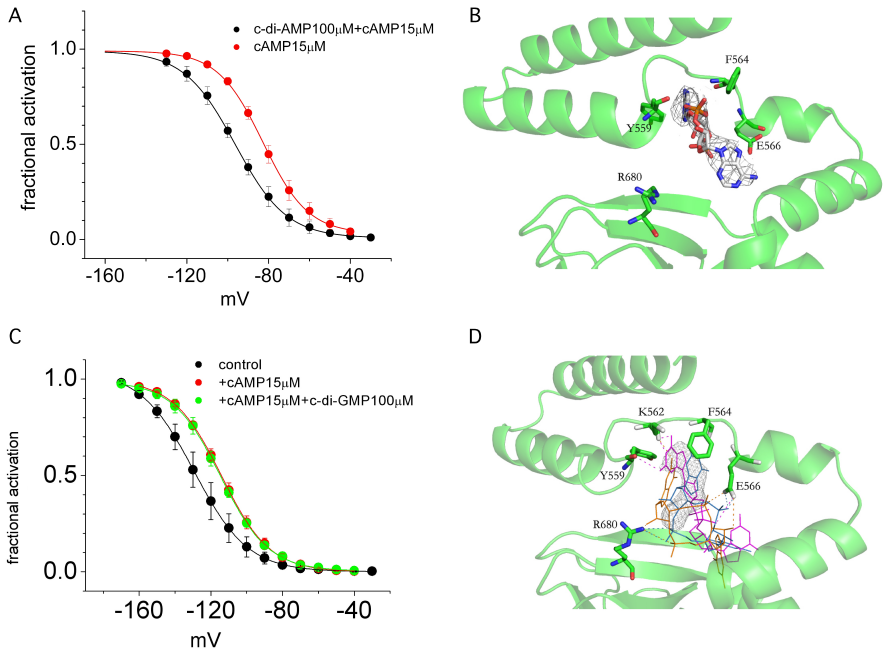

Figure 7.6: **The C-linker region hosts a second binding pocket.** (A) Activation curves of HCN4 recorded in presence of cAMP 15μM and cAMP 15μM+c-di-AMP 100μM ($V_{1/2(+cAMP)}$=−82.7 ± 0.2, $V_{1/2(+c-di-AMP+cAMP)}$=−96.3 ± 0.3 mV). (B) Crystal structure of HCN4 Clinker-CNBD bound to a molecule of c-di-AMP. The molecule of c-di-AMP localized near the loop between B' and C' helices. (C) Activation curves of HCN4 E566K recorded in control solution, in presence of cAMP 15μM and cAMP 15μM+c-di-GMP 100μM ($V_{1/2}$=−129.3 ± 0.2, $V_{1/2(+cAMP)}$=−114.1 ± 0.1, $V_{1/2(+c-di-GMP+cAMP)}$=−114.6 ± 0.1 mV). (D) Crystal structure of HCN4 Clinker-CNBD bound to the c-di-GMP docked in three different poses. Aminoacid E566 interacts in all the three possible docked structures. Data are obtained from average of n≥ 3 experiments.

of the cAMP and that this pocket can bind not only cGMP but also larger molecules as c-di-nucleotides. More than 300.000 molecules were screened and the top 11 ranked according to the calculated affinity were tested on HCN4. These molecules were

divided in two groups and tested separately in whole-cell experiments, adding each mix to the pipette solution, in the presence of cAMP. Each mix contained each compound at a final concentration of 100μM; the selected molecules are highly insoluble, so they were dissolved in DMSO. We tested only the molecules able to dissolve in pipette solution at a final concentration 100μM. The pipette solution had a maximum concentration of DMSO of 0.3%. Control experiments were done maintaining the same DMSO concentration in the pipette solution, to exclude any possible effect of the solvent. Table7.1 shows the $V_{1/2}$ recorded for the two mix. Cells measured in presence of Mix n.1 has an half-activation potential similar to that recorded in presence of cAMP alone, so none of these molecules is able to counteract the effect of the cAMP. Anyway, the Mix n.2 shifted the activation curve at the same position of the control experiments, so at least one of the molecule in the mixture is able to act as an antagonist of the cAMP.

		$\boldsymbol{V_{1/2}}$	$\Delta V_{1/2}$ $(V_{1/2}cAMP - V_{1/2}x)$
Control		-93.9±0.07	14.1 ± 0.4
cAMP		-79.8 ± 0.3	-
MIX 1		-81.9 ± 0.1	2.0 ± 0.4
MIX 2		-96.3 ± 0.5	$\mathbf{16.4 \pm 0.8}$
MIX 2 components	n.5	-82.7 ± 0.3	2.8 ± 0.6
	n.8	-79.9 ± 0.4	0.05 ± 0.4
	n.11	-96.4 ± 0.8	$\mathbf{16.6 \pm 1.1}$

Table 7.1: **Effect of Mix n.1 and Mix n.2 on HCN4 current.** The 11-top ranked compounds obtained docking the second binding pocket were grouped in two mix. Each mix was added in the pipette solution with cAMP 15μM. The table shows the $V_{1/2}$ for each condition and the $\Delta V_{1/2}$ respect the $V_{1/2}$ calculated for cAMP recordings. The compounds of Mix n.2 were individually tested, and the n.11 has been identified as the compound able to revert the cAMP effect.

The molecules in mix n.2 were individually tested, and only one was responsible of the phenotype observed in the mixture. The IUPAC nomenclature of this molecule is N'-biphenyl-2-yl-N-

[1-(3-cyanobenzyl)piperidin-4-yl]-N-(pyridin-3-ylmethyl)urea, hereafter called compound n.11. The effect of the compound n.11 is exactly the same observe with the c-di-GMP, and with the c-di-AMP, but the dose-response curve revealed that it has higher affinity (K_d=$0.42 \pm 0.11 \mu$M) (Fig.7.7).

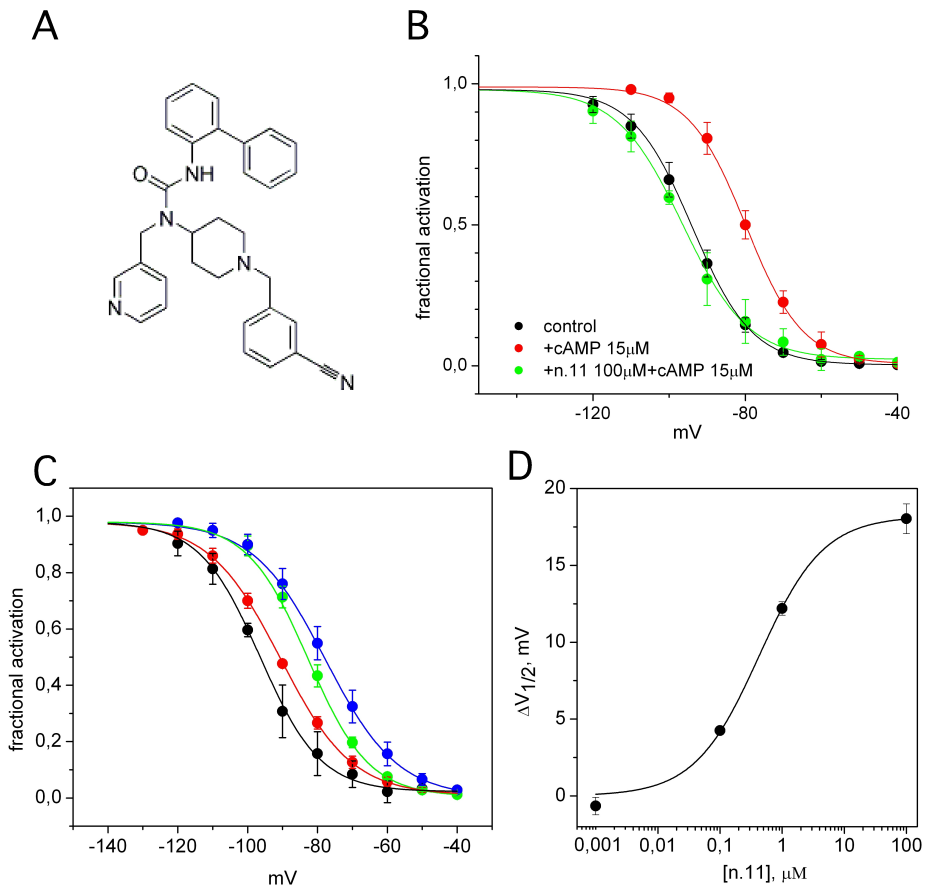

Figure 7.7: **The compound n.11 affects cAMP modulation of HCN4.** (A) Compound n.11: N'-biphenyl-2-yl-N-[1-(3-cyanobenzyl)piperidin-4-yl]-N-(pyridin-3-ylmethyl)urea. (B) Activation curves of HCN4 in pipette control solution, in presence of cAMP, and cAMP+compound n.11. ($V_{1/2}$=−93.9 ± 0.1, $V_{1/2(+cAMP)}$=−79.85 ± 0.3, $V_{1/2(+n.11+cAMP)}$=−96.4 ± 0.8 mV)(C) Activation curves of HCN4 in presence of cAMP 15μM and the compound n.11 at the concentration of 0.1 (●), 1 (●), 10 (●), 100μM (●). (D) Dose-response curve of compound n.11 measured as ΔV respect to the $V_{1/2}$ in presence of cAMP. K_D is 0.42 ± 0.11μM. Data are obtained from average of n≥ 3 experiments.

7.1 Isoform specificity on the effect of c-di-GMP and compound n.11

The C-linker is very conserved in the three isoforms of HCN channels. In order to test isoform-specificity, we repeated the experiments with the c-di-GMP and with the compound n.11 on HCN2. In particular, the residues identified as relevant in the binding of cGMP and c-di-AMP, or c-di-GMP (docking) are identical in HCN2 and HCN4. At the same time, as mentioned in the introduction, the presence of the electron density seemed from the beginning to be isoform-specific, more marked in HCN4 than in HCN2. Cells expressing HCN2 had a $V_{1/2}$ of -94.0 ± 0.1mV in control solution. The addition of cAMP 15μM shifted the $V_{1/2}$ to a value of -74.2 ± 0.5 mV. Cyclic-di-GMP 100μM didn't show any effect on HCN2 current, and we had to increase the concentration of antagonist up to 200μM to observe a shift of $\sim$6mV in the activation curve (Fig.7.8). The compound n.11 was totally ineffective even at the concentration of 200μM (Fig.7.9).

The binding pocket that we identified could be considered as a potential target for drugs, because different molecules, selected in independent ways, affect in the same manner the channel opening in the micromolar and submicromolar range.

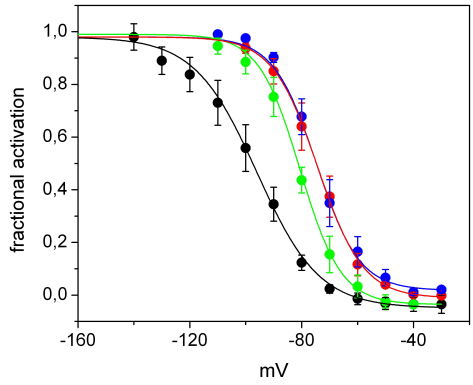

Figure 7.8: **Effect of c-di-GMP on HCN2 current.** Activation curves of HCN2 recorded in control pipette solution (●), in presence of cAMP 15μM (●) and cAMP 15μM+c-di-GMP 100 (●) and 200μM (●) ($V_{1/2}$=−95.9 ± 0.7, $V_{1/2(+cAMP)}$=−74.7 ± 0.5, $V_{1/2(+c-di-GMP100+cAMP)}$=−74.2 ± 0.7, $V_{1/2(+c-di-GMP200+cAMP)}$=−80.6 ± 0.6 mV).

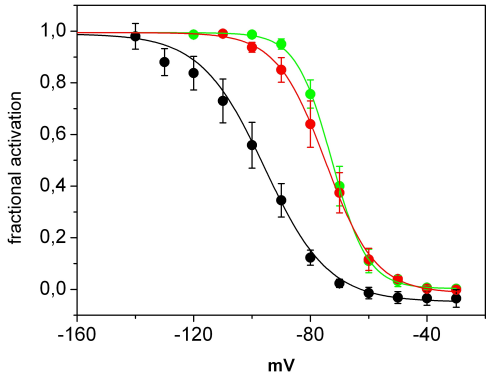

Figure 7.9: **Effect of compound n.11 on HCN2 current.** Activation curves of HCN2 recorded in control pipette solution (●) , in presence of cAMP 15μM (●) and cAMP 15μM+n.11 100μM (●)($V_{1/2}$=−95.7 ± 0.8, $V_{1/2(+cAMP)}$=−74.6 ± 0.6, $V_{1/2(+n.11+cAMP)}$=−72.6 ± 0.4 mV).

7.2 Effect of compound n.11 on the native current I_f

Since HCN4 is the major molecular determinant that underlies the current in the sino-atrial node of the heart, we tested the compound n.11 on the native current I_f, in collaboration with the laboratory of Prof. Dario DiFrancesco (University of Milan, Italy). The experiments were performed in isolated myocytes of the mouse sino-atrial node, in whole-cell configuration, in which the compound was added to the pipette solution. The activation curve recorded in presence of the compound n.11 alone was already left-shifted respect to the control curve: the molecule counteracted the effect of the endogenous cAMP bound to the channel. Anyway, the two activation curves recorded in the presence of the compound n.11, with or without cAMP, are significantly left-shifted respect to the curve recorded in the presence of cAMP alone. As we found in HEK cells, the compound n.11 was able to revert the shift induced by cAMP on the native current (Fig.7.2).

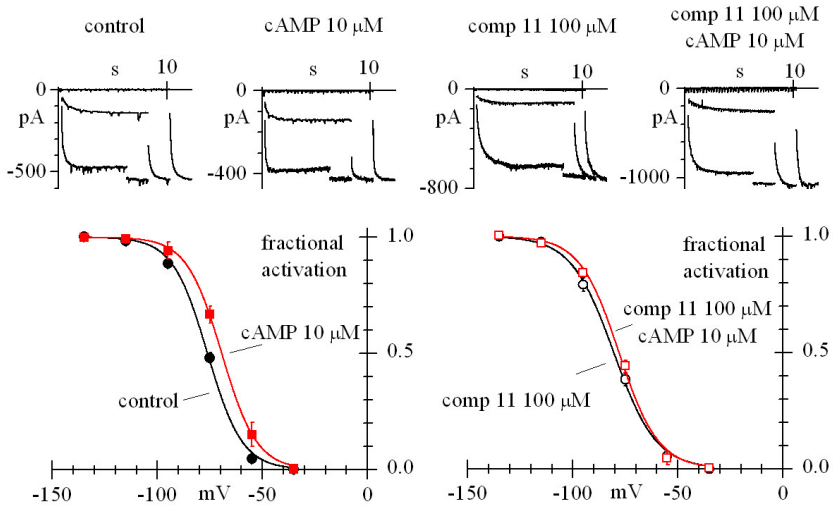

Figure 7.10: **Effect of compound n.11 on I_f in mouse sino-atrial node myocytes.** Traces current recorded at -35mV, -75mV, tail currents at -115mV. cAMP and compound n.11 are added respectively at the concentration of 10μM and 100μM. ($V_{1/2}$=-76.1mV; $V_{1/2(+cAMP)}$=-69.3mV *; $V_{1/2}(+n.11)$=-80.5mV; $V_{1/2(+n.11+cAMP)}$=-78.0mV *. *, P$\leq$ 0.5 versus control value.)

8 DISCUSSION (and future prospects)

In 1991 it has been demonstrated that, in cardiac pacemaker cells, cAMP activates I_f by a mechanism independent of phosphorylation, involving a direct interaction with the channels at their cytoplasmic side. This was the first evidence of an ion channel whose gating is dually regulated by voltage and direct cAMP binding [63]. In the last years many attempts were done in order to understand which mechanism can translate an increase in cAMP concentration into an increase of channel opening. The keystone to interpret the general mechanism is that, upon cAMP binding, the four cytosolic subunits in every channel undergo to a tetramerization, a conformational rearrangement between the subunits that is transmitted to the pore region [8, 78].
In our lab, we now have discovered a new regulation point in HCN4, sited in the C-linker region that provides most of the teramerization contact points in the protein. The finding of a cGMP molecule in this secondary pocket does not seem to correlate with a new function of this nucleotide in the C-linker region. The effect of cGMP on HCN4 current, revealed a similar behaviour previously described in HCN2 [75] and in the native current If [63]. The cGMP acts as an alternative agonist, with lower affinity respect to cAMP, interacting with the binding pocket in the CNBD. Anyway the C-linker binding pocket can host larger molecules, as the dinucleotides (c-di-GMP and c-di-AMP) or the screened compound n.11, and, unlike the cGMP, they can surprisingly counteract the modulation due to cAMP binding. In fact, in the presence of one of these molecules bound

in the second pocket, the effect of cAMP on gating can be partially or completely eliminated, in concentration-dependent manner. This binding pocket could be an interesting target for drug design, because it will be possible to develop molecules that affect the autonomic control on the heart rate, not only in diseases that involve defects of HCN function but also to relieve side effects due to other heart therapies. The known HCN blockers, as ivabradine [80, 81], act as a pore blocker, interrupting the ion flux through the channel. On the contrary, the exploitation of this pocket could allow a fine tuning of the channel activity, in particular when a downregulation of the cAMP effect is required, without perturbing the cAMP concentration in the cell, that is involved in many other regulation pathways [82]. The preference of the molecules that we tested for HCN4, shows a high isoform-specificity, avoiding a general effect on all HCN channels, that are widely expressed in heart, brain and also in the retinal cells [83–85]. The finding of this novel binding pocket raises a great interest from the biophysical point of view. This binding site is situated in tetramerization region of the CNBD, a key point for the trasduction of the cAMP binding effect, a bridge between the binding event and its efficacy. The presence of this binding pocket testify that it is possible to severely affect cAMP modulation acting far from where the binding occurs. How this inhibition, due to c-di-GMP or related molecules, occurs, has to be studied in deep. From our preliminar data is difficult to elaborate a model of the mechanism of c-di-GMP action.
The first hypothesis could be that the binding of c-di-GMP induces a conformational change that is transmitted to the binding pocket of the cAMP, and then it changes the affinity of cAMP for the CNBD. The C-linker region could be an allosteric binding site, antagonizing the effect of cAMP. This idea can explain why the co-crystallization of the CNBD with c-di-GMP failed: the new tertiary and quaternary structure can be less ordered, so difficult to pack properly (we obtained only diffracting crystals at $6\mathring{A}$ resolution). Similar problems have occurred in the crystal-

lization attempts of the "apo-state" of the CNBD of HCN channels, i.e. the CNBD without any ligand bound into the pocket [8]. This, again, suggests that lack of tetramerization, together with the high flexibility of the C-helix in absence of ligand [73, 86], can interfere with the formation of an ordered crystal. In particular, the presence of the c-di-GMP could interfere within the set of interactions established in the "elbow-on-shoulder" [71], in which, via the C-linker, a subunit can contact the neighbouring one. The crystal structure of HCN4 CNBD in the presence of c-di-AMP does not show striking changes in the quaternary assembly, but the c-di-AMP is bound in only two molecules on a total of sixteen, so the averaged structure of the whole crystal shows a tetrameric assembly. Moreover, the low resolution of the crystal, does not allow to estimate if all the interactions present in the cAMP-bound structure are maintained when also c-di-AMP is bound. The second hypothesis involves the possibility that this alternative binding site is due to the quaternary structure of the C-linker only in the cAMP-bound conformation of the C-linker/CNBD. In this case, the c-di-GMP could bind without perturbing the cAMP-CNBD interactions. This hypothesis could explain why the effect of the c-di-GMP is still maintained even upon addition of high concentration of cAMP (1mM), although the effect of c-di-GMP is reversible (data not shown) . In order to explain which mechanism underlies the coupling agonist/antagonist, further experiments are required. In particular, monitoring the binding and unbinding of cAMP would help to understand which structure rearrangements occur in the presence of a molecule interacting in the C-linker region. A couple of options are possible: (1) it's known that an analog of cAMP, the 8-Azido-cAMP, binds covalently to the CNBD upon UV irradiation [87, 88]. Once the cAMP is bound to the CNBD, it will be possible to record or not the effect of c-di-GMP. This will allow to discriminate if the presence of the cAMP in the binding pocket is mandatory or not for c-di-GMP effect. (2) Another analog of cAMP, the fcAMP (8-DY547-AET-cAMP, [77]), binds

with similar affinity and kinetic to the CNBD, and due to its fluorescence, it's possible to follow the binding event together with the measurements of the current. Again, this approach could be useful to understand the events during cAMP/c-di-GMP interaction with the CNBD.
However, the interesting insight of our results, is that the C-linker cannot be merely considered as the covalent bridge between two domains, the pore and the CNBD, but it is a hub of interactions and, in particular, all these interactions are responsible of the relieve of the inhibition exerted from the CNBD upon cAMP binding. This idea was already demonstrated through the functional characterization of chimeras between HCN1 and HCN2, were the C-linker and different parts of the CNBD of the two isoforms were swapped [70]. What it is known is that the deletion of the C-linker/CNBD removes the inhibition of this domain from the channel, shifting the activation curve to less negative voltages. This means that the voltage sensor requires less energy to activate the channel. The same effect is obtained in other two cases: when only the CNBD, but not the C-linker, is deleted, and when, in the wild-type channel, the CNBD is fully ligated to cAMP. From these results, the C-linker alone, does not seem to exert any effect on the transmembrane core of the protein. This can be due to an unfolding of the C-linker in the absence of the CNBD, in which intra- and inter-subunit interactions are lost. The mutant E566K, that we characterized in HCN4, whose phenotype was already showed in HCN2 [65], demonstrates that is possible to uncouple the two mechanisms: the basal position of the activation curve, and the cAMP modulation. In particular, the left-shifted position of the activation curve seems to be assigned to the C-linker (more than the C-linker/CNBD), because the mutation is located in this domain. In this mutant the energy required to open the channel is so high respect to the wild-type, than even when the CNBD is fully ligated, the $V_{1/2}$ is correctly shifted to a more positive value, but it cannot reach the same value than that of HCN4 wild type

(+cAMP: $V_{1/2}$wt=-82mV; $V_{1/2}$E566K=-114mV). The mutated C-linker can exert an inhibiting effect so strong that even the modulation of cAMP is not enough to remove it; this probably suggest a change in interactions between the C-linker and some region of the voltage sensor domain, as the S4-S5 linker. It was postulated that an electrostatic interaction between the C-terminal domain and the S4-S5 linker keeps the channel in a closed conformation. An hyperpolarized stimulus disrupts the interaction and the open state could be reached [89, 90]. This interpretation is supported by the phenotype of another HCN4 mutant that we tested: mutations in the position 564 (F564T, F564A) shift the activation curve to a positive value (-80mV), and no effect is observed upon cAMP addition. Moreover the mutation E566K affects the c-di-GMP effect, a confirmation that this molecule binds in the C-linker region and interacts with this residue and that involves only cAMP modulation, because all the other features of the mutant remains unchanged.
The C-linker is a crossroads where distinct signals meet and are integrated: the voltage sensor can contribute through its movement, the CNBD can modulate the voltage dependence within a range (0-17mV), and the C-linker is responsible of the synthesis of these signals that must be transmitted to the pore. Since the modularity of the channels implies that individual modules maintain their independence [55, 91], a good intermediary is required to interpret this signals, and the C-linker seems to be the best candidate in HCN channels.
Our work demonstrate that the C-linker region contains an allosteric binding site for cAMP modulation, and the isoform specificity confirms, in line with our previous studies of different tetramerization properties of HCN CNBDs [8], that real differences exist within HCN1, HCN2 and HCN4.

Bibliography

[1] J. Kuriyan and D. Eisenberg, "The origin of protein interactions and allostery in colocalization.," *Nature*, vol. 450, pp. 983–90, Dec. 2007.

[2] F. Bezanilla, "How membrane proteins sense voltage.," *Nature reviews. Molecular cell biology*, vol. 9, pp. 323–32, Apr. 2008.

[3] R. D. Nelson, G. Kuan, M. H. Saier, and M. Montal, "Modular assembly of voltage-gated channel proteins: a sequence analysis and phylogenetic study.," *Journal of molecular microbiology and biotechnology*, vol. 1, pp. 281–7, Nov. 1999.

[4] S. S. A. T. G. R. Wainger Brian J., DeGennaro Matthew, Santoro Bina, "Molecular mechanism of cAMP modulation of HCN pacemaker channels," vol. 411, no. June, pp. 805–810, 2001.

[5] Y. Murata, H. Iwasaki, M. Sasaki, K. Inaba, and Y. Okamura, "Phosphoinositide phosphatase activity coupled to an intrinsic voltage sensor.," *Nature*, vol. 435, pp. 1239–43, June 2005.

[6] S. S. Taylor and E. Radzio-Andzelm, "Three protein kinase structures define a common motif," *Structure*, vol. 2, pp. 345–355, May 1994.

[7] B. Plugge, S. Gazzarrini, M. Nelson, R. Cerana, J. L. Van Etten, C. Derst, D. DiFrancesco, A. Moroni, and G. Thiel, "A potassium channel protein encoded by chlorella virus PBCV-1.," *Science (New York, N.Y.)*, vol. 287, pp. 1641–4, Mar. 2000.

[8] M. Lolicato, M. Nardini, S. Gazzarrini, S. Möller, D. Bertinetti, F. W. Herberg, M. Bolognesi, H. Martin, M. Fasolini, J. a. Bertrand, C. Arrigoni, G. Thiel, and A. Moroni, "Tetramerization dynamics of C-terminal domain underlies isoform-specific cAMP gating in hyperpolarization-activated cyclic nucleotide-gated channels.," *The Journal of biological chemistry*, vol. 286, pp. 44811–20, Dec. 2011.

[9] B. Hille, *Ionic Channels of Excitable Membranes*. second ed., 1991.

[10] M. Noda, S. Shimizu, T. Tanabe, T. Takai, T. Kayano, T. Ikeda, H. Takahashi, H. Nakayama, Y. Kanaoka, N. Minamino, K. Kangawa, H. Matsuo, M. A. Raftery, T. Hirose, S. Inayama, H. Hayashida, T. Miyata, and S. Numa, "Primary structure of Electrophorus electricus sodium channel deduced from cDNA sequence," *Nature*, vol. 312, pp. 121–127, Nov. 1984.

[11] W. A. Catterall, "Molecular properties of voltage-sensitive sodium channels.," *Annual review of biochemistry*, vol. 55, pp. 953–85, Jan. 1986.

[12] H. R. Guy and P. Seetharamulu, "Molecular model of the action potential sodium channel.," *Proceedings of the National Academy of Sciences of the United States of America*, vol. 83, pp. 508–12, Jan. 1986.

[13] F. V. Campos, B. Chanda, B. Roux, and F. Bezanilla, "Two atomic constraints unambiguously position the S4 segment

relative to S1 and S2 segments in the closed state of Shaker K channel.," *Proceedings of the National Academy of Sciences of the United States of America*, vol. 104, pp. 7904–9, May 2007.

[14] S.-a. Seoh, D. Sigg, D. M. Papazian, and F. Bezanilla, "Voltage-Sensing Residues in the S2 and S4 Segments of the Shaker K channel," *Neuron*, vol. 16, pp. 1159–1167, 1996.

[15] J. J. Lacroix and F. Bezanilla, "Control of a final gating charge transition by a hydrophobic residue in the S2 segment of a K+ channel voltage sensor.," *Proceedings of the National Academy of Sciences of the United States of America*, vol. 108, pp. 6444–9, Apr. 2011.

[16] D. G. Gagnon and F. Bezanilla, "A single charged voltage sensor is capable of gating the Shaker K+ channel," *Journal of General Physiology*, vol. 133, pp. 467–483, 2009.

[17] R. Olcese, L. Toro, F. Bezanilla, and E. Stefani, "Correlation between Charge Movement and Ionic Current during Slow Inactivation in Shaker K+ channel," *Journal of General Physiology*, vol. 110, no. November, 1997.

[18] E. Stefani, L. Toro, E. Perozo, and F. Bezanilla, "Gating of Shaker K+ channels: I. Ionic and gating currents," *Biophysical Journal*, vol. 66, no. 4, pp. 996–1010, 1994.

[19] N. Schoppa, K. McCormack, M. Tanouye, and F. Sigworth, "The size of gating charge in wild-type and mutant Shaker potassium channels," *Science*, vol. 255, pp. 1712–1715, Mar. 1992.

[20] Y. Jiang, A. Lee, J. Chen, V. Ruta, M. Cadene, B. T. Chait, and R. MacKinnon, "X-ray structure of a voltage-dependent K+ channel.," *Nature*, vol. 423, pp. 33–41, May 2003.

[21] S. B. Long, E. B. Campbell, and R. Mackinnon, "Voltage Sensor of Kv1.2: Structural Basis of Electromechanical Coupling," *Science*, vol. 32, no. August, pp. 903–908, 2005.

[22] R. M. Stephen B. Long, Ernest B. Campbell, "Crystal Structure of a Mammalian Voltage-Dependent Shaker Family K Channel," *Science*, no. August, pp. 897–903, 2005.

[23] S. B. Long, X. Tao, E. B. Campbell, and R. MacKinnon, "Atomic structure of a voltage-dependent K+ channel in a lipid membrane-like environment.," *Nature*, vol. 450, pp. 376–82, Nov. 2007.

[24] J. Payandeh, T. Scheuer, N. Zheng, and W. a. Catterall, "The crystal structure of a voltage-gated sodium channel.," *Nature*, vol. 475, pp. 353–8, July 2011.

[25] V. Yarov-yarovoy, D. Baker, and W. A. Catterall, "Voltage sensor conformations in the open and closed states in ROSETTA structural models of K channels," *Proceedings of the National Academy of Sciences of the United States of America*, 2006.

[26] F. Tombola, M. M. Pathak, P. Gorostiza, and E. Y. Isacoff, "The twisted ion-permeation pathway of a resting voltage-sensing domain.," *Nature*, vol. 445, pp. 546–9, Feb. 2007.

[27] Y. Jiang, A. Lee, J. Chen, V. Ruta, M. Cadene, B. T. Chait, and R. MacKinnon, "X-ray structure of a voltage-dependent K+ channel," *Nature*, vol. 423, pp. 33–41, May 2003.

[28] D. M. Starace and F. Bezanilla, "A proton pore in a potassium channel voltage sensor reveals a focused electric field.," *Nature*, vol. 427, pp. 548–53, Feb. 2004.

[29] M. O. Jensen, V. Jogini, D. W. Borhani, A. E. Leffler, R. O. Dror, and D. E. Shaw, "Mechanism of voltage gating in

potassium channels.," *Science (New York, N.Y.)*, vol. 336, pp. 229–33, Apr. 2012.

[30] E. Vargas, V. Yarov-Yarovoy, F. Khalili-Araghi, W. A. Catterall, M. L. Klein, M. Tarek, E. Lindahl, K. Schulten, E. Perozo, F. Bezanilla, and B. Roux, "An emerging consensus on voltage-dependent gating from computational modeling and molecular dynamics simulations," *The Journal of General Physiology*, vol. 140, pp. 587–594, Nov. 2012.

[31] J. S. Santos, S. M. Grigoriev, and M. Montal, "Molecular Template for a Voltage Sensor in a Novel K + Channel. III. Functional Reconstitution of a Sensorless Pore Module from a Prokaryotic Kv Channel," *The Journal of general physiology*, pp. 651–666, 2008.

[32] D. Shaya, M. Kreir, R. a. Robbins, S. Wong, J. Hammon, A. Brüggemann, and D. L. Minor, "Voltage-gated sodium channel (NaV) protein dissection creates a set of functional pore-only proteins.," *Proceedings of the National Academy of Sciences of the United States of America*, vol. 108, pp. 12313–8, July 2011.

[33] M. Sasaki, M. Takagi, and Y. Okamura, "A voltage sensor-domain protein is a voltage-gated proton channel.," *Science (New York, N.Y.)*, vol. 312, pp. 589–92, Apr. 2006.

[34] S. C. Kohout, Susy CBell, L. Liu, Q. Xu, D. L. M. Jr, and . E. Y. Isacoff, "Electrochemical coupling in the voltage-dependent phosphatase Ci-VSP," *Nature chemical biology*, vol. 6, no. 5, pp. 369–375, 2010.

[35] C. A. Villalba-galea, W. Sandtner, D. M. Starace, and F. Bezanilla, "S4-based voltage sensors have three major conformations," *Proceedings of the National Academy of Sciences of the United States of America*, vol. 105, pp. 17600–17607, 2008.

[36] G. A. Haddad and R. Blunck, "Mode shift of the voltage sensors in Shaker K + channels is caused by energetic coupling to the pore domain," *The Journal of general physiology*, pp. 455–472, 2011.

[37] Z. Lu, A. M. Klem, and Y. Ramu, "Ion conduction pore is conserved among potassium channels.," *Nature*, vol. 413, pp. 809–13, Oct. 2001.

[38] M. Caprini, S. Ferroni, R. Planells-Cases, J. Rueda, C. Rapisarda, A. Ferrer-Montiel, and M. Montal, "Structural compatibility between the putative voltage sensor of voltage-gated K+ channels and the prokaryotic KcsA channel.," *The Journal of biological chemistry*, vol. 276, pp. 21070–6, June 2001.

[39] Z. Lu, "Coupling between Voltage Sensors and Activation Gate in Voltage-gated K+ Channels," *The Journal of General Physiology*, vol. 120, pp. 663–676, Oct. 2002.

[40] A. A. Alabi, M. I. Bahamonde, H. J. Jung, J. I. Kim, and K. J. Swartz, "Portability of paddle motif function and pharmacology in voltage sensors.," *Nature*, vol. 450, pp. 370–5, Nov. 2007.

[41] L. Liu, S. C. Kohout, Q. Xu, S. Müller, C. R. Kimberlin, E. Y. Isacoff, and D. L. Minor, "A glutamate switch controls voltage-sensitive phosphatase function.," *Nature structural & molecular biology*, vol. 19, pp. 633–41, June 2012.

[42] D. Dimitrov, Y. He, H. Mutoh, B. J. Baker, L. Cohen, W. Akemann, and T. Knöpfel, "Engineering and characterization of an enhanced fluorescent protein voltage sensor.," *PloS one*, vol. 2, p. e440, Jan. 2007.

[43] C. Pagliuca, T. A. Goetze, R. Wagner, G. Thiel, A. Moroni, and D. Parcej, "Molecular properties of Kcv, a virus

encoded K+ channel.," *Biochemistry*, vol. 46, pp. 1079–90, Jan. 2007.

[44] A. Abenavoli, M. L. DiFrancesco, I. Schroeder, S. Epimashko, S. Gazzarrini, U. P. Hansen, G. Thiel, and A. Moroni, "Fast and slow gating are inherent properties of the pore module of the K+ channel Kcv.," *The Journal of general physiology*, vol. 134, pp. 219–29, Sept. 2009.

[45] A. Moroni, C. Viscomi, V. Sangiorgio, C. Pagliuca, T. Meckel, F. Horvath, S. Gazzarrini, P. Valbuzzi, J. L. Van Etten, D. DiFrancesco, and G. Thiel, "The short N-terminus is required for functional expression of the virus-encoded miniature K(+) channel Kcv.," *FEBS letters*, vol. 530, pp. 65–9, Oct. 2002.

[46] M. Kang, A. Moroni, S. Gazzarrini, D. Difrancesco, G. Thiel, M. Severino, and J. L. V. Etten, "Small potassium ion channel proteins encoded by chlorella viruses," *Proceedings of the National Academy of Sciences of the United States of America*, vol. 101, no. 15, 2004.

[47] D. a. Doyle, "Structural changes during ion channel gating.," *Trends in neurosciences*, vol. 27, pp. 298–302, June 2004.

[48] L. C. Timpe, T. L. Schwarz, B. L. Tempel, D. M. Papazian, Y. N. Jan, and L. Y. Jan, "Expression of functional potassium channels from Shaker cDNA in Xenopus oocytes.," *Nature*, vol. 331, pp. 143–5, Jan. 1988.

[49] S. C. Kohout, M. H. Ulbrich, S. C. Bell, and E. Y. Isacoff, "Subunit organization and functional transitions in Ci-VSP.," *Nature structural & molecular biology*, vol. 15, pp. 106–8, Jan. 2008.

[50] H. Bao, A. Hakeem, M. Henteleff, J. G. Starkus, and M. D. Rayner, "Voltage-insensitive gating after charge-neutralizing mutations in the S4 segment of Shaker channels.," *The Journal of general physiology*, vol. 113, pp. 139–51, Jan. 1999.

[51] A. Lundby, W. Akemann, and T. Knöpfel, "Biophysical characterization of the fluorescent protein voltage probe VSFP2.3 based on the voltage-sensing domain of Ci-VSP.," *European biophysics journal : EBJ*, vol. 39, pp. 1625–35, Nov. 2010.

[52] Q. Li, V. Jogini, S. Wanderling, D. M. Cortes, and E. Perozo, "Expression, Purification, and Reconstitution of the Voltage-Sensing Domain from Ci-VSP.," *Biochemistry*, Oct. 2012.

[53] L. Slabinski, L. Jaroszewski, L. Rychlewski, I. A. Wilson, S. A. Lesley, and A. Godzik, "XtalPred: a web server for prediction of protein crystallizability.," *Bioinformatics (Oxford, England)*, vol. 23, pp. 3403–5, Dec. 2007.

[54] A. L. HODGKIN and A. F. HUXLEY, "A quantitative description of membrane current and its application to conduction and excitation in nerve.," *The Journal of physiology*, vol. 117, pp. 500–44, Aug. 1952.

[55] B. Chanda and F. Bezanilla, "A common pathway for charge transport through voltage-sensing domains.," *Neuron*, vol. 57, pp. 345–51, Feb. 2008.

[56] K. B. Craven and W. N. Zagotta, "CNG AND HCN CHANNELS: Two Peas, One Pod," *Annual review of physiology*, Feb. 2006.

[57] W. Shi, R. Wymore, H. Yu, J. Wu, R. T. Wymore, Z. Pan, R. B. Robinson, J. E. Dixon, D. McKinnon, and I. S. Co-

hen, "Distribution and Prevalence of Hyperpolarization-Activated Cation Channel (HCN) mRNA Expression in Cardiac Tissues," *Circulation Research*, vol. 85, pp. e1–e6, July 1999.

[58] L. M. Monteggia, A. J. Eisch, M. D. Tang, L. K. Kaczmarek, and E. J. Nestler, "Cloning and localization of the hyperpolarization-activated cyclic nucleotide-gated channel family in rat brain," *Molecular Brain Research*, vol. 81, pp. 129–139, Sept. 2000.

[59] B. SANTORO and G. R. TIBBS, "The HCN Gene Family: Molecular Basis of the Hyperpolarization-Activated Pacemaker Channels," *Annals of the New York Academy of Sciences*, vol. 868, pp. 741–764, Apr. 1999.

[60] D. DiFrancesco, "Pacemaker mechanisms in cardiac tissue.," *Annual review of physiology*, vol. 55, pp. 455–72, Jan. 1993.

[61] D. DiFrancesco and D. Noble, "The funny current has a major pacemaking role in the sinus node.," *Heart rhythm : the official journal of the Heart Rhythm Society*, vol. 9, pp. 299–301, Feb. 2012.

[62] E. A. Accili, C. Proenza, M. Baruscotti, and D. DiFrancesco, "From funny current to HCN channels: 20 years of excitation.," *News in physiological sciences : an international journal of physiology produced jointly by the International Union of Physiological Sciences and the American Physiological Society*, vol. 17, pp. 32–7, Feb. 2002.

[63] D. DiFrancesco and P. Tortora, "Direct activation of cardiac pacemaker channels by intracellular cyclic AMP.," *Nature*, vol. 351, pp. 145–7, May 1991.

[64] R. Milanesi, M. Baruscotti, T. Gnecchi-Ruscone, and D. DiFrancesco, "Familial sinus bradycardia associated with a mutation in the cardiac pacemaker channel.," *The New England journal of medicine*, vol. 354, pp. 151–7, Jan. 2006.

[65] J. C. DiFrancesco, A. Barbuti, R. Milanesi, S. Coco, A. Bucchi, G. Bottelli, C. Ferrarese, S. Franceschetti, B. Terragni, M. Baruscotti, and D. DiFrancesco, "Recessive loss-of-function mutation in the pacemaker HCN2 channel causing increased neuronal excitability in a patient with idiopathic generalized epilepsy.," *The Journal of neuroscience : the official journal of the Society for Neuroscience*, vol. 31, pp. 17327–37, Nov. 2011.

[66] H. C. Pape, "Queer current and pacemaker: the hyperpolarization-activated cation current in neurons.," *Annual review of physiology*, vol. 58, pp. 299–327, Jan. 1996.

[67] R. Männikkö, F. Elinder, and H. P. Larsson, "Voltage-sensing mechanism is conserved among ion channels gated by opposite voltages.," *Nature*, vol. 419, pp. 837–41, Oct. 2002.

[68] B. Santoro, S. Chen, a. Luthi, P. Pavlidis, G. P. Shumyatsky, G. R. Tibbs, and S. a. Siegelbaum, "Molecular and functional heterogeneity of hyperpolarization-activated pacemaker channels in the mouse CNS.," *The Journal of neuroscience : the official journal of the Society for Neuroscience*, vol. 20, pp. 5264–75, July 2000.

[69] U. B. Kaupp and R. Seifert, "Molecular diversity of pacemaker ion channels.," *Annual review of physiology*, vol. 63, pp. 235–57, Jan. 2001.

[70] J. Wang, S. Chen, and S. A. Siegelbaum, "Regulation of hyperpolarization-activated HCN channel gating and cAMP modulation due to interactions of COOH terminus and core

transmembrane regions.," *The Journal of general physiology*, vol. 118, pp. 237–50, Sept. 2001.

[71] W. N. Zagotta, N. B. Olivier, K. D. Black, E. C. Young, R. Olson, and E. Gouaux, "Structural basis for modulation and agonist specificity of HCN pacemaker channels.," *Nature*, vol. 425, pp. 200–5, Sept. 2003.

[72] X. Xu, Z. V. Vysotskaya, Q. Liu, and L. Zhou, "Structural basis for the cAMP-dependent gating in the human HCN4 channel.," *The Journal of biological chemistry*, vol. 285, pp. 37082–91, Nov. 2010.

[73] S. Schünke, M. Stoldt, J. Lecher, U. B. Kaupp, and D. Willbold, "Structural insights into conformational changes of a cyclic nucleotide-binding domain in solution from Mesorhizobium loti K1 channel.," *Proceedings of the National Academy of Sciences of the United States of America*, vol. 108, pp. 6121–6, Apr. 2011.

[74] M. Biel, C. Wahl-Schott, S. Michalakis, and X. Zong, "Hyperpolarization-activated cation channels: from genes to function.," *Physiological reviews*, vol. 89, pp. 847–85, July 2009.

[75] G. E. Flynn, K. D. Black, L. D. Islas, B. Sankaran, and W. N. Zagotta, "Structure and rearrangements in the carboxy-terminal region of SpIH channels.," *Structure (London, England : 1993)*, vol. 15, pp. 671–82, June 2007.

[76] J. Kusch, S. Thon, E. Schulz, C. Biskup, V. Nache, T. Zimmer, R. Seifert, F. Schwede, and K. Benndorf, "How subunits cooperate in cAMP-induced activation of homotetrameric HCN2 channels.," *Nature chemical biology*, vol. 8, pp. 162–9, Feb. 2012.

[77] J. Kusch, C. Biskup, S. Thon, E. Schulz, V. Nache, T. Zimmer, F. Schwede, and K. Benndorf, "Interdependence of receptor activation and ligand binding in HCN2 pacemaker channels.," *Neuron*, vol. 67, pp. 75–85, July 2010.

[78] C. Ulens and S. A. Siegelbaum, "Regulation of Hyperpolarization-Activated HCN Channels by cAMP through a Gating Switch in Binding Domain Symmetry," *Neuron*, vol. 40, pp. 959–970, Dec. 2003.

[79] S. S. Chow, F. Van Petegem, and E. a. Accili, "Energetics of cyclic AMP binding to HCN channel C terminus reveal negative cooperativity.," *The Journal of biological chemistry*, vol. 287, pp. 600–6, Jan. 2012.

[80] J. S. Borer, "Antianginal and Antiischemic Effects of Ivabradine, an If Inhibitor, in Stable Angina: A Randomized, Double-Blind, Multicentered, Placebo-Controlled Trial," *Circulation*, vol. 107, pp. 817–823, Feb. 2003.

[81] G. Riccioni, "Ivabradine: recent and potential applications in clinical practice.," *Expert opinion on pharmacotherapy*, vol. 12, pp. 443–50, Feb. 2011.

[82] D. Walsh and S. Van Patten, "Multiple pathway signal transduction by the cAMP-dependent protein kinase," *FASEB J*, vol. 8, pp. 1227–1236, Dec. 1994.

[83] C. S. Chan, R. Shigemoto, J. N. Mercer, and D. J. Surmeier, "HCN2 and HCN1 channels govern the regularity of autonomous pacemaking and synaptic resetting in globus pallidus neurons.," *The Journal of neuroscience : the official journal of the Society for Neuroscience*, vol. 24, pp. 9921–32, Nov. 2004.

[84] L. Moosmang S, Biel M, Hofmann F and W. A., "Differential Distribution of Four Hyperpolarization-Activated

Cation Channels in Mouse Brain : Biological Chemistry," 1999.

[85] B. Santoro, S. Chen, A. Luthi, P. Pavlidis, G. P. Shumyatsky, G. R. Tibbs, and S. A. Siegelbaum, "Molecular and Functional Heterogeneity of Hyperpolarization-Activated Pacemaker Channels in the Mouse CNS," *J. Neurosci.*, vol. 20, pp. 5264–5275, July 2000.

[86] J. W. Taraska, M. C. Puljung, N. B. Olivier, G. E. Flynn, and W. N. Zagotta, "Mapping the structure and conformational movements of proteins with transition metal ion FRET.," *Nature methods*, vol. 6, pp. 532–7, July 2009.

[87] B. Haley, "Adenosine 3 ,5 cyclic monophosphate binding sites," 1977.

[88] D. Ogried, R. Ekanger, R. H. Suva, J. P. Miller, and S. O. Doskeland, "Comparison of the two classes of binding sites (A and B) of type I and type II cyclic-AMP-dependent protein kinases by using cyclic nucleotide analogs," *European Journal of Biochemistry*, vol. 181, pp. 19–31, Apr. 1989.

[89] N. Decher, J. Chen, and M. C. Sanguinetti, "Voltage-dependent gating of hyperpolarization-activated, cyclic nucleotide-gated pacemaker channels: molecular coupling between the S4-S5 and C-linkers.," *The Journal of biological chemistry*, vol. 279, pp. 13859–65, Apr. 2004.

[90] X. Zong, H. Zucker, F. Hofmann, and M. Biel, "Three amino acids in the C-linker are major determinants of gating in cyclic nucleotide-gated channels.," *The EMBO journal*, vol. 17, pp. 353–62, Jan. 1998.

[91] U.-M. Ohndorf and R. MacKinnon, "Construction of a cyclic nucleotide-gated KcsA K+ channel.," *Journal of molecular biology*, vol. 350, pp. 857–65, July 2005.

Part II

1. **The voltage-sensing domain of a phosphatase gates the pore of a potassium channel**. Accepted manuscript on *Journal of General Physiology*, 14/12/2012

2. **Tetramerization Dynamics of C-terminal Domain Underlies Isoform-specific cAMP Gating in Hyperpolarization -activated Cyclic Nucleotide-gated Channels**. *The Journal of Biological Chemistry*, 2011 Dec 30; 286(52): 44811-20.

3. **A second cyclic nucleotide binding site found in HCN4 eliminates the response of the pacemaker current If to cAMP**. Manuscript in preparation.

The voltage-sensing domain of a phosphatase gates the pore of a potassium channel

Cristina Arrigoni[1], Indra Schroeder[2], Giulia Romani[3], James L. Van Etten[4], Gerhard Thiel[2] and Anna Moroni[1,3,*]

[1] Department of Biosciences, Università degli Studi di Milano, Italy

[2] Plant Membrane Biophysics, TU-Darmstadt, Germany

[3] Institute of Biophysics-Milan, Consiglio Nazionale Ricerche, Italy

[4] Department of Plant Pathology and Nebraska Center for Virology, University of Nebraska, Lincoln, NE 68583-0900, USA,

*Correspondence to: Anna Moroni, Department of Biosciences, Via Celoria 26, 20133 Milano, Italy. Email: anna.moroni@unimi.it, phone +39 02 50314826, Fax: +39 02 503 14815

Running title: Synthetic Kv channel

Abstract:

The modular architecture of voltage-gated potassium (Kv) channels suggests that they resulted from the fusion of a voltage-sensing domain (VSD) to a pore module (PM). Here we show that the VSD of *Ciona intestinalis* phosphatase (Ci-VSP) fused to the viral channel Kcv creates Kv_{Synth1}, a functional voltage-gated, outward rectifying potassium channel. Kv_{Synth1} displays the summed features of its individual components: pore properties of Kcv (selectivity and filter gating) and voltage-dependence of Ci-VSP ($V_{1/2}$ = + 56 mV, z ~1) including the depolarization-induced mode shift. The degree of outward rectification of the channel is critically dependent on the length of the linker more than on its amino acid composition. This highlights a mechanic role of the linker in transmitting the movement of the sensor to the pore and shows that electromechanical coupling can occur without co-evolution of the two domains.

Key words: voltage-sensing domain, Ci-VSP, Kcv, Kv channel, synthetic biology

Introduction

Potassium (K^+) channels are modular proteins, composed of a central pore module (PM) surrounded by sensor domains that perceive external stimuli and convert them into changes of pore activity (gating). This feature and simple assessment of their performance by electrophysiological measurements make ion channels amenable for testing the hypothesis that the pore of Kv channels acquired the voltage- sensing domain (VSD) throughout evolution. The modular building concept has several implications. First, it suggests that single domains, once detached from the original channel, can function independently: for instance the PM of the bacterial KvLm channel forms a functional K^+ channel when separated from its VSD domain(Santos et al., 2008). Second, regulatory modules, which control K^+ channels, are also found in proteins with completely different enzymatic functions. A VSD displaying the hallmarks of those of Kv channels is connected to a soluble phosphatase in the sea squirt *C. intestinalis* Ci-VSP protein(Murata et al., 2005). Third, modularity also implies that domains of different classes of channels can be swapped. So far, attempts to exchange entire membrane modules between K^+ channels have been unsuccessful leaving this third implication unfulfilled (Caprini et al., 2001). Only small portions of the two domains, the "paddle" motif of the VSD and the P loop with part of the transmembrane domains of the pore, could be exchanged between K^+ and Na^+ channels (Lu et al., 2001; Alabi et al., 2007; Bosmans et al., 2008). From this it was concluded that membrane modules have coevolved so intimately in Kv proteins that it is impossible to exchange them entirely without loosing functionality of the chimeric channels.

Here, we show that it is possible to obtain a voltage-gated channel in one step by fusing two full-length modules: the VSD of Ci-VSP and the PM of the viral K^+ channel

Kcv (Plugge et al., 2000). These two membrane modules are evolutionary unrelated and there is not any "a priori" indication that they should be able to make a voltage-sensitive channel. The *Ciona* VSD regulates a soluble enzyme. Recent crystal structures capture this VSD in the "resting" and "active" conformations, revealing a ~5 Å translation of the S4 segment that agrees with the sliding helix gating model (Santoro et al., 1998). It was proposed that this movement underlies VSD control of Ci-VSP phosphatase, yet, it remains speculative if this type of conformational change between these states is sufficient for gating a K^+ channel. The second component, the viral channel Kcv, is clearly not designed to be controlled by external stimuli, such as voltage. Apart from a 12 amino acid long N terminus, the channel comprises only the bare PM and has neither additional membrane nor cytosolic domains (Plugge et al., 2000).

Abbreviations used in this paper: Kv, voltage-gated potassium channel; VSD, voltage-sensing domain; Ci-VSP, *Ciona intestinalis* voltage-sensitive phosphatase; TM, transmembrane domain; WT, wild type.

Materials and Methods

Chimaeric constructs

All constructs were inserted into BamHI and XhoI restriction sites of pSGEM vector (a modified version of pGEM-HE). In vitro transcription was performed on linearized plasmids using T7 RNA polymerase (Promega) and cRNAs were injected (50 ng per oocyte) into *Xenopus laevis* oocytes, as previously reported[6]. Electrophysiological measurements were made 3–4 days after injection. Mutations were inserted by site-directed mutagenesis (QuikChange® site-directed mutagenesis kit (Stratagene)) and confirmed by sequencing. Chimaeric constructs were generated by overlapping-PCR from Ci-VSP and PBCV-1 Kcv. Kv_{Synth1} includes aa 1-239 of Ci-VSP and aa 1-94 of Kcv. All constructs reported in Figure 3 were obtained with this procedure.

Electrophysiological measurements

Two-electrode voltage clamp experiments were performed as indicated previously[6] using a GeneClamp 500 amplifier (Axon Instruments) and filtered at 5 kHz. Data acquisition and analysis were done using the pCLAMP8 software package (Axon Instruments). Electrodes were filled with 3M KCl and had a resistance of 0.2–0.8 MΩ in 50 mM KCl. The oocytes were perfused at room temperature (25–27 °C) at a rate of 2 ml/min with a bath solution containing 50 mM KCl (or NaCl), 1.8 mM $CaCl_2$, 1 mM $MgCl_2$, 5 mM Hepes, adjusted to pH 7.4 with KOH (or NaOH). Mannitol was used to adjust the osmolarity of the solution to 215 mosmol/l. $BaCl_2$ diluted from 1 M stocks was added to the solution as indicated. The standard clamp protocol consisted of steps from the holding voltage of −20 mV to voltages in the range -100 mV to +100 mV; tail currents were measured at −80 mV. Instantaneous and steady-state currents were sampled after 10 ms and at the end of the voltage step respectively.

Results

To test whether the voltage-dependent movement of the *Ciona* VSD is able to gate a channel, we created the fusion protein Kv_{Synth1} by adding amino acids 1- 239 of Ci-VSP to the full length Kcv sequence (amino acid 1-94). The fusion protein and its individual components have been expressed in *Xenopus* oocytes and tested by two electrode voltage clamp. Control experiments show that VSD-injected oocytes (Figure 1A) generate small currents, not different from typical water-injected oocytes. Oocytes expressing Kcv alone (Figure 1B) show the typical K^+ currents, previously characterized (Moroni et al., 2002; Gazzarrini et al., 2004; Kang et al., 2004; Gazzarrini et al., 2006; Abenavoli et al., 2009). The current/voltage relationship of Kcv is linear at moderate voltages. At extreme voltages the Ohmic behavior is lost due to a fast gating mechanism that occurs at the selectivity filter and results in a negative slope conductance (Abenavoli et al., 2009). Kv_{Synth1} generates currents that are very different from those of its single components and shows the typical properties of a voltage-gated K^+ channel (Figure 1C). Depolarizing voltages generate large time-dependent currents on top of a small instantaneous component. The corresponding steady-state current-voltage relationship (I/V) shows a strong outward rectification. To quantify the degree of rectification, we use the ratio of steady state currents at +60mV/-100mV (I_{+60mV}/I_{-100mV}). For Kv_{Synth1} it is 13.3 ± 2 (average of 6 oocytes); this ratio is 1 ± 0.1 in Kcv.

Kv_{Synth1} has the permeability properties of Kcv. Replacement of external K^+ with Na^+ shifts the reversal voltage of the fully activated Kv_{Synth1} current by -80 mV ± 6 (s.d. n=3 oocytes) (Fig. 2A) and reduces the outward current, another typical feature of Kcv (Plugge et al., 2000). The estimated relative permeability P_{Na}/P_K of 0.05 ± 0.01 closely resembles the value of 0.03 ± 0.01 previously reported for Kcv (Chatelain et al., 2009).

Another feature of Kcv that is preserved in Kv_{Synth1} is the aforementioned negative slope conductance of the open channel, in this case already visible at ca. -100 mV (Figure 2A). Hence, the fast gating mechanism of Kcv is maintained in the synthetic channel pore. Supplementary Figure 1 summarizes other Kcv properties preserved in Kv_{Synth1}, including K^+ selectivity, voltage-dependent barium block and biochemical evidence that the protein forms a functional tetramer. We also tested the pore mutation F305A that, as expected from our previous results with the Kcv mutant F66A (Plugge et al., 2000), completely abolished the current in Kv_{Synth1} (Supplementary Figure 1D).),. In summary, Kv_{Synth1} displays the pore properties of Kcv, such as selectivity, fast gating and overall pore architecture; these are not modified by the addition of the VSD.

The new property introduced by the VSD is a strong voltage dependency of the currents. The voltage sensor closes the channel at negative potentials and opens it with a slow kinetics at voltages more positive than zero mV ($t_{1/2}$ = 450 ± 74 ms at +60 mV (n=4 oocytes), Figure 1C). The activation curve shown in Figure 2B was determined from the tail currents after subtraction of the instantaneous component (inset of Figure 2B). Kv_{Synth1} has an apparent half activation voltage ($V_{1/2}$) of +56 mV and channel opening is caused by the movement of the equivalent of about one electronic charge across the membrane (z = 0.92). These parameters strongly resemble those reported for the sensing currents of Ci-VSP, either with or without the phosphatase (Murata et al., 2005; Villalba-Galea et al., 2008). The shallow voltage dependency of Kv_{Synth1} with an estimated transfer of ~1 electronic charge is in agreement with the "one click" gating mechanism, recently proposed on the basis of the structural changes of the VSD[7]. To confirm that the VSD is responsible for the voltage-dependent properties of $Kv_{Synth1,}$ we replaced two of the four arginines in the S4 segment, R229 and R232, with glutamines. In Ci-VSP this double

mutation eliminates the 'sensing' currents and generates a voltage-insensitive phosphatase (Murata et al., 2005; Murata and Okamura, 2007). In Kv_{Synth1} the double mutation R229Q/R232Q results in a very small and quasi-Ohmic current (Supplementary Figure 1D); the mutated VSD has apparently lost its tight control on channel opening and voltage-dependency. Another interesting mutation that shifts the Q/V curve of Ci-VSP to the left by 46 mV, is the single neutralization of the gating charge R217 to Q (Villalba-Galea et al., 2008). The same mutation in Kv_{Synth1} resulted in a channel that is already more open at the holding voltage because the activation curve is shifted by 38 mV to the left (Figure 2C, D). Judging from the behavior of these mutants, we conclude that the properties of the VSD are transmitted to the gating of the pore. To examine further details of the causal interplay between VSD and channel gating, we tested whether Kv_{Synth1} also reveals the mode-shift, which has been described for the sensor domain (Villalba-Galea et al., 2008). During a long-lasting depolarization, the voltage sensor enters a "relaxed" conformation in which the voltage–dependency is markedly shifted towards negative potentials. To test this, we measured the tail currents of Kv_{Synth1} R217Q, after holding the same oocyte at two different pre-conditioning voltages, -100 mV and +40 mV. Figure 2E shows that the activation curve is shifted to more negative potentials when the membrane is maintained depolarized for long periods of time. The observed negative shift of about 30 mV (n = 3 oocytes), matches quite well the direction and the amplitude of the shift reported for the VSD (Villalba-Galea et al., 2008). These data further confirm that the properties of the sensor are transmitted to the gating of the pore.

Considerable evidence supports the role of the S4-S5 linker in Kv channels as the transducing element between sensor movement and pore gating (Long et al., 2005). In Kv_{Synth1}, the VSD is directly connected to Kcv, after removal of the 16 amino acid linker

that in Ci-VSP couples the VSD to the phosphatase (Figure 3A, B). Hence, the 12 aa long N terminus of Kcv acts here as the S4-S5 linker of Kv channels and transmits the conformational changes of the sensor to the pore. To study if and how the linker influences gating we varied its length and composition, by combining the N terminus of Kcv and the linker of the VSD, as shown in Figure 3B. All constructs produced functional channels, apart from that with the 28 aa linker that barely expressed and was not further analyzed. Figure 3C shows exemplary currents from constructs with 4, 6 and 20 aa linkers and their corresponding I/V relationships. The first and most cogent observation is that there is a minimum linker length required for efficient control of the voltage sensor on the pore and that the transition is quite sharp. The construct with 4 aa is quite similar to the original channel Kcv, while that with 6 aa shows the typical features of Kv_{Synth1}, rectification and slow kinetics. Extending the linker up to 12 aa doesn't change significantly the properties of Kv_{Synth1} (data not shown), while trespassing this length results in a gradual disappearance of the properties, as evident from the construct with 20 aa linker, showing a predominant instantaneous component and an increase in inward current (see also the corresponding I/V curves in Figure 3C). This trend is summarized in Figure 3D where we have plotted the degree of rectification (I_{+60mV}/I_{-100mV}) as a function of linker length, for all measurable constructs. Interestingly, rectification was not influenced by the amino acid composition because two constructs with a linker of the same length, 20 aa, but of different sequence (see 3B), gave the same result.

Discussion

The addition of Ci-VSD to Kcv is sufficient and necessary to transform a voltage-independent K^+ channel into a Kv type outward rectifier. This finding has several corollaries. First of all it shows unambiguously that the shallow voltage dependency and the sliding helix-type movement of the S4 of *Ciona* VSD[7] are sufficient to gate a channel pore and suggests that this might represent a common mechanism of voltage-dependent gating in ion channels.

Second, it proves that electromechanical coupling between the VSD and the pore can occur even without co-evolution of the interacting surfaces of the two, an apparent requirement in Kv channels (Long et al., 2005; Lee et al., 2009). Another remarkable finding is that coupling is a function of linker length, with an apparent optimal length between 6 and 12 aa, and appears independent of its amino acid composition. We obtained functional coupling in Kv_{Synth1} with completely unrelated sequences, such as the N terminus of Kcv and the C terminus of *Ciona* VSD (see Fig. 3).

Our analysis is in agreement with the idea that a rigid connection, which is presumably provided by a short linker, favors the mechanical coupling between voltage sensor and pore. There is nevertheless a minimal linker length that has to be > 4aa to function.

Third and last, because a primitive channel with poor control on gating can acquire sophisticated voltage regulation via fusion with a regulatory element from another source, it is possible that the appearance of Kv channels occurred in one evolutionary step, as previously suggested (Chanda and Bezanilla, 2008).

References

Abenavoli, A., M.L. DiFrancesco, I. Schroeder, S. Epimashko, S. Gazzarrini, U.P. Hansen, G. Thiel, and A. Moroni. 2009. Fast and slow gating are inherent properties of the pore module of the K+ channel Kcv. *The Journal of general physiology*. 134:219-229.

Alabi, A.A., M.I. Bahamonde, H.J. Jung, J.I. Kim, and K.J. Swartz. 2007. Portability of paddle motif function and pharmacology in voltage sensors. *Nature*. 450:370-375.

Bosmans, F., M.F. Martin-Eauclaire, and K.J. Swartz. 2008. Deconstructing voltage sensor function and pharmacology in sodium channels. *Nature*. 456:202-208.

Caprini, M., S. Ferroni, R. Planells-Cases, J. Rueda, C. Rapisarda, A. Ferrer-Montiel, and M. Montal. 2001. Structural compatibility between the putative voltage sensor of voltage-gated K+ channels and the prokaryotic KcsA channel. *The Journal of biological chemistry*. 276:21070-21076.

Chanda, B., and F. Bezanilla. 2008. A common pathway for charge transport through voltage-sensing domains. *Neuron*. 57:345-351.

Chatelain, F.C., S. Gazzarrini, Y. Fujiwara, C. Arrigoni, C. Domigan, G. Ferrara, C. Pantoja, G. Thiel, A. Moroni, and D.L. Minor, Jr. 2009. Selection of inhibitor-resistant viral potassium channels identifies a selectivity filter site that affects barium and amantadine block. *PloS one*. 4:e7496.

Gazzarrini, S., A. Abenavoli, D. Gradmann, G. Thiel, and A. Moroni. 2006. Electrokinetics of miniature K+ channel: open-state V sensitivity and inhibition by K+ driving force. *The Journal of membrane biology*. 214:9-17.

Gazzarrini, S., M. Kang, J.L. Van Etten, S. Tayefeh, S.M. Kast, D. DiFrancesco, G. Thiel, and A. Moroni. 2004. Long distance interactions within the potassium channel pore are revealed by molecular diversity of viral proteins. *The Journal of biological chemistry*. 279:28443-28449.

Kang, M., A. Moroni, S. Gazzarrini, D. DiFrancesco, G. Thiel, M. Severino, and J.L. Van Etten. 2004. Small potassium ion channel proteins encoded by chlorella viruses. *Proceedings of the National Academy of Sciences of the United States of America*. 101:5318-5324.

Lee, S.Y., A. Banerjee, and R. MacKinnon. 2009. Two separate interfaces between the voltage sensor and pore are required for the function of voltage-dependent K(+) channels. *PLoS biology*. 7:e47.

Li, Q. et al. Structural mechanism of voltage-dependent gating in an isolated voltage-sensing domain. *Science* Submitted.

Long, S.B., E.B. Campbell, and R. Mackinnon. 2005. Voltage sensor of Kv1.2: structural basis of electromechanical coupling. *Science*. 309:903-908.

Lu, Z., A.M. Klem, and Y. Ramu. 2001. Ion conduction pore is conserved among potassium channels. *Nature*. 413:809-813.

Moroni, A., C. Viscomi, V. Sangiorgio, C. Pagliuca, T. Meckel, F. Horvath, S. Gazzarrini, P. Valbuzzi, J.L. Van Etten, D. DiFrancesco, and G. Thiel. 2002. The short N-terminus is required for functional expression of the virus-encoded miniature K(+) channel Kcv. *FEBS letters*. 530:65-69.

Murata, Y., H. Iwasaki, M. Sasaki, K. Inaba, and Y. Okamura. 2005. Phosphoinositide phosphatase activity coupled to an intrinsic voltage sensor. *Nature*. 435:1239-1243.

Murata, Y., and Y. Okamura. 2007. Depolarization activates the phosphoinositide phosphatase Ci-VSP, as detected in Xenopus oocytes coexpressing sensors of PIP2. *The Journal of physiology*. 583:875-889.

Plugge, B., S. Gazzarrini, M. Nelson, R. Cerana, J.L. Van Etten, C. Derst, D. DiFrancesco, A. Moroni, and G. Thiel. 2000. A potassium channel protein encoded by chlorella virus PBCV-1. *Science*. 287:1641-1644.

Santoro, B., D.T. Liu, H. Yao, D. Bartsch, E.R. Kandel, S.A. Siegelbaum, and G.R. Tibbs. 1998. Identification of a gene encoding a hyperpolarization-activated pacemaker channel of brain. *Cell*. 93:717-729.

Santos, J.S., S.M. Grigoriev, and M. Montal. 2008. Molecular template for a voltage sensor in a novel K+ channel. III. Functional reconstitution of a sensorless pore module from a prokaryotic Kv channel. *The Journal of general physiology*. 132:651-666.

Villalba-Galea, C.A., W. Sandtner, D.M. Starace, and F. Bezanilla. 2008. S4-based voltage sensors have three major conformations. *Proceedings of the National Academy of Sciences of the United States of America*. 105:17600-17607.

Acknowledgements. We thank Dan Minor (UCSF) for the generous gift of the Ci-VSP clone and for helpful discussion. This work was partially supported by PRIN 2008, SAL-49 Progetto di Cooperazione Scientifica e Tecnologica Regione Lombardia, Cariplo 2009-3519, (AM), by LOEWE initiative Soft Control (GT) and by NSF-EPSCoR (grant EPS-1004094 (JLVE) and grant P20-RR15635 from the COBRE program of the National Center for Research Resources (JLVE).

Figure legends

Figure 1- The synthetic channel Kv_{Synth1} is an outward rectifier.

Top: cartoons of the individual components and of the fusion protein Kv_{Synth1}. (A) VSD is the voltage-sensing domain (aa 1-239) of Ci-VSP (*2*); S1-S4 indicate the 4 transmembrane domains of the VSD. (B) Kcv is the full length (aa 1-94) viral K^+ channel *(6)*; TM1, TM2 and P indicate respectively the two transmembrane domains and the pore loop of Kcv. (C) Kv_{Synth1} is the 333 aa fusion protein of VSD and Kcv. Middle: Currents recorded by TE-voltage clamp in oocytes injected with the three constructs. Dotted line indicates zero current level. Voltage protocol: V_h -20 mV, test voltages +100 to -100 mV (-200 mV for Kcv), tail -80 mV. Test pulse length is 8.5 s in A and C and 0.6 s in B. Bottom: corresponding steady state I/V relationships. All experiments were performed in 50 mM $[K^+]_{out}$.

Figure 2- Biophysical properties of Kv_{Synth1}. (A) Kv_{Synth1} selects K^+ over Na^+. Current reversal potential recorded from the same oocyte was -20 mV in 50 mM $[K^+]_{out}$ (●) and -98 mV in 50 mM $[Na^+]_{out}$ (○). Voltage protocol: pre-pulse voltage step at +60 mV followed by testing voltages from +60 to -180 mV. Arrowhead marks the point of data collection. (B) Voltage dependency of Kv_{Synth1}. Activation curve of Kv_{Synth1} constructed from tail currents (inset) after subtracting the instantaneous current offset. Voltage protocol as in Figure 1C. Data sets (n=6) were jointly fitted to a two-state Boltzmann equation (dotted line) of the form $y = (1 + e^{zF(V - V_{1/2}) / RT})^{-1}$ where z is the effective charge, $V_{1/2}$ is the half activation voltage, F, R and T have their usual thermodynamic meaning. Data were normalized to the extrapolated maximum current. Points represent mean ± s.e.m. $V_{1/2}$ = 56 mV, z = 0.92. (C) Exemplary currents recorded from wt Kv_{Synth1}

(control) and its R217Q mutant. Traces have been normalized to the current value recorded at +60 mV. (D) Activation curve of the R217Q mutant (●) constructed as in B from 4 data sets: $V_{1/2}$ = 18 mV, z = 1.1. The curve of the wt (dotted line) is re-plotted from B for comparison. (E) The activation of the R217Q mutant depends on the pre-conditioning voltage. The same R217Q expressing oocyte was subjected to the following protocol: pre-conditioning (5 s) at either -100 mV or + 40 mV; test pulses (1.2 s) from -120 mV to +30 mV. Tail currents (at -80 mV) are plotted for pre-conditioning at -100 mV (○) or at + 40 mV (●). The test pulses were kept short to maintain the effect of the preconditioning voltages; hence data in E do not reflect full activation of the channel.

Figure 3- The length of the linker connecting the VSD to the pore affects the degree of rectification in Kv_{Synth1} constructs. (A) Expanded view of the sequences of the two sequences that where variably combined to form the Kv_{Synth1} linker. (B) List of linkers that have been tested in Kv_{Synth1}, their amino acid (aa) length and amino acid sequences (color coded as in panel A). (C) Exemplary current traces recorded from Kv_{Synth1} constructs with the 4, 6 and 20 aa linkers and their corresponding current-voltage relationships (color coded). (D) The degree of current rectification (I_{+60mV}/I_{-100mV}) is plotted as a function of linker length for all functional constructs. Data are mean ± s.e.m. ($n \geq 3$). Experimental data (with the exclusion of the value corresponding to the construct with a 4 aa linker that loses the rectification) have been interpolated with a logistic function (black line) in which the lower asymptote was set to 1, corresponding to the value measured in Kcv that lacks rectification (dotted line).

Figure 1

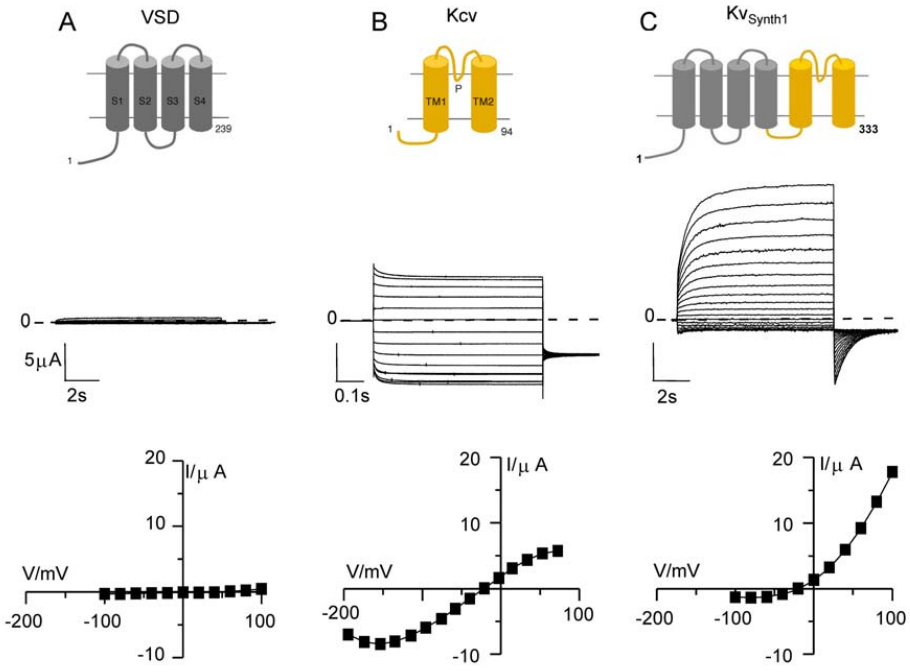
A
VSD
S1
S2
S3
S4
239
1
B
Kcv
P
TM1
TM2
1
94
C
Kv Synth1
333
1
0
5μA
2s
0
0.1s
0
2s
20
I/μ A
10
V/mV
-200
-100
100
-10
20
I/μ A
10
V/mV
-200
100
-10
20
I/μ A
10
V/mV
-200
-100
100
-10

Figure 2

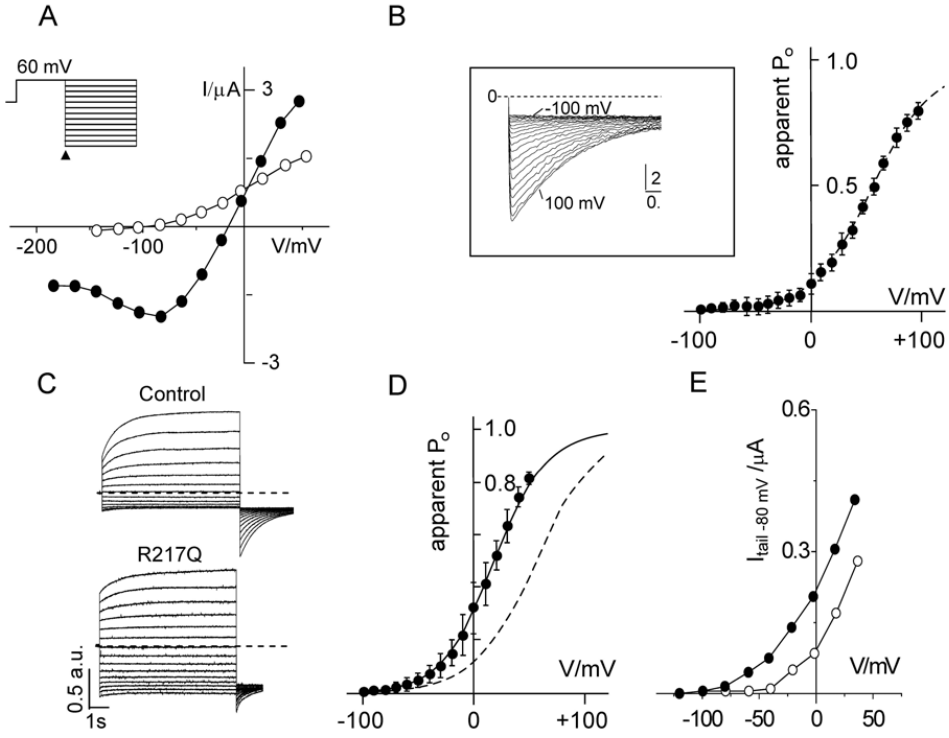
A
60 mV
I/μA
3
-3
-200
-100
V/mV
B
0
-100 mV
100 mV
2
0.
apparent P$_o$
1.0
0.5
V/mV
-100
0
+100
C
Control
R217Q
0.5 a.u.
1s
D
apparent P$_o$
1.0
0.8
V/mV
-100
0
+100
E
0.6
0.3
I$_{tail\ -80\ mV}$ /μA
V/mV
-100
-50
0
50

Figure 3

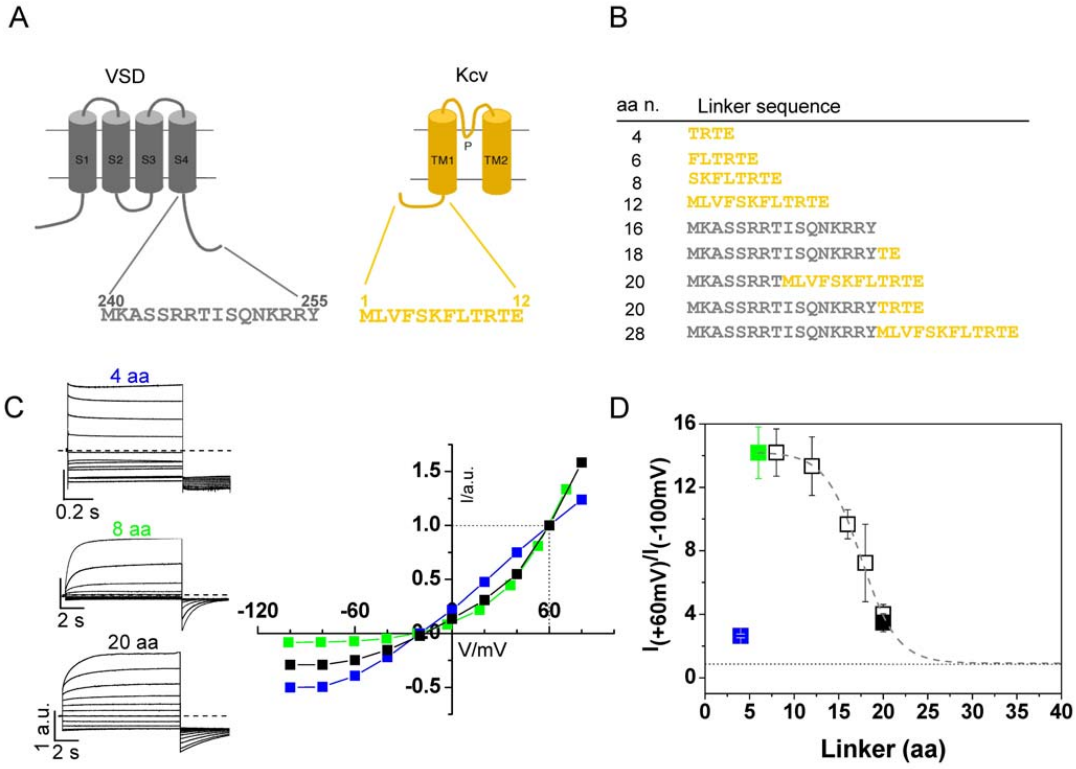
A
VSD
Kcv
S1
S2
S3
S4
TM1
P
TM2
240
255
MKASSRRTISQNKRRY
1
12
MLVFSKFLTRTE
B
aa n.
Linker sequence
4 TRTE
6 FLTRTE
8 SKFLTRTE
12 MLVFSKFLTRTE
16 MKASSRRTISQNKRRY
18 MKASSRRTISQNKRRYTE
20 MKASSRRTMLVFSKFLTRTE
20 MKASSRRTISQNKRRYTRTE
28 MKASSRRTISQNKRRYMLVFSKFLTRTE
C
4 aa
0.2 s
8 aa
2 s
20 aa
1 a.u.
2 s
-120
-60
60
V/mV
1.5
1.0
0.5
-0.5
I/a.u.
D
I(+60mV)/I(-100mV)
16
12
8
4
0
0
5
10
15
20
25
30
35
40
Linker (aa)

Supplementary Figure 1

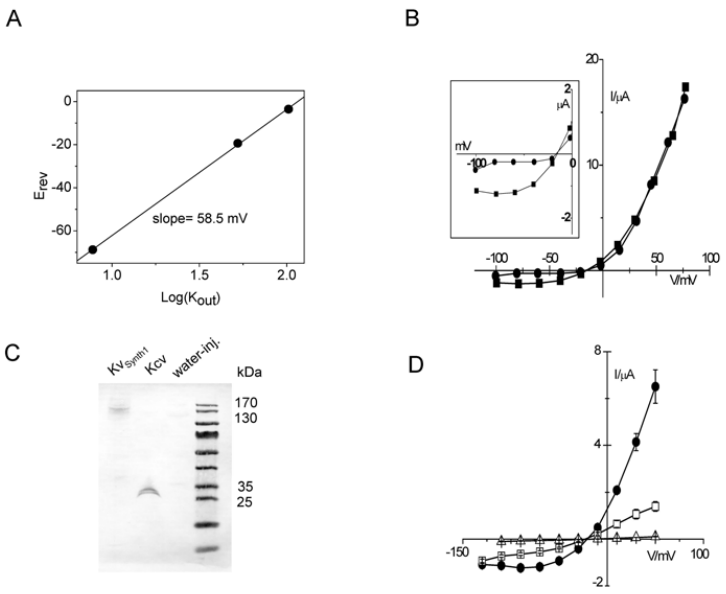

Supplementary Figure 1- K^+ selectivity, barium block, tetramerization and effect of mutations in Kv_{Synth1}.

(A) Nernst plot: Kv_{Synth1} current reversal potential (E_{rev}) plotted as a function of external K^+ concentration (Lg[K^+]out). Black line is the linear regression to mean E_{rev} values (n=3). (B) Effect of Barium on Kv_{Synth1} current. Steady-state currents recorded in: (■) control solution (50 mM K^+) and (●) + 1mM $BaCl_2$. The addition of barium blocks the inward current and affects the outward current, as previously reported for native Kcv channel *(6)*. (C) Western blot analysis performed total protein extract from oocytes with a monoclonal antibody (8D6) that recognizes the tetramer of Kcv, but not the monomer. The expected MW of Kcv and Kv_{Synth1} tetramers are 42,5 and 149 kDa, respectively. (D) Steady state current/voltage relationships of the single mutant F305A (Δ), the double mutant R229Q/R232Q (□) and the wt Kv_{Synth1} (●). Points represent mean ± s.e.m. (n=6). Currents in B and D were recorded from a holding potential (V_h) of -20 mV to the indicated test voltages (8.5 s in B, 600 ms in D).

THE JOURNAL OF BIOLOGICAL CHEMISTRY VOL. 286, NO. 52, pp. 44811–44820, December 30, 2011

Tetramerization Dynamics of C-terminal Domain Underlies Isoform-specific cAMP Gating in Hyperpolarization-activated Cyclic Nucleotide-gated Channels*[S]

Received for publication, August 25, 2011, and in revised form, October 13, 2011 Published, JBC Papers in Press, October 17, 2011, DOI 10.1074/jbc.M111.297606

Marco Lolicato[‡], Marco Nardini[§], Sabrina Gazzarrini[‡], Stefan Möller[¶], Daniela Bertinetti[¶], Friedrich W. Herberg[¶], Martino Bolognesi[§], Holger Martin[‡], Marina Fasolini[‖], Jay A. Bertrand[‖], Cristina Arrigoni[‡], Gerhard Thiel[**], and Anna Moroni[‡1]

From the [‡]Department of Biology and Consiglio Nazionale delle Ricerche-Istituto di Biofisica and the [§]Department of Biomolecular Sciences and Biotechnology, University of Milan, Via Celoria 26, 20133 Milan, Italy, the [¶]Department of Biochemistry, University of Kassel, Heinrich Plett Strasse 40, 34132 Kassel, Germany, [‖]Nerviano Medical Sciences Srl, Oncology, Viale Pasteur 10, 20014 Nerviano (MI), Italy, and the [**]Institute of Botany, Technische Universität Darmstadt, Schnittspahnstrasse 3, 64287 Darmstadt, Germany

Background: HCN2 and HCN4 respond to cAMP, whereas HCN1 does not.
Results: The C-linker plus CNBD of HCN2 and HCN4 show cAMP-induced tetramerization, whereas that of HCN1 contains prebound cAMP and is tetrameric.
Conclusion: HCN1 does not respond to the addition of cAMP because its CNBD contains cAMP already.
Significance: Tetramerization of the C terminus controls ligand gating in HCN channels.

Hyperpolarization-activated cyclic nucleotide-gated (HCN) channels are dually activated by hyperpolarization and binding of cAMP to their cyclic nucleotide binding domain (CNBD). HCN isoforms respond differently to cAMP; binding of cAMP shifts activation of HCN2 and HCN4 by 17 mV but shifts that of HCN1 by only 2–4 mV. To explain the peculiarity of HCN1, we solved the crystal structures and performed a biochemical-biophysical characterization of the C-terminal domain (C-linker plus CNBD) of the three isoforms. Our main finding is that tetramerization of the C-terminal domain of HCN1 occurs at basal cAMP concentrations, whereas those of HCN2 and HCN4 require cAMP saturating levels. Therefore, HCN1 responds less markedly than HCN2 and HCN4 to cAMP increase because its CNBD is already partly tetrameric. This is confirmed by voltage clamp experiments showing that the right-shifted position of $V_{½}$ in HCN1 is correlated with its propensity to tetramerize *in vitro*. These data underscore that ligand-induced CNBD tetramerization removes tonic inhibition from the pore of HCN channels.

Hyperpolarization-activated cyclic nucleotide-gated (HCN)[2] channels underlie the I_f/I_h cation currents that control pacemaker activity in the heart and brain (1–3). HCN channels belong to the superfamily of the six-transmembrane domain segment voltage-gated K^+ channels and are dually activated by membrane hyperpolarization and binding of cAMP to their cyclic nucleotide binding domain (CNBD) (4–6). Increase in the cytosolic cAMP concentration shifts the channel voltage dependence to more positive potentials, thereby increasing the open probability and current at a given voltage. In this respect, the three most studied isoforms, HCN1, HCN2, and HCN4, behave differently. HCN2 and HCN4 respond to saturating cAMP levels by shifting the activation curve of +17 mV, whereas HCN1 only shifts it by +4 mV (7). Interestingly, the behavior of HCN1 seems not to be due to a lower affinity of this isoform for cAMP because dose-response curves obtained in patch clamp recordings in inside-out configuration indicate similar nanomolar affinity for HCN1 and HCN2 activation (7, 8).

The current understanding of ligand-induced gating in HCN channels is that cAMP binding releases the tonic inhibition exerted by the cytoplasmic CNBD on the channel pore. This mechanism probably involves cAMP-induced tetramerization of the CNBD and is supported by two lines of evidence. On one side, removal of the cytosolic domain, by enzymatic digestion in the native I_f channels (9) or by gene manipulation in HCN clones (10), mimics the action of cAMP and shifts the activation curve of the channels to more depolarized potentials. On the other side, the addition of saturating cAMP concentrations promotes the tetramerization of the isolated cytosolic fragment (consisting of the CNBD and the C-linker) of HCN2 and HCN4 in solution (11, 12). Furthermore, it has been shown in HCN2 that promotion of tetramerization induced by a tripeptide

* This work was supported in part by European Union Grant EDICT (European Drug Initiative on Channels and Transporters) and Progetto di Cooperazione Scientifica e Tecnologica Regione Lombardia (to A. M.) and European Union grant Affinity Proteome and Affinomics (to F. W. H.).
[S] The on-line version of this article (available at http://www.jbc.org) contains supplemental Tables I–IV and Figs. 1–3.
The atomic coordinates and structure factors (codes 3U0Z, 3U10, 3U11) have been deposited in the Protein Data Bank, Research Collaboratory for Structural Bioinformatics, Rutgers University, New Brunswick, NJ (http://www.rcsb.org/).
[1] To whom correspondence should be addressed: Dept. of Biology, CNR-IBF, Via Celoria 26, 20133 Milan, Italy. Tel.: 02-5031-4826; Fax: 02-5031-4815; E-mail: anna.moroni@unimi.it.
[2] The abbreviations used are: HCN, hyperpolarization-activated cyclic nucleotide-gated; CNBD, cyclic nucleotide binding domain; MBP, maltose-binding protein; FP, fluorescence polarization; SPR, surface plasmon resonance; ITC, isothermal titration calorimetry; 8-AHA-cAMP, 8-(6-aminohexylamino)-adenosine-3′,5′-cyclic monophosphate.

mutation in the C-linker facilitated channel opening in the absence of cAMP (13).

With this background, we have focused our attention on HCN1 in order to explain its peculiar properties that include, besides a weak response to cAMP, also a right-shifted activation curve, when compared with the other isoforms (7, 8, 10), indicating that this isoform might partially lack the inhibition of the CNBD. To this end, we have solved the crystal structures of the cytosolic fragment (C-linker plus CNBD) of HCN1, HCN2, and HCN4 and compared them. Furthermore, we have systematically analyzed the ligand binding and ligand-induced tetramerization properties of the three proteins in solution. Our results show that the C-terminal fragment of HCN1 differs from those of HCN2 and HCN4 because it forms tetramers already at basal cAMP concentration, whereas tetramerization of the C-terminal domain of HCN2 and HCN4 requires saturating cAMP levels. This finding explains the modest response of HCN1 to the addition of cAMP *in vivo* and, in general, offers an experimental proof to the leading hypothesis that cAMP-induced tetramerization of the C-terminal domain of HCN channels removes the inhibition exerted by this domain on the pore gating.

EXPERIMENTAL PROCEDURES

Protein Preparation—The cDNA fragments comprised the C-linker and CNBD (CB) and encoded the following residues: 470–672 (human $HCN2_{CB}$), 521–723 (human $HCN4_{CB}$), 390–592 (mouse $HCN1_{CB}$), and 441–592 (ΔC-linker $HCN1_{CNBD}$).

The fragments were cloned into a modified pET-24b downstream of a double His_6-maltose-binding protein (MBP) tag and transformed into *Escherichia coli* Rosetta strain. Cells were grown at 37 °C in Luria broth to 0.6 A_{600} and induced with 0.4 mM isopropyl 1-thio-β-D-galactopyranoside overnight at 20 °C. The cells were collected by centrifugation and resuspended in ice-cold lysis buffer (30 mM Hepes, pH 7.4, 500 mM NaCl, 10% glycerol, 1 mM β-mercaptoethanol) with the addition of 10 μg/ml DNase, 0.25 mg/ml lysozyme, 100 μM phenylmethylsulfonyl fluoride, 5 μM leupeptin, and 1 μM pepstatin. The cells were sonicated on ice 12 times for 20 s each, and the lysate was cleared by centrifugation. The proteins were purified by affinity chromatography on Ni^{2+}-NTA and eluted in lysis buffer plus 300 mM imidazole. The His_6-MBP was removed by HRV3C cleavage overnight at 4 °C. The cleavage reaction was loaded onto an amylose resin (New England Biolabs), and the flow-through was collected and loaded onto a HiLoad 16/60 Superdex 200 prep grade size exclusion column (GE Healthcare) that was equilibrated with lysis buffer. Analysis presented in Fig. 3 and Fig. 5 was performed with Superdex 200 5/150 GL (GE Healthcare). Protein concentration was 1.5 mg/ml. Buffer contained 100 mM NaCl, 20 mM Hepes, pH 7.0, 10% glycerol with or without cAMP.

Fluorescence Polarization—The direct fluorescence polarization (FP) assay was performed following in principle the procedure from Moll *et al.* (14). 8-Fluo-cAMP and 8-Fluo-cGMP were purchased from the Biolog Life Science Institute (Bremen, Germany). Fine chemicals (research grade) were purchased from Sigma. The measurements were performed in 150 mM NaCl, 20 mM MOPS, 0.005% (v/v) CHAPS, pH 7.0, using the Fusion™ α-FP microtiter plate reader at room temperature in a 384-well microtiter plate (PerkinElmer, Optiplate, black). The protein concentration was varied (from 50 μM to 12 pM), and the concentration of 8-Fluo-cAMP/8-Fluo-cGMP was fixed at 1 nM. The FP signal was detected for 2 s at excitation of 485 nm and emission FP filter of 535 nm with a photomultiplier tube voltage of 1,100. Data were analyzed with GraphPad Prism 5.03 (GraphPad Software, San Diego, CA) by plotting the FP signal in millipolarization units (mPol) against the logarithm of the HCN concentration.

Isothermal Titration Calorimetry—Measurements were carried out at 25 °C using an iTC_{200} microcalorimeter (MicroCal, GE Healthcare). The volume of sample cell was 0.2 ml; the reference cell contained water. The proteins were extensively dialyzed against PBS plus 10% glycerol, and the same buffer was used to dissolve cAMP. The proteins (11–75 μM) were titrated with cAMP (250–900 μM) using injection volumes of 1–2 μl. Calorimetric data were analyzed with Origin software (version 7, MicroCal), using equations described for the single-site binding model (15).

Surface Plasmon Resonance Measurements—Protein/nucleotide interactions were monitored as solution competition experiments and were performed using a Biacore 3000 instrument (Biacore GE Healthcare) at 20 °C.

A carboxymethylated sensor chip surface (CM5, research grade, Biacore GE Healthcare) was activated for covalent coupling of 8-AHA-cAMP as described previously (16). Running buffer was PBS, pH 7.4, plus 0.005% (v/v) surfactant P20. Proteins (100 nM) were preincubated with varying concentrations of free cAMP and injected over the 8-AHA-cAMP surface. Surface plasmon resonance (SPR) signals indicate binding of the respective proteins to the cAMP analog 8-AHA-cAMP covalently linked to the sensor chip. The association was monitored for 3 min, and the binding signal was collected at the end of the association phase. The resulting binding signals were plotted against the logarithm of the free cAMP concentration, and the EC_{50} values were calculated form the dose-response curve.

Crystallization—Crystallization trials were set up in 96-well sitting drop plates (Greiner) using the Oryx 8.0 crystallization robot (Douglas Instruments) and stored at 4 °C. Crystals of the mHCN1-cAMP complex (protein concentration 10 mg/ml, 5 mM cAMP) were grown by vapor diffusion, using as a precipitant solution 20–22% PEG 3350, 400 mM sodium acetate buffer, pH 5.0. Crystals usually grew in 2 weeks and were cryoprotected with the same crystallization well solution supplemented with 30% glycerol prior to cryocooling in liquid nitrogen. A full data set was collected to 2.9 Å resolution using synchrotron radiation (ID29 beamline, ESRF, Grenoble, France). Crystals of the human HCN2-cAMP complex (protein concentration 10–13 mg/ml, 5 mM cAMP) were grown by vapor diffusion, using as a precipitant solution 20% PEG 8000, 500 mM NaCl, 100 mM citrate buffer, pH 4.6, 10% glycerol. A full data set was collected to 2.3 Å resolution (ID23-2 beamline, ESRF, Grenoble, France). Crystals of the human HCN4-cAMP complex (protein concentration 10 mg/ml, 5 mM cAMP) were grown by vapor diffusion using as a precipitant solution 25% PEG 3350, 400 mM sodium acetate buffer, pH 5.0 (with/without 500 mM dibasic ammonium phosphate). A full data set was collected to 2.5 Å resolution (ID29 beamline, ESRF, Grenoble, France). Raw data were

processed with Mosflm (17) and Scala (18), and the structures were solved by molecular replacement using the program MolRep (19). The crystal structure of mouse HCN2 in complex with cAMP (11) (Protein Data Bank entry 1Q43) was used as search model. To avoid model bias, the bound cAMP was removed from the search model, and the side chains were truncated to Ala in cases of mismatch between the amino acid sequences. Several cycles of manual rebuilding, using the program COOT (20), and refinement, using the program REFMAC (21) (rigid body and restrained refinement), were carried out to improve the electron density map, and the side chains omitted in the search model were rebuilt into the electron density.

The final *R*-factor/*R*-free for HCN1-cAMP, HCN2-cAMP, and HCN4-cAMP are 20.5%/27.5%, 20.2%/27.1%, and 19.3%/27.7%, respectively (supplemental Table 1). Residue 586 of HCN4-cAMP has been modeled and refined as *S*-hydroxycysteine (probably induced by x-ray oxidation). The program Procheck (22) was used to assess protein stereochemical quality. The program PISA (23) was used to identify and analyze the quaternary assemblies. Atomic coordinates and structure factors have been deposited with the Protein Data Bank, with entry codes 3U0Z, 3U10, and 3U11 for HCN1-cAMP, HCN2-cAMP, and HCN4-cAMP, respectively.

Analytical Ultracentrifugation—Sedimentation Velocity experiments were performed at 20 °C using a Optima XL-I Ultracentrifuge (Beckman Coulter) with an An50 Ti rotor at a rotor speed of 50,000 rpm. Data were acquired by monitoring absorbance at 280 nm through sapphire cell windows, in Epon sectors. Proteins (2.5 mg/ml) were run at 100 μM, and the related gel filtration buffer was used as a blank (20 mM Hepes, pH 7.0, 150 mM NaCl, 10% glycerol). cAMP at a concentration of 0.3 mM was added directly to the protein and reference solutions. Data were analyzed with the software SEDFIT (24) to determine the sedimentation coefficients of the proteins in solution. Solvent density (1.028 g/ml), partial specific volume (0.7354 ml/g), and viscosity (0.013284 g/s/cm) were calculated using the SEDNTERP program (available on the World Wide Web). The oligomeric states of the proteins were determined by comparing the sedimentation coefficients from SEDFIT with those calculated using the crystallographic coordinates and the program HYDROPRO (25).

Dynamic Light Scattering—Experiments were conducted using a Protein Solutions DynaPro 99 instrument with a DynaProMSTC200 microsampler (Protein Solutions, Charlottesville, VA). Protein concentration was 1 mg/ml. Buffer contained 20 mM Hepes, pH 7.0, 150 mM NaCl, 10% glycerol with or without 2.5 mM cAMP. Acquisition was performed at 10 °C with Dynamics 5, 30–50 scans, 30 s/scan. Data analysis was performed with Dynamics 6 software.

Determination of cAMP Content— cAMP was released by boiling the protein sample (~1 mg) in 100 μl of lysis buffer for 2 min. The boiled sample was centrifuged at maximum speed for 10 min at room temperature, and the supernatant was collected and added with 900 μl of 5 mM ammonium bicarbonate. The sample was loaded onto an anion exchange chromatography column (HiTrapQ (1 ml), GE Healthcare), previously equilibrated with 5 mM ammonium bicarbonate. Unbound molecules were washed out with 7 ml of 5 mM ammonium bicarbonate. The cAMP was eluted with a linear gradient of ammonium bicarbonate (5–1000 mM) in 20 column volumes.

Electrophysiology—Site-directed mutagenesis on pGHE:: mHCN1 was performed using the QuikChange mutagenesis kit (Stratagene). All of the constructs were linearized and transcribed into cRNA using T7 polymerase (T7 Riboprobe® system, Promega). Oocyte preparation and cRNA transcription were performed according to standard procedures as reported previously (26). Oocytes were injected with 50 nl of cRNA solution each, at a concentration of 0.5 μg/μl. Two-electrode voltage clamp recordings were performed 2 days after cRNA injection using a GeneClamp 500 amplifier (Axon Instruments) and digitized at 50 kHz with a Digidata 1200 (Axon Instruments). Data acquisition and analysis were done using the pCLAMP8 software package (Axon Instruments). Microelectrodes filled with 3 M KCl had resistances of 0.5–2.0 megaohms. Oocytes were bathed in extracellular solution containing 98 mM KCl, 2 mM NaCl, 5 mM HEPES, pH 7.5, 1.8 mM $CaCl_2$, and 1 mM $MgCl_2$. Three-second-long voltage steps were applied in 10-mV increments from a holding potential of −30 mV. Peak tail current amplitudes were measured at −40 mV, and tail current *I*-V curves were fitted using the Boltzmann equation, $I(V) = A1 + A2/(1 + \exp((V - V_{½})/s))$.

RESULTS

cAMP Binding Affinity Measurements—We have prepared three constructs, hereafter termed $HCN1_{CB}$, $HCN2_{CB}$, and $HCN4_{CB}$, comprising the C-linker and the CNBD domains of mouse HCN1, human HCN2, and human HCN4, respectively. The three constructs differ by 26 substitutions in total, 14 of which occur in $HCN1_{CB}$ (supplemental Fig. 1). The purified proteins were tested for cyclic nucleotide binding with three different techniques: FP, SPR, and isothermal titration calorimetry (ITC). The three proteins showed similar binding affinities when tested with the same technique (Table 1), but different techniques gave quite different absolute values (12). In FP measurements, all three proteins bind the 8-Fluo-cAMP analog in the nanomolar range (Table 1). Notably, the highest affinities were measured with the maltose-binding protein fused at the N terminus of the HCN proteins (MBP-HCN_{CB}). Fig. 1 shows exemplary curves in which K_D values of 39.7, 82.0, and 39.2 nM were calculated for MBP-HCN1, MBP-HCN2, and MBP-HCN4 constructs, respectively. These results are remarkably similar to the $K_{½}$ values obtained in patch clamp experiments: 60 and 100 nM for HCN1 and HCN2, respectively (8).

The measured affinity of the HCN proteins for 8-Fluo-cGMP was significantly lower than that for 8-Fluo-cAMP, at least for HCN2 and HCN4, but still in the nanomolar range. Notably, patch experiments had previously reported micromolar $K_{½}$ for HCN2 (11, 27). This observation suggests that the higher $K_{½}$ values for cGMP might be related to a lower efficacy of this ligand in promoting gating.

When we measured binding with other techniques, we obtained 10 times lower affinities. Binding of cAMP by ITC showed micromolar affinity with and without the MBP constructs: for MBP-$HCN2_{CB}$, $K_D = 3.06 \pm 0.7$ μM; for MBP-$HCN4_{CB}$, $K_D = 0.97 \pm 0.7$ μM; and for $HCN2_{CB}$, $K_D = 3.6 \pm 1.3$ μM (Table 1 and supplemental Fig. 2). For unclear reasons, we

TABLE 1

Comparison of binding constants for cyclic nucleotide binding to the C termini of HCN proteins (HCN_{CB}) derived from FP, SPR, and ITC measurements

	K_D (from FP) ± S.E.[a]		EC_{50} (from SPR) ± S.D. for cAMP	K_D (from ITC) ± S.D. for cAMP
	8-Fluo-cAMP	8-Fluo-cGMP		
	nM		*μM*	*μM*
MBP-$HCN1_{CB}$	116 ± 26 (n = 4)	208 ± 51 (n = 5)	ND[b]	Not measurable
MBP-$HCN2_{CB}$	115 ± 18 (n = 4)	286 ± 34[c] (n = 5)	ND	3.06 ± 0.7 (n = 9)
MBP-$HCN4_{CB}$	111 ± 36 (n = 4)	414 ± 56[d] (n = 3)	ND	0.97 ± 0.7 (n = 4)
$HCN1_{CB}$	382 ± 87 (n = 4)	386 ± 76 (n = 3)	5 ± 1[e] (n = 5)	Not measurable
$HCN2_{CB}$	606 ± 219 (n = 3)	752 ± 236 (n = 3)	10 ± 4 (n = 3)	3.6 ± 1.3 (n = 3)
$HCN4_{CB}$	167 ± 36 (n = 4)	694 ± 121[d] (n = 4)	11 ± 2 (n = 3)	ND
$HCN1_{CB}$ ΔC-linker	ND	ND	5 ± 2[e] (n = 3)	ND
$HCN1_{CB}$ G510S/S515G/S516N	ND	ND	7.3 ± 1.6[e] (n = 3)	ND

[a] FP experiments were in duplicate or triplicate.
[b] ND, not determined.
[c] Mean $p < 0.05$; values are significantly different from that of 8-Fluo-cAMP (analyzed by paired t test, p value two-tailed, confidence interval 99%, GraphPad Prism version 5.03).
[d] Mean $p < 0.01$; values are significantly different from that of 8-Fluo-cAMP (analyzed by paired t test, p value two-tailed, confidence interval 99%, GraphPad Prism version 5.03).
[e] Protein concentration was 500 nM instead of 100 nM.

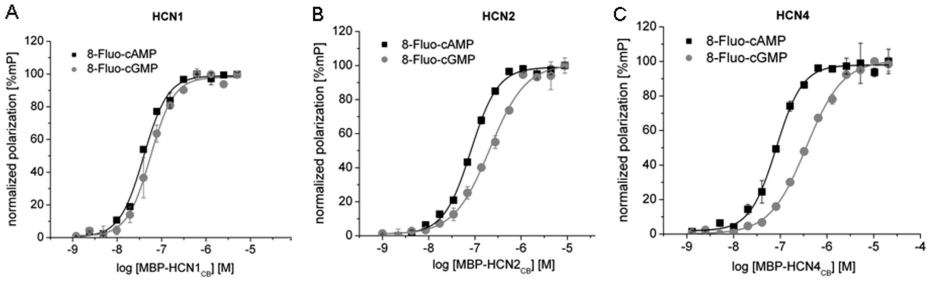

FIGURE 1. **Determination of the dissociation constant K_D for 8-Fluo-cAMP (*black square*) and 8-Fluo-cGMP (*gray circle*) to MBP-tagged $HCN1_{CB}$ (*A*), $HCN2_{CB}$ (*B*), and $HCN4_{CB}$ (*C*) using fluorescence polarization.** K_D values for 8-Fluo-cAMP and 8-Fluo-cGMP are as follows: for MBP-$HCN1_{CB}$, K_D = 40 and 60 nM; for MBP-$HCN2_{CB}$, K_D = 82 and 209 nM; for MBP-$HCN4_{CB}$, K_D = 40 nM and 135 nM.

were not able to record binding with the $HCN1_{CB}$ constructs. Micromolar binding was also measured by SPR with immobilized 8-AHA-cAMP in a solution competition experiment. In this case, the signal obtained with $HCN1_{CB}$ was low but measurable. The calculated EC_{50} values where roughly the same for the three proteins: 5 ± 1, 10 ± 4, and 11 ± 2 μM for $HCN1_{CB}$, $HCN2_{CB}$, and $HCN4_{CB}$, respectively.

Altogether, the binding data show no dramatic difference in the binding affinities of the three proteins. Notably, different techniques yielded different results; the most plausible explanation is that different cAMP and cGMP analogs indeed have different affinities for the proteins, as reported for HCN2 (28). But these results are not necessarily due to technical reasons. They may highlight a high and a low affinity state of the same protein. The low to absent signal of HCN1 observed in two cases (SPR and ITC measurements) highlights a difference from HCN2 and HCN4, probably in the fraction of protein available for binding. We did not observe a systematic difference in binding due to the presence of the MBP (*e.g.* see the ITC results for HCN2 in Table 1).

CNBD Structural Comparison—We next determined the crystal structures of $HCN1_{CB}$, $HCN2_{CB}$, and $HCN4_{CB}$ (at 2.9, 2.3, and 2.5 Å resolutions, respectively) (supplemental Table I). Fig. 2*A* shows a *top view* of the three-dimensional structure of mouse $HCN1_{CB}$. It crystallized as a tetramer in the presence of 5 mM cAMP, as shown previously for mouse HCN2 (11) and, more recently, for human HCN4 (12). Fig. 2*B* shows the tertiary structure of the $HCN1_{CB}$ protomer, with the seven α-helices of the C-linker (A′–F′) in *gray* and the CNBD, composed of four α-helices (A, P, B, and C) and eight β-sheets (numbered 1–8) in *gold*. Fig. 2*C* shows a *side view* of the tetramer, highlighting the contacts provided by the C-linker, where the A′ and B′ helices contact the C′ and D′ of the neighboring subunit. The cAMP binding mode (with the cAMP molecule adopting the *anti*-conformation) and the most relevant protein-ligand interactions are conserved in $HCN1_{CB}$, $HCN2_{CB}$, and $HCN4_{CB}$ (Fig. 2*D* and supplemental Table II). The tertiary structure of $HCN1_{CB}$ superimposes well with those of $HCN2_{CB}$ (average root mean square deviation of 0.85 Å over 198 Cα atoms) and of $HCN4_{CB}$ (average root mean square deviation of 1.05 Å over 197 Cα atoms) (Fig. 2*E*). The only deviations of the Cα backbones emerge for two short regions located at the C-linker and at the loop between strands β4 and β5 (facing the cAMP binding pocket, *circled* in Fig. 2*E*). Such discrepancies are not surprising because most of the residue substitutions of $HCN1_{CB}$ cluster in these regions (supplemental Fig. 1). Analysis of the subunit interfaces reveals that all HCN structures share similar

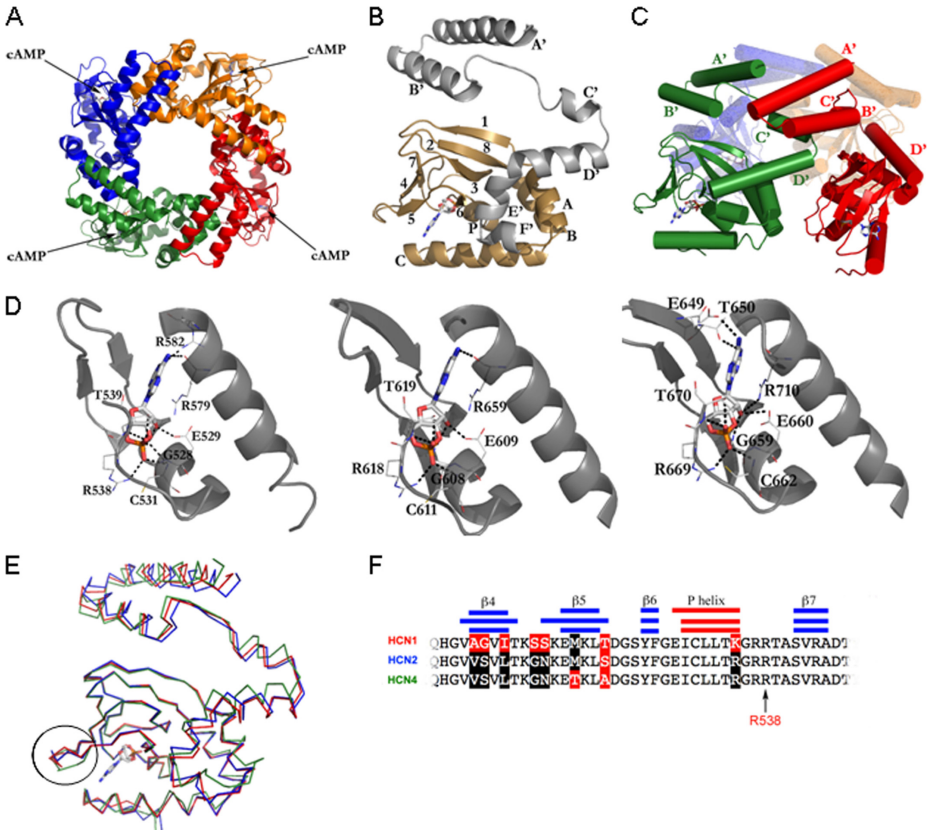

FIGURE 2. **Crystal structure of the soluble portion CB (C-linker plus CNBD) of HCN1 bound to cAMP.** *A*, $HCN1_{CB}$ tetramer viewed parallel to the 4-fold axis. Each subunit is shown in a different *color*. *B*, the protomer of $HCN1_{CB}$ with cAMP. The C-linker, helices A′–F′, is in *gray*; the CNBD, β-sheets 1–8 and helices A, B, P, and C, is in *gold*. *C*, subunit-subunit interactions mediated in the tetramer by the C-linker; helices A′ and B′ form a helix-turn-helix motif that interacts with the helix-turn-helix motif formed by the C′ and D′ helices of the neighboring subunit. The C-linker of one monomer (*red*) contacts two other subunits in the tetramer (*green* and *orange*). *Cylinders* and *arrows* represent helices and strands, respectively. *D*, from *left* to *right*, cAMP binding site of $HCN1_{CB}$, $HCN2_{CB}$, and $HCN4_{CB}$, showing hydrogen bonds and salt bridges that stabilize the cAMP molecule. The binding amino acids are conserved among the three HCN isoforms. In particular, six polar contacts are strictly preserved between the same atoms (see supplemental Table II for the list of interactions). In addition, the residue Cys-531 (HCN1) makes a salt bridge (not present in the other two isoforms) between its nitrogen and the O1P of the cAMP, stabilizing the cyclic nucleotide inside the binding pocket. Another stabilizing element is the polar contact between residue Arg-582 (Arg-659 in HCN2 and Arg-632 in HCN4) and the atom N1 of the cAMP. The same atom contacts residue Arg-579, fundamental for the affinity for the cNMP (27). Also visible in our HCN2 structure are two more polar contacts (not reported in Ref. 11) between the atoms O2* and O2P (cAMP) and the nitrogen atoms of the residues Cys-611 and Gly-608, completing the range of strictly preserved amino acids mentioned above. *E*, differences in the structures highlighted by the superimposition of $HCN1_{CB}$ (*red*), $HCN2_{CB}$ (*blue*), and $HCN4_{CB}$ (*green*). The β4-β5 loop at the entrance of the cAMP binding site in the CNBD is *circled*. *F*, alignment of the amino acid sequences of the three proteins in the *circled region*. Secondary structures are indicated by the *blue*/*red bars*. Residues identical in HCN1 and HCN2 (*black*) but different in HCN1 (*red*) are highlighted. The conserved arginine, Arg-538 in HCN1, important for cAMP binding, is indicated by an *arrow*.

buried surface areas between adjacent subunits (average of 1085 $Å^2$) and mostly conserved polar interactions.

In conclusion, the comparative structural analysis of cAMP-bound HCN proteins (*i.e.* the end products of cAMP binding and tetramerization processes) did not highlight systematic structural differences that would group $HCN1_{CB}$ separately from $HCN2_{CB}$ and $HCN4_{CB}$. This prompted us to look for possible differences between $HCN1_{CB}$ and the other isoforms in the apo-form, a state in which $HCN1_{CB}$ diverges substantially from the other two, as for cAMP-induced gating *in vivo*.

CNBD Oligomerization Propensity—To test this hypothesis, a solution experimental approach was undertaken on the apo-

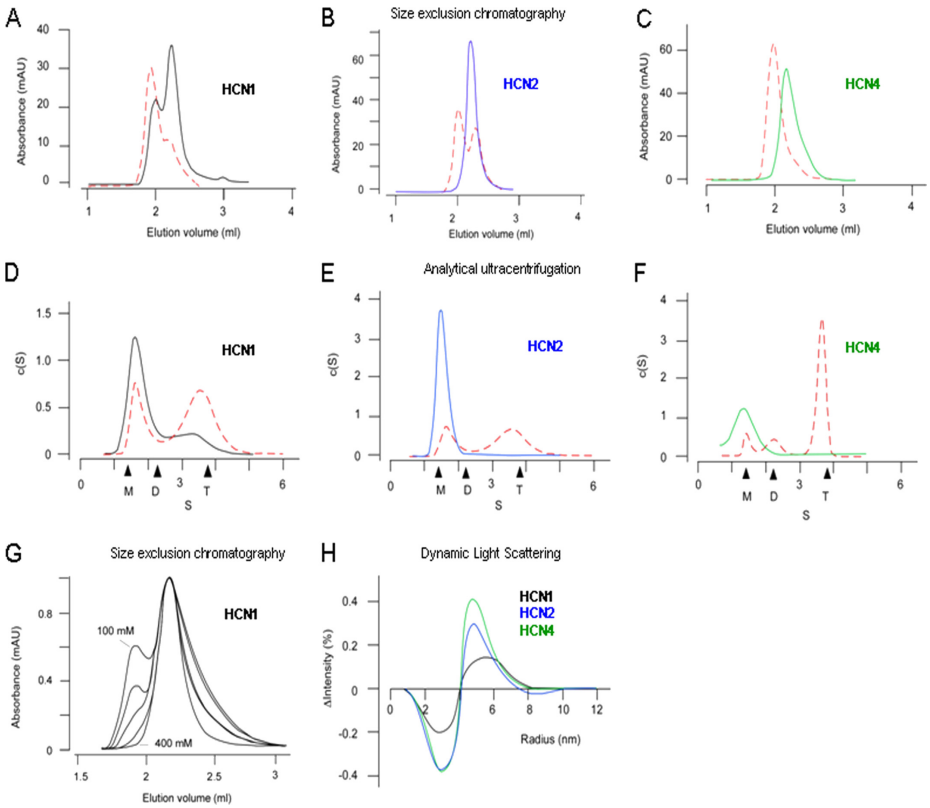

FIGURE 3. **$HCN1_{CB}$ tetramerizes in the absence of added cAMP.** *A–C*, size exclusion chromatography profiles of $HCN1_{CB}$ (*black*), $HCN2_{CB}$ (*blue*), and $HCN4_{CB}$ (*green*) proteins in the absence (*solid line*) and in the presence (*dashed red line*) of 1 mM cAMP; *D–F*, distribution of the sedimentation coefficient (*c*(*s*)), as calculated from sedimentation velocity experiments for $HCN1_{CB}$, $HCN2_{CB}$, and $HCN4_{CB}$ in the absence (*solid line*) and in the presence (*dashed red line*) of 0.3 mM cAMP; *black arrowheads* indicate from *left* to *right* the theoretical values for monomer, dimer, and tetramer (supplemental Table III); *G*, size exclusion chromatography profiles of $HCN1_{CB}$ obtained in the absence of cAMP at increasing NaCl concentration: 100, 150, 200, 300, and 400 mM. The absorbance values are normalized to the peak at 2.2 ml of elution volume. *H*, differential curves showing the cAMP-induced change in protein radius estimated by dynamic light scattering. Curves were obtained by fitting individual dynamic light scattering spectra in the presence and absence of 2.5 mM cAMP with single Gaussians. After normalizing the fitted curves to the same ordinate, the difference spectra were obtained by subtracting the curves in the presence from those in the absence of cAMP. Each pair includes ≥4 data sets.

forms of the three constructs. Fig. 3 summarizes three independent lines of evidence highlighting that $HCN1_{CB}$ has different oligomerization properties from the others: $HCN1_{CB}$ is present in a tetrameric form already in the absence of added cAMP, whereas $HCN2_{CB}$ and $HCN4_{CB}$ form tetramers only in its presence. In size exclusion chromatography, $HCN2_{CB}$ and $HCN4_{CB}$ elute as a single peak (Fig. 3, *B* and *C*, *solid line*), whereas $HCN1_{CB}$ elution shows an additional peak at higher molecular weight (Fig. 3*A*, *solid line*). The higher molecular weight peak appears in $HCN2_{CB}$ and $HCN4_{CB}$ only upon the addition of cAMP (Fig. 3, *A–C*, *dashed red lines*). Sedimentation velocity analytical ultracentrifugation studies assign a proper size to the two forms (Fig. 3, *D–F*, and supplemental Table III). In the absence of added cAMP, $HCN2_{CB}$ and $HCN4_{CB}$ were mainly identified as monomers, with only a small amount of dimeric component (Fig. 3, *E* and *F*, *solid line*). In contrast, $HCN1_{CB}$ exists as a mixture of monomers, dimers, and tetramers (Fig. 3*D*, *solid line*). These oligomeric states are observed for $HCN2_{CB}$ and $HCN4_{CB}$ only after adding saturating amounts of cAMP (Fig. 3, *D–F*, *dashed red line*). Interestingly, the equilibrium between monomer/dimer and tetramer observed in the $HCN1_{CB}$ protein depends on the ionic strength of the solution. Fig. 3*G* shows the effect of increasing salt concentration, from 100 to 400 mM, on the elution profile of

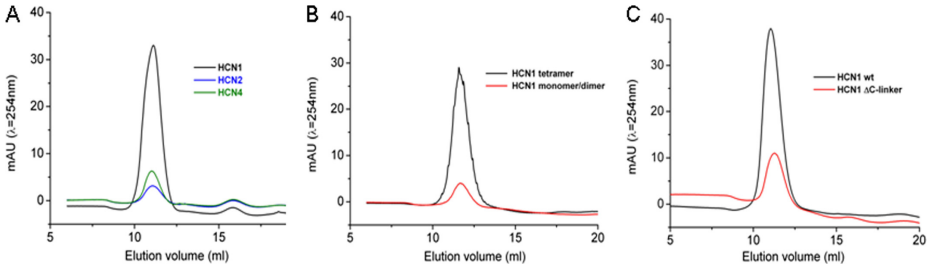

FIGURE 4. **Quantification of the cAMP molecules released by the HCN proteins.** Cyclic AMP content was estimated by the absorbance at $\lambda = 254$ nm (calibration curve shown in supplemental Fig. 3). *A*, absorbance profiles of cAMP released by the three HCN_{CB} proteins after boiling (for experimental details, see "Experimental Procedures"). *B*, comparison between the cAMP content of the monomer/dimer and of the tetramer form of $HCN1_{CB}$. *C*, comparison between the cAMP content of the WT $HCN1_{CB}$ and the HCN1 ΔC-linker protein (see Table 2 for molar ratios).

$HCN1_{CB}$. The disappearance of the tetrameric form of the protein implies an electrostatic nature for the stabilizing interactions. This is strengthened by the observation that, in the tetramer of $HCN1_{CB}$, all 14 substitutions that distinguish this isoform from the other two are exposed to the solvent, and five of them (Ile-432, Asn-437, Asp-444, Ala-496, and Val-497) are at the interface between monomers (not shown).

Finally, dynamic light scattering analysis indicates that, in the absence of added cAMP, $HCN2_{CB}$ and $HCN4_{CB}$ are mainly dimers, whereas $HCN1_{CB}$ is a mixture of dimers and tetramers. The addition of cAMP promotes the full tetramerization of $HCN2_{CB}$ and $HCN4_{CB}$ as well as the residual tetramerization of $HCN1_{CB}$ (supplemental Table IV). The differential signal in the dynamic light scattering peaks, which is due to the addition of cAMP, is illustrated in Fig. 3*H*, indicating the presence of tetrameric $HCN1_{CB}$ protein in the absence of added cAMP.

cAMP Retention after Purification—On the basis of the above reported evidence, a clear and systematic difference emerges between $HCN1_{CB}$ and the other two proteins; whereas $HCN2_{CB}$ and $HCN4_{CB}$ form tetramers only after the addition of saturating concentrations of cAMP, $HCN1_{CB}$ is found as a tetramer already without the addition of exogenous cAMP. This raises the question of whether $HCN1_{CB}$ has a high propensity to tetramerize in the apo-state or if this behavior is due to some tightly prebound cAMP. We then analyzed the endogenous cAMP content associated with the protein after purification. As a negative control, we prepared the mutant protein R538E $HCN1_{CB}$. Mutation of this invariant amino acid (Arg-591 in HCN2 and Arg-669 in HCN4) that interacts with the exocyclic oxygen of the cAMP phosphate (29) reduces the affinity of HCN CNBD for the ligand by more than 3 orders of magnitude (7, 27, 30). Fig. 4*A* shows that $HCN1_{CB}$ contains a significantly higher amount of endogenous cAMP than $HCN2_{CB}$ and $HCN4_{CB}$. The measured molar ratio (protein/cAMP) in $HCN1_{CB}$ is 6. In contrast, this ratio is 24 in $HCN4_{CB}$ and 50 in $HCN2_{CB}$. The value found in the negative control $HCN1_{CB}$ R538E is 40 (Table 2). Furthermore, separate analysis of the two forms of $HCN1_{CB}$, monomer/dimer and tetramer, showed that almost all cAMP is in the tetrameric form, where we found a protein/cAMP ratio of 2 (Fig. 4*B* and Table 2). From these experiments, we must conclude that the tetrameric, but not the monomeric/dimeric, form of $HCN1_{CB}$ contains endogenous cAMP and binds it with high affinity because the ligand is not released during the purification procedure. Altogether our data confirm that cAMP binding to CNBD promotes tetramerization of the C-terminal fragment (11, 12) and suggest that cAMP binds with high affinity to the $HCN1_{CB}$ tetramer, resulting in ligand trapping. We further tackled this point by checking 1) the tetramer formation of an HCN1 mutant with a reduced affinity for cAMP and 2) the cAMP content in a protein with altered tetramerization properties.

TABLE 2
Cyclic AMP content in purified HCN_{CB} proteins expressed as molar ratio (protein/cAMP)

	Molar ratio (protein/cAMP)	*n*
$HCN1_{CB}$	6 ± 2	5
$HCN2_{CB}$	49.5 ± 8.5	4
$HCN4_{CB}$	24 ± 5	3
$HCN1_{CB}$ monomer/dimer	17 ± 2.7	3
$HCN1_{CB}$ tetramer	2.2 ± 0.36	3
$HCN1_{CB}$ ΔC-linker	25 ± 3	3
$HCN1_{CB}$ R538E	40	1

Point one was addressed by testing the elution profile in size exclusion chromatography of the R538E mutant that, as previously mentioned, has a decreased affinity for cAMP. As shown in Fig. 5*A*, R538E protein elutes as a monomer/dimer and does not show the tetramer peak found in the wild type. As expected, the mutant also does not tetramerize upon the addition of 1 mM cAMP.

In regard to point two, in order to prevent tetramerization, we modified the C-linker, because it establishes extensive interactions that mediate the assembly of the four subunits (Fig. 2*C*). We deleted the first three helices (A′, B′, and C′) and tested the resulting protein fragment, ΔC-linker $HCN1_{CB}$, for tetramerization and cAMP binding. For control, we have also performed the same deletion in $HCN2_{CB}$ and $HCN4_{CB}$. We found that ΔC-linker $HCN1_{CB}$ does not show the tetramer peak in size exclusion chromatography and that addition of cAMP does not induce its tetramerization (Fig. 5, *B* and *C*, and supplemental Table IV). The same behavior was found for ΔC-linker $HCN2_{CB}$ and ΔC-linker $HCN4_{CB}$ (data not shown). It is worth noting that ΔC-linker $HCN1_{CB}$ is still able to dimerize, as determined by dynamic light scattering (supplemental Table IV).

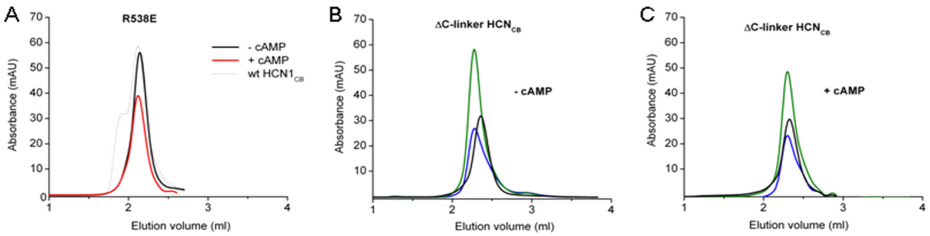

FIGURE 5. **Size exclusion chromatography profile of HCN_{CB} mutants.** *A*, elution profile of $HCN1_{CB}$ R538E mutant, in the presence (*red lines*) and in the absence (*black lines*) of 1 mM cAMP. The profile of $HCN1_{CB}$ WT is shown for comparison as a *dotted line*. Shown are elution profiles of ΔC-linker HCN_{CB} proteins (HCN1 (*black*), HCN2 (*blue*), and HCN4 (*green*)) in the absence (*B*) and in the presence (*C*) of 1 mM cAMP.

The results of these experiments show that tetrameric assembly requires the presence of an intact C-linker region, in agreement with the proposed role of the C-linker in oligomerization (11, 13). We then tested if this construct could trap cAMP. Interestingly, ΔC-linker HCN1 has a very low content of cAMP (protein/cAMP ratio = 25) (Fig. 4*C* and Table 2), showing that an intact C-linker is needed to establish the high affinity state, which traps cAMP in the CNBD. It is worth noting that this construct shows micromolar affinity for cAMP by SPR (Table 1), indicating that this affinity value corresponds to that of the low affinity state. The question is why $HCN1_{CB}$ behaves differently from the other two isoforms. To answer this question, we have reconsidered the divergence in the β4-β5 loop found in the holo-structures because it was recently reported that this linker modulates binding in HCN4 (12). Three residues that are conserved in the β4-β5 region of HCN2 and HCN4 but not in HCN1 have been tested by performing the following mutations in HCN1: the single mutation G510S, the double mutation S515G/S516N, and the triple mutation G510S/S515G/S516N. We tested their impact on cAMP binding to $HCN1_{CB}$ and on the electrophysiological properties of the full-length channel expressed in *Xenopus* oocytes. None of the mutations changed the binding properties of $HCN1_{CB}$ or the tetramerization behavior in gel filtration and the cAMP content of the protein (data not shown). Thus, we have to conclude that the β4-β5 loop does not determine the peculiar biochemical properties of $HCN1_{CB}$. Similar results were obtained by measuring, in intact oocytes, the activation curves of wild type and mutant channels. Table 3 reports the calculated values for half-activation voltage of WT HCN1 and the mutants. None of the mutations affected this parameter. We further extended our analysis to the β5 strand and tested the mutation M519T, previously reported to affect $K_{½}$ in HCN2 without affecting the binding (12). Again, we observed no effect either on $V_{½}$ (Table 3) or on binding (not shown). As controls for the voltage clamp experiments, we used the wild type HCN2 and the low affinity mutant HCN1 R538E. Both channels showed an equally left-shifted $V_{½}$ (−76 mV) when compared with HCN1, as reported previously (7). From these experiments, we conclude that the right-shifted position of the $V_{½}$ of HCN1 is correlated with its property of eluting as a tetramer *in vitro*. This is in line with the finding that the two controls, HCN2 and HCN1 R538E, that do not form tetramers, are left-shifted *in vivo*.

TABLE 3
Effect of mutations in the β4-β5 linker and in β-sheet 5 on the half-activation voltage of HCN1 ($V_{1/2}$), measured by two-electrode voltage clamp in intact oocytes

Channel	$V_{1/2}$	*n*
HCN1 WT	−67.5 ± 0.13	11
G510S	−66.5 ± 0.25	4
S515G/S516N	−65.6 ± 0.23	5
G510S/S515G/S516N	−67.9 ± 0.34	5
M519T	−66.5 ± 0.65	3
R538E	−75.9 ± 0.35	4
HCN2 WT	−76.5 ± 0.04	7

DISCUSSION

In this paper, we have addressed the behavior of the pacemaker channel isoform HCN1, which, unlike HCN2 and HCN4, shows a right-shifted activation curve and responds weakly to saturating cAMP levels *in vivo*. According to the current view, this behavior is reminiscent of a lack of inhibition by the CNBD. To test this hypothesis, we have solved the crystal structure of the isolated C-terminal domain of HCN1 and compared it with those of HCN2 and HCN4; furthermore, we have tested their biophysical and biochemical properties *in vitro* and validated them by electrophysiology.

In the cAMP-bound form, all three HCN isoforms show similar tertiary and quaternary structures. The holoproteins are tetrameric, with the C-linkers mediating the "elbow on shoulder" assembly of the four subunits (11). A deviation of the Cα backbones emerges only in the β4-β5 loop, where the substitutions among the three proteins are clustered (Fig. 2).

This loop is in proximity to the ligand binding pocket and, therefore, could potentially control ligand affinity (12); our mutational analysis of this region has shown no relevant changes in the properties of the purified $HCN1_{CB}$ fragment and, notably, also of the channel expressed in oocytes. Therefore, we can conclude that, at least in HCN1, there is no obvious correlation between the β4-β5 loop and the processes of ligand binding and/or gating. Because the fully saturated cAMP-bound form of the HCN tetramer is similar in all isoforms, the structural differences able to justify the different biochemical behaviors of HCNs should reside in the apo-form of the proteins. Unfortunately, any attempt to crystallize HCNs in the unbound state failed. Only the HCN2 structure has been reported also in the cAMP-free state, but its structure is identical to the holo-form due to the presence of two bromide ions located in the cyclic nucleotide binding pocket, one of which

occupied the position equivalent to the phosphate group of cAMP in the holo-state structure (31). Size exclusion chromatography, sedimentation velocity analytical ultracentrifugation, and dynamic light scattering were used to analyze the HCN isoforms in their unbound state in solution. Our results indicate that in the absence of added cAMP, $HCN1_{CB}$ has a different oligomerization behavior relative to $HCN2_{CB}$ and $HCN4_{CB}$. $HCN2_{CB}$ and $HCN4_{CB}$ were mainly identified as monomers with only a small amount of dimeric component (Fig. 3, *E* and *F*, *solid line*). In contrast, $HCN1_{CB}$ exists as a mixture of monomers, dimers, and tetramers (Fig. 3*D*, *solid line*). These oligomeric states are observed for $HCN2_{CB}$ and $HCN4_{CB}$ only after adding saturating amounts of cAMP (Fig. 3, *D–F*, *dashed red line*). Thus, one of the main findings is that $HCN1_{CB}$ has a higher propensity to tetramerize than $HCN2_{CB}$ and $HCN4_{CB}$ in the same experimental conditions. Remarkably, this property clearly pools $HCN1_{CB}$ separately from $HCN2_{CB}$ and $HCN4_{CB}$ and closely mirrors the grouping established by the *in vivo* response to cAMP, with HCN2 and HCN4 linked by the strong response to cAMP and separated from HCN1.

The analysis of the different HCN species separated by size exclusion chromatography revealed that $HCN1_{CB}$ contains a significantly higher amount of endogenous cAMP than $HCN2_{CB}$ and $HCN4_{CB}$ (molar protein/cAMP ratios of 6, 24, and 50, respectively) (Table 2) and that almost all endogenous cAMP is bound to the $HCN1_{CB}$ tetramer, with a cAMP/tetramer molar ratio of 2. The correlation between tetramerization and cAMP binding is unraveled by analyzing the behavior of the $HCN1_{CB}$ R538E mutant and the ΔC-linker $HCN1_{CB}$. The first mutant has an altered cAMP-binding site, resulting in a reduced affinity for cAMP. The $HCN1_{CB}$ R538E mutant elutes as a monomer/dimer (Fig. 5*A*), and tetramerization does not occur even upon the addition of 1 mM cAMP. The ΔC-linker $HCN1_{CB}$ mutant construct has an intact cAMP-binding site but cannot tetramerize because it is missing the C-linker region. ΔC-linker $HCN1_{CB}$ shows a strong reduction in cAMP content, comparable with those of the other HCN isoforms. We can conclude that cAMP binding promotes tetramerization and that in the tetrameric form, cAMP is bound tightly, because the complex survives extensive dialysis during purification. On the contrary, cAMP-trapping is not a property of the monomeric/dimeric HCN isoforms. Our data suggest that cAMP-induced tetramerization, which is mediated by the C-linker, forces $HCN1_{CB}$ into a high affinity state that in turn stabilizes the tetramer. This finding is in line with the reports of state-dependent affinity of HCN channels for their ligand (30, 32) and agrees with the cyclic allosteric model proposed for HCN channels that postulates the coexistence of the protein in resting and active states with different affinities for the ligand (30, 33, 34). Furthermore, the presence of a stable tetrameric structure agrees with the finding that cAMP traps channels in an open state that kinetically affects the depolarization-dependent deactivation (35).

As for the possibility of measuring *in vitro* these two affinity states, our data show that when probed with the same technique, the affinities of the three C-terminal fragments appear similar and do not highlight an obvious difference between HCN1 and the others. However, as to the absolute values, different techniques yielded very different results. Whereas the K_D and EC_{50} values obtained by ITC and SPR are in the micromolar range, we obtained much higher affinities, in the nanomolar range, by FP. The possibility that the fluorescein-modified analog of cAMP (8-Fluo-cAMP) used in FP experiments has a higher affinity than cAMP because of its chemical modification is ruled out by the evidence that 8-Fluo-cAMP and cAMP produced similar results in ITC when tested on mHCN2 (12). We can speculate that different techniques might highlight a high and a low affinity state of the same protein. In this context, the observation that $HCN1_{CB}$ yielded very poor to absent signals in SPR and ITC but not in FP may be relevant.

The presence of different cAMP affinities, depending on the oligomerization state, can be a general property of HCNs, but $HCN1_{CB}$ differs from $HCN2_{CB}$ and $HCN4_{CB}$ because it tetramerizes already at basal cAMP concentration and with a cAMP/tetramer ratio of 2. Thus, in full-length HCN channels, the CNBD of HCN1, but not that of HCN2 and HCN4, should exist as tetramers already at basal cAMP concentrations. This property of HCN1 protein fully explains the right-shifted position of the activation curve and the weak response to an increase of cAMP level *in vivo*. In regard to the cAMP/tetramer ratio of 2 found in $HCN1_{CB}$, half-saturation of the tetramer appears more likely than half of the tetramers being fully saturated because the second hypothesis would imply that tetramerization is not mandatorily cAMP-driven. Tetramer formation with only half of the binding sites being occupied by cAMP is, on the contrary, consistent with other reports (36) and would explain other experimental findings, such as the small additional shift (2–4 mV) induced by saturating cAMP on the already right-shifted activation curve of HCN1. In this view, full saturation of the tetramer by high cAMP promotes a residual conformational change that, *in vivo*, results in the additional shift in activation curve. The evidence that a tetramer can form even if it is not fully saturated by cAMP has a general relevance for HCN channels that extends beyond the peculiar properties of HCN1. This is in agreement with the report that in HCN2, increasing the number of available binding sites from 1 to 4 progressively increases the number of mV in the shift (36). More recently, Kusch *et al.* (32) have shown by patch clamp fluorimetry that only two of the four binding sites in the tetrameric HCN2 channel have to be occupied for maximal activation. Ulens and Siegelbaum (36) have suggested, on the basis of the stoichiometry of cAMP gating, that a 4-fold symmetric gating ring forms from a 2-fold symmetric dimer of dimers.

CONCLUSIONS

We showed that the C-terminal domain of HCN1 is different from those of HCN2 and HCN4 because it partly purifies as a tetramer, half-saturated with cAMP. Given the well known effect of cAMP-induced tetramerization in removing the inhibition exerted by this domain on the pore gating, we conclude that the property of the HCN1 CNBD to accumulate in the tetrameric state can explain the right-shifted position observed in HCN1 before the addition of saturating cAMP, whereas its half-saturation with cAMP can explain the weak response to saturating cAMP levels. Specifically, we propose the following model that recapitulates well known properties of HCN chan-

nels. The C-terminal region exerts a tonic inhibition on the pore when the C-linker plus CNBD domains are in a non-tetrameric form (probably dimers (this paper) (13, 36)). When the cAMP concentration increases, the C-linker/CNBD region tetramerizes and releases the inhibition from the pore gate. This event results in the positive shift of 16–20 mV in the activation curve of HCN2 and HCN4. In the case of HCN1, a large fraction of C-linker/CNBD is already tetrameric at basal cAMP concentrations. Therefore, it does not exert inhibition and retains the right shifted position of the activation curve. The addition of cAMP saturates the tetramerization process and affects the HCN1 activation curve only marginally, reflected in the modest shift of 2–4 mV.

Acknowledgments—We thank Dan Minor (University of California, San Francisco) and Bina Santoro (Columbia University, New York) for helpful discussion and the generous gift of MBP and mHCN1 clones, Michaela Hansch and Maike Vetter for technical assistance, and Xention (Cambridge, UK) for human HCN2 and HCN4 clones.

REFERENCES

1. DiFrancesco, D. (1993) *Annu. Rev. Physiol.* **55,** 455–472
2. Robinson, R. B., and Siegelbaum, S. A. (2003) *Annu. Rev. Physiol.* **65,** 453–480
3. Santoro, B., and Baram, T. Z. (2003) *Trends Neurosci.* **26,** 550–554
4. Santoro, B., Liu, D. T., Yao, H., Bartsch, D., Kandel, E. R., Siegelbaum, S. A., and Tibbs, G. R. (1998) *Cell* **93,** 717–729
5. Gauss, R., Seifert, R., and Kaupp, U. B. (1998) *Nature* **393,** 583–587
6. Ludwig, A., Zong, X., Jeglitsch, M., Hofmann, F., and Biel, M. (1998) *Nature* **393,** 587–591
7. Chen, S., Wang, J., and Siegelbaum, S. A. (2001) *J. Gen. Physiol.* **117,** 491–504
8. Wang, J., Chen, S., and Siegelbaum, S. A. (2001) *J. Gen. Physiol.* **118,** 237–250
9. Barbuti, A., Baruscotti, M., Altomare, C., Moroni, A., and DiFrancesco, D. (1999) *J. Physiol.* **520,** 737–744
10. Wainger, B. J., DeGennaro, M., Santoro, B., Siegelbaum, S. A., and Tibbs, G. R. (2001) *Nature* **411,** 805–810
11. Zagotta, W. N., Olivier, N. B., Black, K. D., Young, E. C., Olson, R., and Gouaux, E. (2003) *Nature* **425,** 200–205
12. Xu, X., Vysotskaya, Z. V., Liu, Q., and Zhou, L. (2010) *J. Biol. Chem.* **285,** 37082–37091
13. Zhou, L., Olivier, N. B., Yao, H., Young, E. C., and Siegelbaum, S. A. (2004) *Neuron* **44,** 823–834
14. Moll, D., Prinz, A., Gesellchen, F., Drewianka, S., Zimmermann, B., and Herberg, F. W. (2006) *J. Neural Transm.* **113,** 1015–1032
15. Wiseman, T., Williston, S., Brandts, J. F., and Lin, L. N. (1989) *Anal. Biochem.* **179,** 131–137
16. Moll, D., Schweinsberg, S., Hammann, C., and Herberg, F. W. (2007) *Biol. Chem.* **388,** 163–172
17. Leslie, A. G. (2006) *Acta Crystallogr. D Biol. Crystallogr.* **62,** 48–57
18. Evans, P. (2006) *Acta Crystallogr. D Biol. Crystallogr.* **62,** 72–82
19. Vagin, A., and Teplyakov, A. (2010) *Acta Crystallogr. D Biol. Crystallogr.* **66,** 22–25
20. Emsley, P., and Cowtan, K. (2004) *Acta Crystallogr. D Biol. Crystallogr.* **60,** 2126–2132
21. Murshudov, G. N., Vagin, A. A., and Dodson, E. J. (1997) *Acta Crystallogr. D Biol. Crystallogr.* **53,** 240–255
22. Laskowski R. A., MacArthur, M. W., Moss, D. S., and Thornton, J. M. (1993) *J. Appl. Cryst.* **26,** 283–291
23. Krissinel E., and Henrick, K. (2005) in *CompLife LNBI 3695* (Berthold, M. R., Glen, R., Diederichs, K., and Kohlbacher, O., eds) pp. 163–174, Springer, Berlin
24. Schuck, P., Perugini, M. A., Gonzales, N. R., Howlett, G. J., and Schubert, D. (2002) *Biophys. J.* **82,** 1096–1111
25. García De La Torre, J., Huertas, M. L., and Carrasco, B. (2000) *Biophys. J.* **78,** 719–730
26. Kang, M., Moroni, A., Gazzarrini, S., DiFrancesco, D., Thiel, G., Severino, M., and Van Etten, J. L. (2004) *Proc. Natl. Acad. Sci. U.S.A.* **101,** 5318–5324
27. Zhou, L., and Siegelbaum, S. A. (2007) *Structure* **15,** 655–670
28. Scott, S. P., Shea, P. W., and Dryer, S. E. (2007) *Biochemistry* **46,** 9417–9431
29. Weber, I. T., and Steitz, T. A. (1987) *J. Mol. Biol.* **198,** 311–326
30. Wu, S., Vysotskaya, Z. V., Xu, X., Xie, C., Liu, Q., and Zhou, L. (2011) *Biophys. J.* **100,** 1226–1232
31. Taraska, J. W., Puljung, M. C., Olivier, N. B., Flynn, G. E., and Zagotta, W. N. (2009) *Nat. Methods* **6,** 532–537
32. Kusch, J., Biskup, C., Thon, S., Schulz, E., Nache, V., Zimmer, T., Schwede, F., and Benndorf, K. (2010) *Neuron* **67,** 75–85
33. Wang, J., Chen, S., Nolan, M. F., and Siegelbaum, S. A. (2002) *Neuron* **36,** 451–461
34. Altomare, C., Bucchi, A., Camatini, E., Baruscotti, M., Viscomi, C., Moroni, A., and DiFrancesco, D. (2001) *J. Gen. Physiol.* **117,** 519–532
35. Wicks, N. L., Wong, T., Sun, J., Madden, Z., and Young, E. C. (2011) *Proc. Natl. Acad. Sci. U.S.A.* **108,** 609–614
36. Ulens, C., and Siegelbaum, S. A. (2003) *Neuron* **40,** 959–970

A second cyclic nucleotide binding site found in HCN4 eliminates the response of the pacemaker current I_f to cAMP

Lolicato[1]*, M., Zucca[1]*, S., Arrigoni[1]* C., Nardini[1], M., Bucchi[1], A., Schroeder[2], I., Simmons[3], Fishwick, C.W.G[3], Johnson, A.P[3], K., Bolognesi[1], M., Di Francesco[1], D., Schwede[4], F., Thiel[2], G., Moroni[1,5,§] A.

[1] Department of Biosciences, University of Milan, Italy

[2] TU-Darmstadt, Darmstadt, Germany

[3] University of Leeds, UK

[4] BIOLOG Life Science Institute, Forschungslabor und Biochemica-Vertrieb GmbH

D-28199 Bremen, Germany

[5] IBF-CNR, Sezione di Milano, Italy

§ corresponding author: Anna Moroni, Dept. of Biosciences, Via Celoria 26, 20133 Milnao, Italy, anna.moroni@unimi.it, tel +390250314826, fax +390250314815

* These Authors equally contributed to this work;

Running title: allosteric regulation of cAMP-induced activation in HCN4

Abstract

We have identified a binding pocket for cyclic nucleotides at the interface between the C-linker and the CNBD of HCN4. Occupancy of this pocket by the prokaryote second messenger c-di-GMP prevents cAMP-induced activation of the channel. Cyclic-di-GMP exerts this inhibitory effect with micromolar affinity ($k_{1/2}$=1.6 μM) on HCN4 and on the I_f current in sino-atrial node myocytes leading to a decrease in heart rate. Virtual high-throughput screening identified compound #11, a molecule unrelated to c-di-GMP, that inhibits cAMP-induced activation in recombinant and native channels with nanomolar affinity ($k_{1/2}$ = 0.4 uM). Occupancy of the pocket and effect on the current of c-di-GMP and compound #11 is isoform – specific and was not observed in HCN2.

Our results highlight the presence of an allosteric modulatory pathway in HCN channels, indicate a potential drug binding site for heart rate modulation and advance understanding of the mechanism of efficacy of cAMP binding in HCN channels.

Key words: HCN, I_f, cAMP, c-di-GMP, SAN

Introduction

Autonomic regulation of the heart rate is shouldered by the funny current (I_f) that responds to changes in cytosolic cAMP concentration by changing its open probability, thus affecting the slope of the diastolic depolarization in the sinoatrialnode (SAN) action potential. First shown in 1991 by DiFrancesco and Tortora, direct binding of cAMP to the cardiac pacemaker channels was explained in its molecular details when the corresponding genes HCN1-4 (hyperopolarization activated cyclic nucleotide gated) were cloned (Ludwig et al. 1998, Santoro et al. 1998) and the cyclic nucleotide binding domain (CNBD) of HCN2 eventually crystallized (Zagotta et al. 2003). As any member of the superfamily of Kv channels, functional HCN channels are tetrameric. Each monomer contains a transmembrane domain (TMD) connected through a 90 amino acid sequence, the C-linker, to the cyclic nucleotide binding domain (CNBD). Direct binding of cAMP to the canonical binding site in the CNBD, promotes its tetramerization that, in turn, exerts an effect on the TMD, i.e. the voltage sensor and the pore. As a result, voltage-dependent activation is shifted towards less negative potentials and pore opening is facilitated. Although cAMP is the most effective ligand, the pacemaker current I_f is also activated by cGMP (DiFrancesco and Tortora, 1991). Affinity to cGMP was tested so far only for HCN2 (Ludwig et al. 1998, Zagotta et al. 2003) but not for HCN4 that is, among the HCN isoforms, the most highly (ref rabbit) or the only isoform expressed (mouse) in mammalian sinoatrial node (SAN). This work stems from our initial aim to extend investigation on cGMP binding to HCN4 and HCN1. To this end we have co-

crystallized the C-linker + CNBD (CL-CNBD) portion of the channels with cGMP and solved the structures with a cGMP molecule inside the canonical cyclic nucleotide binding pocket. In the case of HCN4, we found a second cGMP molecule bound to a yet unknown binding pocket in the tetramerization domain of the protein. This discovery has started our investigation leading to the unexpected finding that occupancy of this binding site by c-di-GMP, a prokaryote signaling molecule (Jenal and Malone, 2006), inhibits cyclic nucleotide regulation of the channel and reduces heart rate in SAN myocytes.

Results

The I_f current of the sinoatrial node of the heart is modulated by cGMP, albeit with a roughly 40 fold lower sensitivity compared to that for cAMP (DiFrancesco and Tortora, 1991). Although HCN4 is the HCN isoform most expressed in the sinoatrial node, so far no available evidence shows that this isoform is indeed regulated by cGMP. As a starting point in the study of the effect of HCN4 to cGMP, we have co-crystallized the C-linker + CNBD of HCN4 with cGMP. We used HCN4 with cAMP as a searching model (Lolicato et al. 2011) and obtained the phase information by molecular replacement. The atomic structure was refined at 2.7 Å resolution (Table supplementary) and shows a tetrameric assembly of the protomers in which the C-linkers provide most of the subunit contacts (Figure 1a). No significant differences were observed with the structure of HCN4 with cAMP (Lolicato et al. 2011 : the average RMSD of C-α atoms being less than 0.8 A close up view of the binding pocket reveals also perfect agreement with that of HCN2 co-crystallized with cGMP (Zagotta et al. 2003). The cGMP molecule is found in

the syn configuration, between the beta roll and the C helix. All the agonist-protein interactions found in HCN2 are conserved (Table S1), including the purine-specific hydrogen bonds with Thr 670 of the beta-roll and with Arg 710 of the C helix

To determine the effect of cGMP on HCN4, we expressed the channel in HEK293 cells. Inside-out patch clamp recordings from these channels showed a behavior very similar to that reported for the native current I_f. In Figure 1d it can be seen that the current recorded in one such patch during hyperpolarization to –130 mV increases during perfusion of cGMP at the intracellular side due to a positive shift in the activation curve of 11.6 mV (Figure 1e). Cyclic GMP induced-shifts were measured for different cGMP concentrations and the dose-response relationship is plotted in Figure 1f. Hill-plot fitting yielded values of 13.2 μM for the half maximal cGMP concentration ($k_{1/2}$) and 0.72 for the Hill coefficient *n*. Maximal shift was 12 mV. For comparison, the equivalent values reported for I_f are: $k_{1/2}$ = 7.9 μM, *n* = 0.7 and maximal shift 11 mV (DiFrancesco and Tortora, 1991). From the structural and functional data we conclude that HCN4 is regulated by cGMP with modalities closely reflecting those of the native current I_f, as expected. The unexpected finding was a residual electron density at the interface between the C-linker and the CNBD in 4 out of 4 protomers of the unit cell. The presence of the density is clearly cGMP-specific since co-crystallization with cAMP did not produce it (Lolicato et al. 2011). Furthermore, it is also concentration-dependent, being more evident at 50 mM than at 5 mM cGMP. For all these reasons we refined a cGMP molecule inside the density and the result is reported in Figure 2a. A close up view of the binding pocket shows

that the molecule is found in the syn configuration between helices B' and C' of the C-linker and β8 of the β roll. The purine ring interacts exclusively with the C-linker, H bonding with Y559 on helix B' and K562 and F564 on the B'-C' linker. The ribose and cyclic phosphate interact with the C linker and the β roll, H bonding E566 on helix C' and Arg 680 on the β sheet 8 Moreover, the presence of c-GMP in this novel binding pocket is isoform–specific and it only occurs in HCN4 despite the fact that the interacting residues are conserved in HCN1 and HCN2. In order to test if the occupancy of this site, presumably occurring at high concentrations only, would affect the channel behavior, we tested the effect of high cGMP concentrations on HCN4 channel. As shown in Figure 2c, at the test voltage of -110 mV addition of 5 mM or 10 mM cGMP produces the increase in current, as expected by its binding to the canonical binding site in the CNBD. Anomalously high concentrations of cGMP therefore do not exert side effects on the current. Along the same line, we have tested if abnormal concentrations of cGMP can affect the effect of cAMP. The experiment in Figure 2d shows that this is not the case, as addition of cGMP up to 2.5 mM does not change the current recorded in the presence of 5 mM cAMP. In this case, the very high concentration of cAMP was chosen to exclude competition between the two agonists for the canomical binding pocket in the CNBD since the $k_{1/2}$ of HCN4 for cAMP is 1.5 μM (Milanesi et al. 2006).

Thus, the cGMP molecule cannot be considered an alternative modulator of the channel, although it was found in the crystal structure. A more detailed analysis of the structure revealed that the portion of protein, in which the second cGMP was found, is rich of charged residues that create a deeper tunnel

(compared to the cGMP electron density) able to allocate a larger molecule. Ideally a couple of cGMP molecules can fit perfectly on that site, so we tried to dock in the new binding pocket a molecule of c-di-GMP (Fig. XX panel a). Surprisingly, most of the docking poses overlap substantially with the cGMP electron density and the rest of the docked molecule can insert itself through the charged amino acids. As an example in Fig. XX panel a is shown a single c-di-GMP docking pose. We therefore tested whether c-di-GMP could affect the properties of HCN4 expressed in HEK 293 cells. In this case the experiments were first performed in whole cell configuration with the agonist in the pipette solution. The presence of 100 μM c-di-GMP did not affect the currents that appeared indistinguishable from the control. This is shown in Figure 3a, displaying exemplary current recordings and the average activation curves showing no shift in the open probability of the channel. Surprisingly different results were obtained when the experiment was repeated in the presence of cAMP (3b). In this case the presence of c-di-GMP completely abolished the increase in current induced by cAMP, left-shifting the activation curve by 16 mV back to the control position. Panel 3c shows the dose-response curve for the effect of c-di-GMP evaluated as the difference in the half activation potential ($V_{1/2}$) recorded in the presence of cAMP. The $k_{1/2}$ is 1.58 +/- 0.24 (n=3), while the Hill coefficient *n* is 1.2. To test whether c-di-GMP is directly acting on the HCN4 channel, we repeated the experiments in inside-out configuration. Figure 3d shows a typical experiment (n >10): after the control current is recorded at -140 mV (black), addition of 15 μM cAMP induces the expected increase in amplitude (red). Further addition of 100 μM c-di-GMP to the same solution (green), completely abolishes the effect of

cAMP on the current amplitude and kinetics. This result is further supported by the activation curves reported in panel e that were obtained with a ramp protocol from another patch. The presence of c-di-GMP left-shifted the activation curve recorded in the presence of c-AMP of about 14 mV, similarly to what reported for the whole cell experiments of Panels b. The very negative position of the curves is due to the run down, a known phenomenon occurring in inside-out previously described in HCN channels (DiFrancesco et al. 1986). These results confirm that c-di-GMP competes with cAMP on the activation of HCN4. In order to discriminate between a direct competition with cAMP for the canonical cyclic nucleotide binding pocket and an indirect competition that would result from the occupancy of the second binding pocket highlighted in the crystal, we have increased the cAMP concentration up to 1mM in order to compete out the c-di-GMP from the canonical pocket. Since we have not seen any change (panel f), we concluded that c-di-GMP counteracts the effect of cAMP by binding to another site on the channel that must be downstream of the cAMP binding and that we have presumably identified on the crystal structure as being at the interface between the C-linker and the CNBD.

As additional proof, the c-di-GMP molecule was *in silico* docked on the canonical binding site of the human HCN4 structure previously published using the docking software eHiTS (Zsoldos et al., 2006, Zsoldos et al., 2007) , removing the cAMP from that site. Docking attempts showed that the c-di-GMP molecule was too large to be accommodated in the cAMP binding pocket.

Several attempts were performed to co-crystallize the HCN4 protein with the c-di-GMP molecule in the allosteric pocket. The presence of c-di-GMP clearly disturbs the crystals that diffracted at quite low resolution and always above 6 Å. We could nonetheless solve the structure of the protein in the presence of c-di-AMP at a resolution of 3.7 Å.

In this case we could solve the molecule inside the density even though we could not see the position of the side chains in the amino acids surrounding the pocket.

Interestingly, we found the c-di-AMP bound in only two monomers of sixteen (four tetramers) in the asymmetric unit, and there with occupancy <1. This finding allowed the protein to diffract at a reasonable resolution, indicating that the protein was only partially disturbed by the presence of the molecule. On the contrary what happened with the c-di-GMP.

This achievement confirms that cyclic dinucleotides can occupy the allosteric pocket, but worth noting that both the cGMP (gray electron density) and the docked c-di-GMP (blue sticks) assume a different orientation compared with the crystallized c-di-AMP (red sticks, vedi figure sovrapposte) indicating possible different interactions with the protein.

As the fig. sovrapposte shows, the crystallized c-di-AMP protrudes outside the "hot spot" of the allosteric binding pocket. Potentially, this lack of contacts with the protein is significant for the binding affinity and allowed the tetramer to pack properly.

The effect of c-di-AMP was therefore tested on HCN4 current by adding 100 μM of the ligand in the pipette in the presence of cAMP. As shown by the

curves reported in Figure 4a, also this molecule prevents cAMP-induced activation of the current.

Looking at the three docking poses of c-di-GMP shown in Figure 4b the amino acid E566 is the only one that interacts with all of them, appearing as a relevant residue for binding. As predicted, mutation E556K in hHCN4, removes the response to c-di-GMP, as shown in Figure 4, panel b.

The evidence that binding of a small molecule to this site induces such a drastic and relevant effect on the HCN channel current, prompted us to screen for unrelated molecules by using the in silico virtual high-throughput screening program eHiTS. More than 300000 molecules from the Maybridge (http://www.maybridge.com/portal/alias__Rainbow/lang__en/tabID__146/DesktopDefault.aspx), Chembridge (http://www.hit2lead.com/) and Peakdale Molecular Scientific (http://www.peakdale.co.uk/products/screening-compounds.html) screening libraries were screened. The top 1000 compounds were further examined using the de novo design software SPROUT (Gillet et al., 1995, Gillet et al., 1994, Law et al., 2003, Zsoldos et al., 2003) and the most promising scaffold chosen according to synthetic accessibility and desirable solubility properties as well as predicted binding affinity. Eleven of the most structurally diverse compounds were selected for testing on HCN4. Out of 11, the best effect was found with the compound N'-biphenyl-2-yl-N-[1-(3-cyanobenzyl)piperidin-4-yl]-N-(pyridin-3-ylmethyl)urea (IUPAC name, hereafter called compound 11) . Figure 5 shows in panel a the molecule inside the allosteric pocket and, in a close up view, the main protein-ligand interactions. When tested on the channel by patch clamp experiments, this molecule was able to abolish the effect of cAMP in a dose-dependent way.

Panel b shows an exemplary experiment performed in whole cell in which the presence of 100 μM compound 11 in the pipette was able to abolish the increase in current induced by the addition in the bath of the membrane permeant 8-Br-cAMP. Panel c shows the average activation curves recorded with the mix of three molecules 5, 8 and 11 (out of 11 selected by docking), and with the single molecules, to show that only compound 11 was found active. The dose-response curve of compound n.11 evaluated on the cAMP-induced shift (panel d) highlights a $k_{1/2}$ of 0.42 +/- 0.11 μM, higher than that of c-di-GMP. This result shows that the pocket identified in this work can be considered a potential drug binding target, inasmuch unrelated molecules, selected in totally independent ways, induce the effect on the current upon micromolar or submicromolar binding.

Thinking along this line, another property that appears appealing for a potential drug binding site is isoform-specificity. Indeed, as previously mentioned, the electron density found in the presence of cGMP, was more evident in the structure of HCN4 than in other HCN isoforms, when crystallized in the same experimental conditions. We have therefore determined the effect of c-di-GMP on the current of human HCN2 in HEK 293 cells. Figure 6 panels a and b show respectively that 100 μM c-di-GMP and 200 μM compound 11 do not revert the action of cAMP thus confirming that this binding site is isoform-specific.

The next step was to verify if the native current I_f in the cardiac sinoatrial node, was similarly affected by the two molecules, c-di-GMP and compound n.11. It is known that HCN4 is the major (rabbit) and in some cases the only (mouse) molecular determinant of the native channel expressed in the pacemaker region of the mammalian heart. To this end we acutely isolated sinoatrial node (SAN)

myocytes from mouse heart and recorded the native current I_f in whole cell configuration. Figure 7a shows exemplary currents recorded in SAN myocytes in control solution and in the presence of 10 μM cAMP. The addition of c-di-GMP or compound 11 is able to block the effect of cAMP on the current. This is clearly shown by the activation curve of panel b, showing the reversion of the shift in the activation curve to the control position induced by c-di-GMP or compound 11. Last, we tested if the addition of compound n.11 or c-di-GMP was able to affect the heart rate.

Discussion

1-interest from a molecular biophysics point of view: Novel binding pocket identifies a region of the protein that controls the efficacy of cAMP. We can mention here that all mutants in the pocket (so far we have tested 3) are affected either in the response to cAMP and/or in the basal position of the activation curve.

If with the flash exp we can show the relationship to the affinity in the CNBD, we will stress the point that this is a hub that transducer the voltage sensor movement in the TMD into a change in affinity in the CNBD during activation and vice-versa, transduces the binding of cAMP into a facilitated opening of the pore.

Evidences that this is a hub for cAMP effect: the mutant F564T is already shifted and does not respond to cAMP.

We have previously highlighted differences in the biochemical properties of the three C-terminal proteins, in particular in the dynamics of cAMP–induced tetramerization (Lolicato et al). Therefore, differential binding of cGMP in a position that seems to be relevant for the tetramerization of the proteins, does not come totally unexpected.

2- interest for drug design: this is a potential binding site for drugs because binding of molecules in this pocket controls the autonomic control on the heart rate, an important aspect of therapy during heart failure; it is isoform-specific

excluding side effects on HCN2 (HCN1 is not important because cAMP-induced shift does not occur in HCN1); it acts at nanomolar affinity;

3-interest for c-di-GMP:

Cyclic di-(3':5')- guanosine monophosphate (c-di-GMP) is a prokaryotic second messenger, recently found also in lower eukaryotes (Chen and Schaap, 2012). As a second messenger, it regulates bacteria motility and biofilm formation (Jenal and Malone, 2006). Cyclic-di-GMP induces a potent immune response in infected cells and for this role it is frequently used as a co-adjuvant in vaccinations (Hu et al.,2009). Recently, it was shown to induce a type I interferon response that depends on its direct binding to STING (stimulator of interferon genes) (Yin, Q. et al. 2012, Huang et al. 2012), a ER-localized transmembrane receptor that links cytosolic detection of bacterial DNA to interferon synthesis.

REFERENCES

Battye, T. G. G., Kontogiannis, L., Johnson, O., Powell, H. R. & Leslie, A. G. W. (2011). Acta Cryst. D67, 271-281.

Chen and Schaap. The prokaryote messenger c-di-GMP triggers stalk cell differentiation in Dictyostelium. Nature (2012) vol. 488 (7413) pp. 680-3

DiFrancesco et al. Properties of the hyperpolarizing-activated current (if) in cells isolated from the rabbit sino-atrial node. J Physiol (Lond) (1986) vol. 377 pp. 61-88

DiFrancesco and Tortora. Direct activation of cardiac pacemaker channels by intracellular cyclic AMP. Nature (1991) vol. 351 (6322) pp. 145-7

Emsley P, Cowtan K (2004) Coot: model-building tools for molecular graphics Acta Crystallographica Section D-Biological Crystallography 60: 2126-2132 Part 12 Sp.

Gillet et al. SPROUT: recent developments in the de novo design of molecules. J Chem Inf Comput Sci (1994) vol. 34 (1) pp. 207-17

Gillet 1995

Hu et al. c-di-GMP as a vaccine adjuvant enhances protection against systemic methicillin-resistant Staphylococcus aureus (MRSA) infection. Vaccine (2009) vol. 27 (35) pp. 4867-73

Huang et al. The structural basis for the sensing and binding of cyclic di-GMP by STING. Nat Struct Mol Biol (2012) vol. 19 (7) pp. 728-30

Jenal and Malone. Mechanisms of cyclic-di-GMP signaling in bacteria. Annu Rev Genet (2006) vol. 40 pp. 385-407

Krissinel E. and Henrick K.(2007).Inference of macromolecular assemblies from crystalline state. J. Mol. Biol. 372, 774--797.

Laskowski R A, MacArthur M W, Moss D S, Thornton J M (1993). PROCHECK - a program to check the stereochemical quality of protein structures. J. App. Cryst., 26, 283-291.

Law 2003

Lebedev, A. A., Young, P., Isupov, M. N., Moroz, O. V., Vagin, A. A. & Murshudov, G. N. (2012). Acta Cryst. D68, 431-440.

Lolicato et al. Tetramerization dynamics of C-terminal domain underlies isoform-specific cAMP gating in hyperpolarization-activated cyclic nucleotide-gated channels. J Biol Chem (2011) vol. 286 (52) pp. 44811-20

Ludwig et al. A family of hyperpolarization-activated mammalian cation channels. Nature (1998) vol. 393 (6685) pp. 587-91

McCoy, A. J., Grosse-Kunstleve, R. W., Adams, P. D., Winn, M. D., Storoni, L. C. & Read, R. J. (2007). J. Appl. Cryst. 40, 658-674.

Milanesi et al. Familial sinus bradycardia associated with a mutation in the cardiac pacemaker channel. N Engl J Med (2006) vol. 354 (2) pp. 151-7

Murshudov G.N., Vagin A.A. andDodson E.J. (1997) Refinement of Macromolecular Structures by the Maximum-Likelihood Method. Acta Cryst. D53, 240-255.

Murshudov, G.N., Skubak P., Lebedev A.A., Pannu N.S. , Steiner R.A., Nicholls R.A., Winn M.D., Long and Vagin A.A. (2011) REFMAC5 for the Refinement of Macromolecular Crystal Structures. Acta Cryst. D67, 355-367.

Nicholls R.A., Long F. and Murshudov G.N. (2012) Low Resolution Refinement Tools in REFMAC5. Acta Cryst. D.

Santoro et al. Identification of a gene encoding a hyperpolarization-activated pacemaker channel of brain. Cell (1998) vol. 93 (5) pp. 717-29

Vagin A.A. and Isupov M.N. Spherically averaged phased translation function and its application to the search for molecules and fragments in electron-density maps. Acta Cryst.D,(2001) 57, pp 1451-1456

Zagotta et al. Structural basis for modulation and agonist specificity of HCN pacemaker channels. Nature (2003) vol. 425 (6954) pp. 200-5

Yin et al. Cyclic di-GMP sensing via the innate immune signaling protein STING. Mol Cell (2012) vol. 46 (6) pp. 735-45

Zsoldos et al. eHiTS: an innovative approach to the docking and scoring function problems. Curr Protein Pept Sci (2006) vol. 7 (5) pp. 421-35

Figure legends

Figure 1

(a) Tetrameric assembly of the HCN4 C-linker+CNBD in the presence of cGMP.

(b) Close-up view of one monomer with the cGMP molecule in the canonical binding site.

(c) Electron density map (top) and polar contact (bottom) of a molecule of cGMP in the canonical binding pocket.

(d) Example trace current recording of HCN4 channel in the absence (black) and in the presence (red) of the ligand cGMP.

(e) Activation curves of the apo (black) and cGMP-bound (red) HCN4 channel.

(f) Titration curve of cGMP recorded onto HCN4 channels.

Figure 2

(a) Cartoon representation of a monomer of the crystallized HCN4 in the presence of cGMP in both the canonical binding pocket and in the new additional regulation site. The electron density (gray net) of the cGMP in the new site is also represented.

(b) Polar contacts occurring between the cGMP in the new binding site and its coordination aminoacids of HCN4.

(c,d) High concentrations of cGMP do not reduce the effect of cAMP. We haveused 5 mM cAMP to exclude competition on the canomical binding pocket.

Figure XX

>(a)

Close-up view of the C-linker region of HCN4.

The gray trace is the electron density, countered at 1.5 sigma, of the cGMP crystallized in the allosteric binding pocket.

The blue sticks represent a single pose of the docked c-di-GMP, with substantially overlapping region with the cGMP electron density.

The side chains of charged aminoacids are, also, represented, highlighting a "charged tunnel" able to allocate a larger molecule.

(b)

Structure superposition of HCN4 CNBD in the presence of c-di-AMP (red sticks and cyan backbone) and the docked c-di-GMP (blue sticks). The green backbone is of the crystal structure of HCN4 in the presence of cGMP in the allosteric pocket (gray grid countered at 1.5 sigma).

Figure 3

(a) Example trace record (top) and activation curves (bottom) of HCN4 channels in the presence (red) and in the absence (black) of the molecule c-di-GMP.

(b) Same as (a), but also in the presence of saturating amount (15uM) of cAMP.

(c) Dose-response curve of the c-di-GMP

(d) Inside-out experiments on HCN4 currents in the presence of c-di-GMP (green, together with cAMP). The control curve is represented in black, while the control in the presence of only cAMP is represented in red.

(e) Ramp protocol of HCN4 in the presence of cAMP alone (black) or in the presence of c-di-GMP (red).

(f) Competition experiments conducted with 1mM cAMP (blue track). Experiments performed as same as (d).

Figure 4

(a) Crystal structure of HCN4 in the presence of a molecule of c-di-AMP (green cartoons) flanked by a sketch representation of the molecule (left) and the effect of the molecule on the channel behavior in the presence of cAMP (right).

(b) Same as (a), except for the cartoon representation: here are presented three docking poses (cyan, magenta and orange) of the molecule c-di-GMP on the crystal structure of HCN4.

Figure 5

(a) Cartoon representation of HCN4 crystal structure with a molecule of compound 11 docked in the new binding pocket (left). The aminoacids involved in the stabilization of the molecule in the pocket are shown in the right panel.

(b) Effect of the selected compounds on HCN4 current. The compound 11 was the only one able to give a measurable effect on the channel. The dose-response curve is represented in the right figure.

Figure 6

Effect of c-di-GMP (a) and the compound 11 (b) on HCN2 channels. Experiments performed in whole-cell configuration.

FIGURES

Figure 1

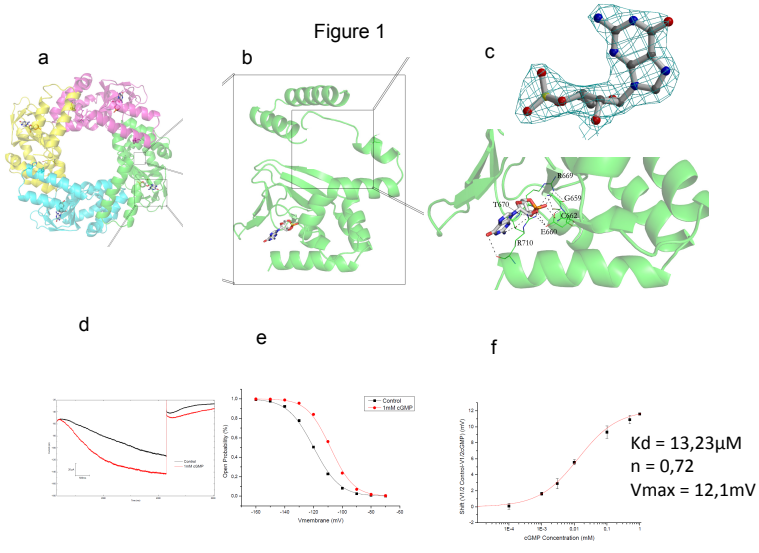

Figure 2

a

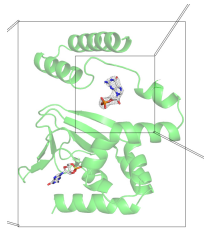

b

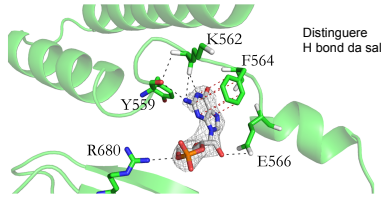

Distinguere
H bond da salt bridges

c

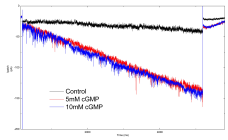

d

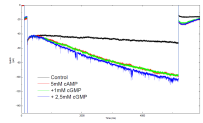

High concentrations of cGMP do not reduce
the effect of cAMP. We haveused 5 mM cAMP

to exclude competition on the canomical binding pocket.

Figure XX

a

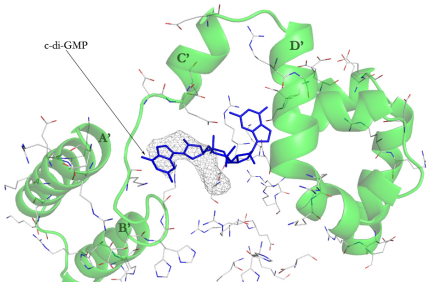

b

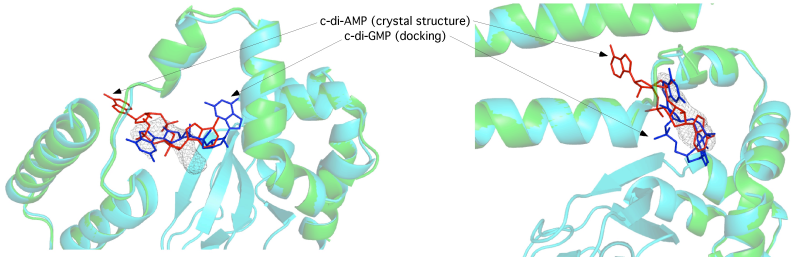

Figure 3

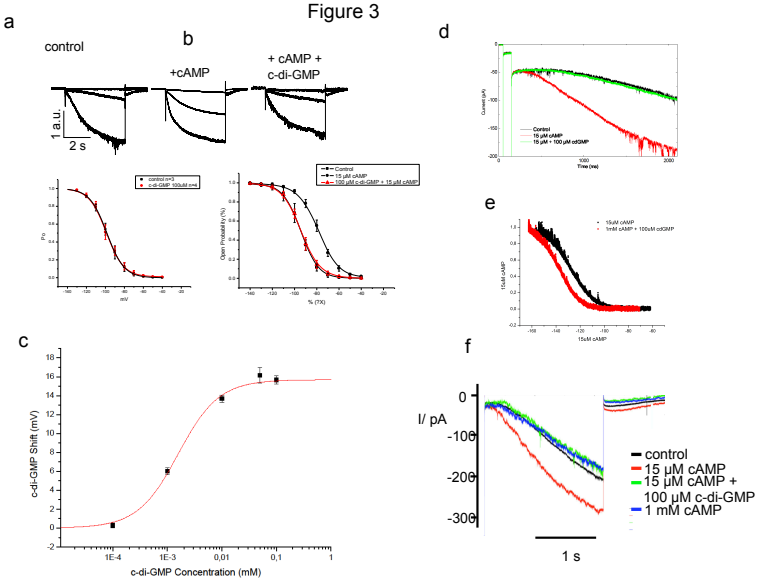

Figure 4

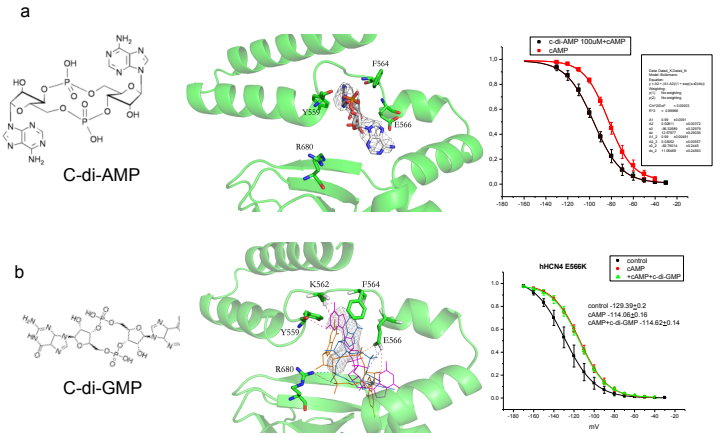

Figure 5

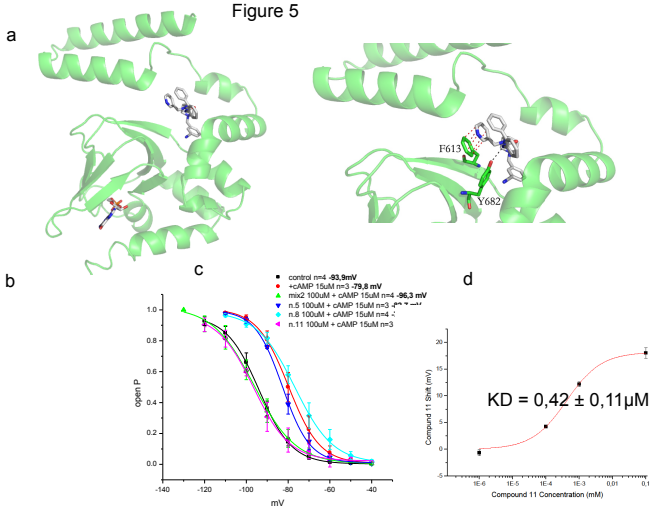

Figure 6

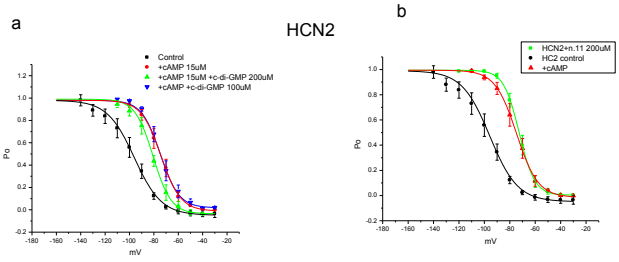

Methods

Electrophysiology

Wild-type HCN4 channel complementary DNA (cloned in pcDNA1.1, kindly provided by Prof. DiFrancesco D.) was transfected for transient functional expression into HEK293 cells with a plasmid containing green fluorescent protein, as described previously. From one to five days after transfection, the cells were dispersed by trypsin and plated on 35-mm plastic petri dishes. A dish was placed under the stage of an inverted micro- scope, and GFP-expressing cells were selected for patch-clamp analysis at room temperature (25 to 26° C). The pipettes used in the whole-cell patch-clamp experiment contained 10 mM sodium chloride, 130 mM potassium chloride, 1 mM egtazic acid (EGTA), 0.5 mM magnesium chloride, 2 mM ATP (sodium salt), 0.1 mM guanosine triphosphate (sodium salt), 5 mM phosphocreatine, and 5 mM HEPES potassium hydroxide buffer (pH 7.2). The control extra- cellular solution in whole-cell experiments contained 110 mM sodium chloride, 30 mM potassium chloride, 1.8 mM calcium chloride, 0.5 mM magnesium chloride, and 5 mM HEPES sodium hydroxide buffer (pH 7.4); 1 mM barium chloride, 2 mM manganese chloride, 100 μM nickel chlo- ride, and 20 μM nifedipine were added to improve dissection of the pacemaker current. The pipettes used in inside-out macropatch experiments contained 70 mM sodium chloride, 70 mM potassium chloride, 1.8 mM calcium chloride, 1 mM magnesium chloride, 1 mM barium chloride, 2 mM manganese chloride, and 5

mM HEPES sodium hydroxide buffer (pH 7.4); bath solution contains 130 mM potassium aspartate, 10 mM sodium chlo- ride, 2 mM calcium chloride, 5 mM EGTA potassium hydroxide, and 10 mM HEPES potassium hydroxide buffer (pH 7.2). (Milanesi et al. 2006)

Virtual high-throughput screening using eHiTS

The electronic high-throughput screening program eHiTS (Zsoldos et al., 2006, Zsoldos et al., 2007) utilises an exhaustive systematic search algorithm that considers all docking poses that lack severe steric clashes with the protein. The system employs a unique graph matching algorithms and dock tables which are stored in SQL databases. Unlike DOCK or FlexX (http://www.biosolveit.de/FlexX-C/), eHiTS does not use an incremental construction method but instead attempts to find the global optimum by enumerating combinations of independent fragment dockings.

The eHiTS software has a novel flexible docking ligand method that exhaustively produces all ligand poses that avoid severe steric clashes between the protein receptor and the ligand. In the first instance, the binding pocket is defined by a steric grid which divides regions into separate pockets and identifying all possible interaction sites. The ligand is divided into rigid fragments and connecting flexible chains. Each fragment is wrapped into a polyhedron shape with chemical properties assigned to the vertices of the polyhedron. All rigid fragments are docked to every possible place in the newly identified binding site and scored for predicted binding affinity.

Initially, a simple and fast chemical flag based statistical scoring function is used during the rigid fragment-docking and pose-matching phases. This function is not too sensitive to small variations in the interaction geometry, interaction distance and hydrogen-bonding angle.

All ring systems are considered rigid and their conformation is preserved as given in the input. Therefore, it is desirable to use multiple ring conformers (e.g. chair, boat and twist boat for a cyclohexane) for complete conformational sampling. These can be generated using a conformer generation program such as Corina (Schwab, 2010). An exhaustive matching of compatible rigid fragment pose sets is performed to yield complete structures. Typically, the program evaluates several million mappings of the rigid fragment polyhedra to cavity polyhedra. The reconstructed solutions define a rough binding pose which is then refined using a local energy minimisation in the targeted site of the protein receptor. A more sensitive, empirical-scoring function is used during the final local energy minimization phase. This scoring function has smooth curves representing the distance and angle dependency of the interactions while supporting efficient gradient-based optimization.

The final resulting poses are evaluated using a third, more time consuming scoring function that combines both statistical and empirical components, plus additional grid based geometrical terms as well as entropy loss estimation and another novel scoring element based on the coverage of receptor surface area. This final scoring function attempts to estimate the binding free energy more

accurately. The result of the final accurate scoring is used to rank the generated solutions (Zsoldos et al., 2007).

Using the high-throughput screening mode within the program (version 9.0), three compound libraries containing a total of 300 000 commercially available compounds from Maybridge(http://www.maybridge.com), Chembridge(http://www.chembridge.com) and Peakdale(http://www.peakdale.co.uk) were screened against the new x-ray crystal structure of HCN4.

From the library of commercially available molecules, 1000 compounds were selected for further evaluation and consensus scoring using the *de novo* design program SPROUT (Gillet et al., 1995, Gillet et al., 1994, Law et al., 2003, Zsoldos et al., 2003). These 1000 compounds were selected based on their predicted binding to the protein as calculated using the eHiTS scoring algorithm. From this set, 11 molecules were selected for purchase. These 11 compounds were chosen based upon their predicted binding affinity to the protein as determined using the eHiTS and SPROUT scoring functions and also their predicted binding pose, as visualised using the SPROUT protein boundary surface representation.

High-resolution mass spectroscopy was used to confirm the integrity of the purchased compounds.

Protein preparation

The cDNA fragment comprised the C-linker (CL) and CNBD region of human HCN4 and encoded residues 521-723, were cloned into a modified pET-24b, transformed into *E. coli* Rosetta strain and overexpressed as previously

described (Lolicato et al. 2011). Briefly, cells were grown at 37 °C in LB broth to 0.6 OD_{600} and induced with 0.4 mM isopropyl-1-thioβ-D-galactopyranoside (IPTG) O.N. at 20 °C. The cells were collected by centrifugation and resuspended in ice-cold lysis buffer (30 mM Hepes pH 7.4, 500 mM NaCl, 10% glycerol, 1 mM β-mercaptoethanol) with the addition of 10 µg/ml DNAse, 0.25 mg/ml lysozyme, and inhibitor cocktail. The cells were sonicated on ice 12 x 20 sec and the lysate cleared by centrifugation. The proteins were purified by affinity chromatography on Ni^{2+}-NTA and eluted in lysis buffer plus 300 mM imidazole. The tag was removed by HRV3C cleavage O.N. at 4 °C. The cleavage reaction was further purified by amylose resin (New England Biolabs) followed by a size-exclusion chromatography onto a HiLoad 16/60 Superdex 200 column (GE Healthcare).

Crystallization

Crystallization trials were set up in 96-well sitting drop plates (Greiner) using the Orxy 8.0 crystallization robot (Douglas Instruments) and stored at 4 °C. Crystals were further optimized in 24-well hanging-drop plates.

Crystals of the HCN4-cGMP complex (protein concentration 7-13mg/ml, 5-50 mM cGMP) were grown by vapor-diffusion using as a precipitant solution 10-15% PEG3350, 200mM sodium acetate buffer, pH 5.0 and 200mM Ammonium phosphate.

Crystals were cryoprotected with the same solution plus 5% PEG3350 and 25% glycerol.

A full data set was collected to 2.7 Å resolution (IDxx beamline, ESRF, Grenoble, France).

Crystals of the HCN4-cGMP-cidiGMP complex (protein concentration 10mg/ml, 5mM cAMP and 5-50mM c-di-GMP) were grown by vapor-diffusion using as a precipitant solution 200mM K/Na tartrate (with/without 100mM MES, pH=6.5 or 100mM Tris-Cl, pH=7.5). 15-30 crystals were tested for diffraction but none of them reached a resolution better then 6.0 Å, so no dataset were collected. (IDxx beamline, ESRF, Grenoble, France and XALOC beamline, ALBA, Barcelona).

Moreover soaking experiments with 50mM c-di-GMP (biolog.de) on crystal grown in the presence of cGMP were performed. Crystals were tested for diffraction (XALOC beamline, ALBA, Barcelona, Spain), but no dataset were collected due to poor diffraction.

Crystals were cryoprotected with the same grow solution plus 5% precipitant and 25% glycerol or 25% PEG400.

Crystals of the HCN4-cGMP-cidiAMP complex were obtained by soaking (48 hours) of HCN4-cGMP protein crystals on a cryo-solution containing 20mM c-di-AMP (Biolog.de), 15% PEG3350, 200mM Ammonium phosphate, 200mM Sodium acetate, pH=5.0 and 25% Glycerol.

Crystals were directly frozen in liquid nitrogen.

A full data set was collected to 3.7 Å resolution (XALOC beamline, ALBA, Barcelona, Spain).

Raw data were processed with Mosflm (Battye et al. 2011) and Scala and the structures were solved by molecular replacement using the program MolRep (Vagin and Isupov, 2001) (HCN4-cGMP) or Phaser (HCN4-cGMP-cdiAMP) (McCoy et al. 2007). The crystal structure of human HCN4 in complex with cAMP (Lolicato et al. 2011) (PDB entry-code 3U11) was used as search model.

To avoid model bias, the bound-cAMP was removed from the search model. Several cycles of manual rebuilding, using the program COOT (Emsley and Cowtan, 2004), and refinement, using the program REFMAC5 (Murshudov et al. 2011 and Murshudov et al. 1997) (rigid body and restrained refinement), were carried out to improve the electron density map.

For the complex with c-di-AMP molecule, ligand restraints were generated by the program JLigand (Lebedev et al. 2012) and additional cycles of refinement with REFMAC5 using TLS restraints together with additional restraints generated by PROSMART (Nicholls et al. 2012) were used to improve the final model.

The final R-factor/R-free are 20/25 . The programs Procheck (Laskowski et al. 1993) was used to assess protein stereochemical quality. The program PISA (Krissinel and Henrick, 2007) was used to identify and analyze the quaternary assemblies. Atomic coordinates and structure factors have been deposited with the Protein Data Bank, with entry codes XXXX and YYYY for HCN4-cGMP, and HCN4-cGMP-cdiAMP, respectively.